GA-A13238
UC-77

GAS-COOLED FAST BREEDER REACTOR

QUARTERLY PROGRESS REPORT

FOR THE PERIOD AUGUST 1, 1974 THROUGH OCTOBER 31, 1974

by

Project Staff

Prepared for the
U.S. Atomic Energy Commission
San Francisco Operations Office
Under
Contract AT(04-3)-167
Project Agreement No. 23

General Atomic Project 393

December 12, 1974

GENERAL ATOMIC

GENERAL ATOMIC COMPANY
P.O. BOX 81608
SAN DIEGO, CALIFORNIA 92138

PROGRESS REPORT SERIES

GA-5537	November 1, 1963 to July 31, 1964
GA-6667	August 1, 1964 to July 31, 1965
GA-7645	August 1, 1965 to July 31, 1966
GA-8107	August 1, 1966 to July 31, 1967
GA-8787	August 1, 1967 to July 31, 1968
GA-8895	August 1, 1968 through October 31, 1968
GA-9229	November 1, 1968 through January 31, 1969
GA-9359	February 1, 1969 through April 30, 1969
GA-9639	May 1, 1969 through July 31, 1969
GA-9811	August 1, 1969 through October 31, 1969
GA-9838	November 1, 1969 through January 31, 1970
GA-10517	February 1, 1970 through January 31, 1971
GA-10645	February 1, 1971 through April 30, 1971
GA-A10803	May 1, 1971 through July 31, 1971
GA-A10906	August 1, 1971 through October 31, 1971
GA-A12003	November 1, 1971 through January 31, 1972
GA-A12165	February 1, 1972 through April 30, 1972
GA-A12252	May 1, 1972 through July 31, 1972
GA-A12421	August 1, 1972 through October 31, 1972
GA-A12530	November 1, 1972 through January 31, 1973
GA-A12635	February 1, 1973 through April 30, 1973
GA-A12728	May 1, 1973 through July 31, 1973
GA-A12824	August 1, 1973 through October 31, 1973
GA-A12894	November 1, 1973 through January 31, 1974
GA-A13021	February 1, 1974 through April 30, 1974
GA-A13148	May 1, 1974 through July 31, 1974

ABSTRACT

The tasks of the Gas-Cooled Fast Breeder Reactor (GCFR) program that are supported by the U.S. Atomic Energy Commission include: development of GCFR fuel, blanket, and control elements; fuels and materials development; nuclear analysis and reactor physics for GCFR core design; development of the pressure-equalization system for fuel; structural-thermal-flow tests of core assemblies; an in-pile loop facility test program plan; reactor engineering to assess the thermal, hydraulic, and structural performance of the core and core support structure, to evaluate and develop the reactor control-rod, shutdown-rod, and core components locking mechanisms, and to evaluate the capability of PCRV internal structures to serve as postaccident fuel containment; to evaluate the pressure-boundary integrity of the prestressed concrete reactor vessel (PCRV); reactor safety; refueling-system development; component development engineering, in particular, the steam generator, helium circulator, and PCRV; shielding requirements of the GCFR; and fuel-rod engineering to evaluate the steady-state and transient performance of the GCFR fuel and blanket rods.

CONTENTS

Figures

Tables

I. INTRODUCTION

The various tasks of the Gas-Cooled Fast Breeder Reactor (GCFR) program sponsored by the U.S. Atomic Energy Commission are discussed in the following sections of this quarterly progress report.

The GCFR Utility Program, which is supported by a large number of electric utility companies, rural electric cooperatives, and General Atomic Company, is primarily directed toward the development of a GCFR demonstration plant. This utility-sponsored work and the AEC-sponsored work are complementary.

To establish the basis for the design of the GCFR fuel, blanket, and control element assemblies, analytical, experimental, and fabrication development is being done under the core-element development task.

The results of thermal, hydraulic, stress, and distortion analyses of the assemblies and component parts and performance analyses under transient conditions are presented. Current progress on the rod-spacer interaction tests, fuel-element vibration test planning, and the development of fabrication techniques is also presented. The various subtasks of the core-element development and the work accomplished during this reporting period are discussed in Section II.

In the fuels and materials development program, thermal-flux and fast-flux irradiation programs are being conducted to establish conditions and design features specific to GCFR fuel rods, such as vented fuel, fission-product traps, and surface-roughened cladding. In addition, a test program is being conducted of GCFR cladding specimens, both smooth and surface-roughened, to determine materials behavior in an irradiation environment. These fuels and materials tests and analytical studies and the results to date are presented in Section III.

The validation and verification of the nuclear design methods that will be applied to the GCFR core design are the objectives of the nuclear

analysis and reactor physics task. A critical experiments program will be carried out to evaluate the methods developed. The critical assembly design and analysis and methods development are presented in Section IV.

The technology to support the design and construction of the pressure-equalization system for GCFR fuel is being developed. This includes the development of design models and computer codes that will be verified by test programs and testing of materials and seals and developing fabrication processes for the pressure-equalization system, as discussed in Section V.

Program plans for out-of-pile and in-pile tests of GCFR element assemblies are discussed in Sections VI and VII. The out-of-pile heat-transfer and fluid-flow tests are to demonstrate the ability of the GCFR assemblies to meet design goals and to verify analytical predictions that describe design operation and postulated accident behavior.

In the reactor engineering program, analytical methods and models are being evaluated and developed to assess the thermal, hydraulic, and structural performance of the GCFR core and core support; a program to develop the control rods, shutdown rods, and core component locking mechanisms is being carried out; and materials behavior models are being developed to assess the capability of the PCRV internal structures to serve as postaccident fuel containment. The work on these tasks is discussed in Section VIII.

An evaluation of the design of the prestressed concrete reactor vessel (PCRV) pressure-boundary system is being made to determine the integrity of the system, which includes the PCRV liner and thermal and pressure barriers. This program is discussed in Section IX.

The reactor safety task, which is discussed in Section X, is to study the safety aspects of the GCFR using logical probabilistic methods to determine the probabilities associated with accident initiation and progression sequences.

In the development of the GCFR refueling system, an evaluation of the reference design and design verification of the refueling equipment are being conducted. This task includes analysis of system requirements

for spent-fuel cooling and shielding. Program plans for the development and testing of the GCFR refueling system are being developed. This task is discussed in Section XI.

The development of the main components of the GCFR nuclear steam supply system is being carried out under the component engineering task. Initial work on this task is the preparation of development program plans for the steam generator, helium circulator, and PCRV. These are discussed in Section XII.

The verification of the physics and engineering analytical methods and data for the design of the GCFR shields and an evaluation of the effectiveness of various shield configurations are to be conducted under the shielding requirements task. The results of radial shield analyses and the work being done on structural analysis are presented in Section XIII.

Under the fuel-rod engineering task, the steady-state and transient performance of the fuel and blanket rods is being evaluated to determine performance characteristics, operating limits, and design criteria. These studies are presented in Section XIV.

II. CORE ELEMENT DEVELOPMENT (189a No. 13125)

The analytical, experimental, and fabrication development program necessary to establish the basis for the design of the fuel, blanket, and control assemblies is being carried out under this task. Thermal, hydraulic, stress, and distortion analyses of the assemblies and component parts will be performed as well as performance analyses under transient conditions. Rod-spacer interaction tests, fuel-element vibration tests, and development of fabrication techniques are also being carried out as part of this task.

2.1. FUEL- AND CONTROL-ASSEMBLIES DEVELOPMENT

The analytical basis, in conjunction with experimental results, for the design and development of the GCFR fuel and control assemblies will be developed under this subtask. Because complete prototype in-pile tests will not be conducted, a strong analytical base, supported by development tests, is required to design the core assemblies. The current emphasis is to develop an adequate transient analysis capability and to perform both thermal-hydrodynamic and structural transient analyses, which will provide a basis for the assembly design criteria and for specific test requirements. A further objective during FY-75 is to complete the development program plan for the assemblies. Although some transient analyses have been performed previously, and some of the analyses to be performed are extensions of the previous work, much of the work for the current year will be based on newly developed methods; therefore, the completion of the analytical work during FY-75 is dependent on the adequacy of those methods. Thus, it is assumed that adequate methods will be successfully developed for the analyses and that for the future, the appropriate experimental results will be available.

During the previous reporting period, the fuel- and control-assemblies development work was centered on determining the deflections of the rod

spacers and the duct. The structural analyses were performed under subcontract to Battelle Pacific Northwest Laboratories (PNL), and spacer deflections and duct dilations were calculated with the finite-element models constructed. The COBRA thermal analysis code was also modified by PNL for application of the code to the flow of helium in the GCFR core.

During this reporting period, the modified COBRA code was made operational on the GA computer and was evaluated. The evaluation will be extended to include transient problems. The development of a new thermal analysis code, FLOMAX, was initiated during this period, and the solution method of FLOMAX is described in detail. Further analysis of the assembly duct dilation problem was performed at GA during this period. The dilation was calculated with an exact viscoelastic creep solution, which compares well with the PNL finite-element solutions.

2.1.1. COBRA-IV Evaluation and Development

The COBRA-IV computer code for the thermal and hydraulic performance of fuel-rod arrays was received from PNL and made operational on the GA computer. The GA version of COBRA-IV was designed specifically for use with helium as the coolant and contains all but the transient computational procedures from the PNL general version of COBRA-IV. The transient computational procedures are those from the older COBRA-III-C code.

To evaluate the computational performance of COBRA-IV, the code was applied to the existing model of the rod bundle, which is shown in Fig. 2.1. The model represents an experimental fuel assembly for in-pile testing of GCFR fuel rods in the BR-2 helium loop at Mol, Belgium. To model the assembly in Fig. 2.1 with COBRA-IV requires iteration on the inlet conditions to satisfy a two-point boundary-value problem. To determine the convergence of the COBRA-IV solutions with the number of iterations, a numerical experiment was conducted with the above model. The steady-state, relative outlet temperatures of the subchannels as functions of the number of iterations are plotted in Fig. 2.2. It can be seen that approximately fifteen iterations are sufficient for the convergence of the problem. The number of iterations required for the solution of a problem is important in limiting the computational cost of the problem. This is illustrated in Fig. 2.3 where the number of iterations are related to the

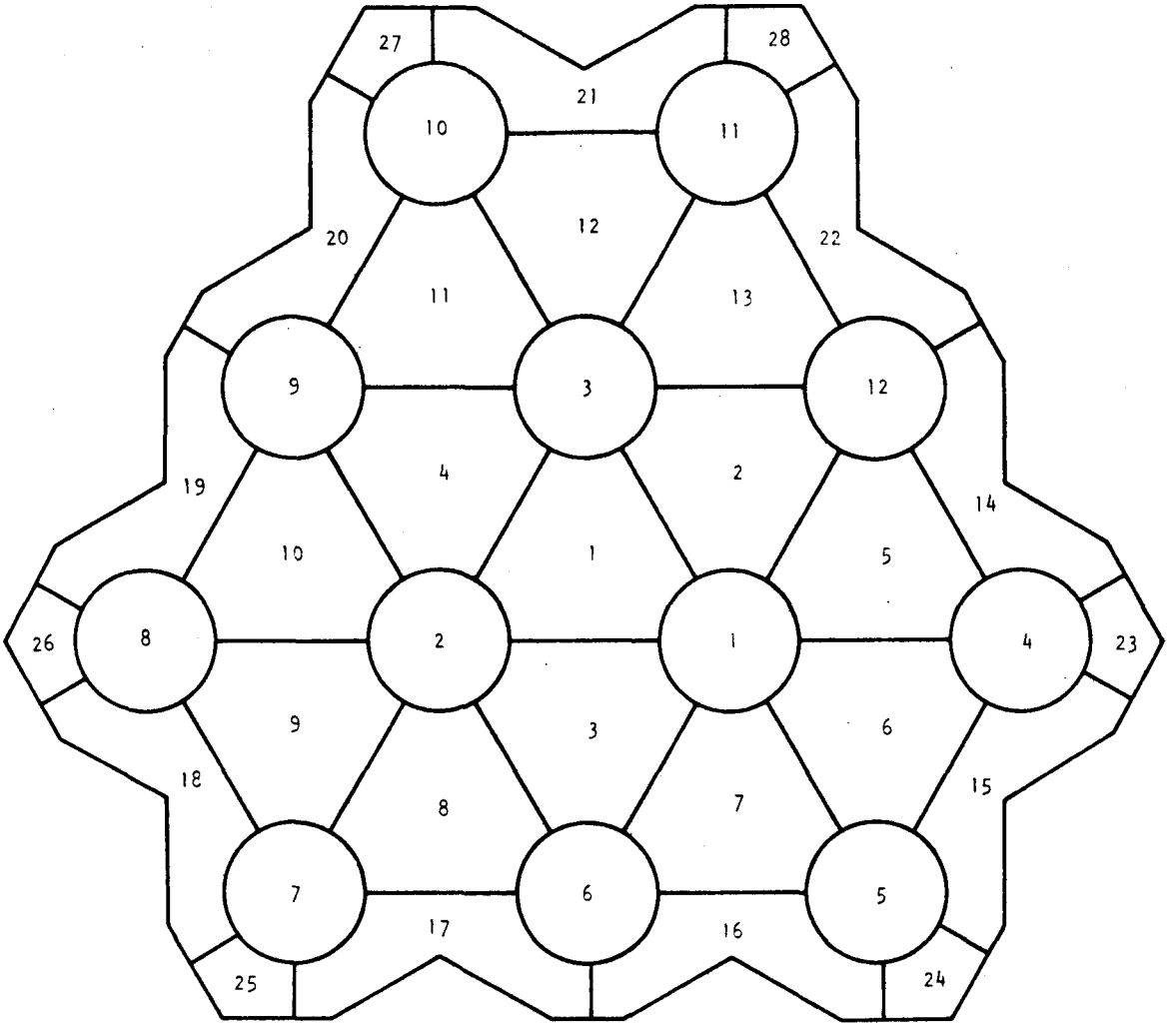

Fig. 2.1 Subchannel layout of an experimental fuel assembly (not to scale)

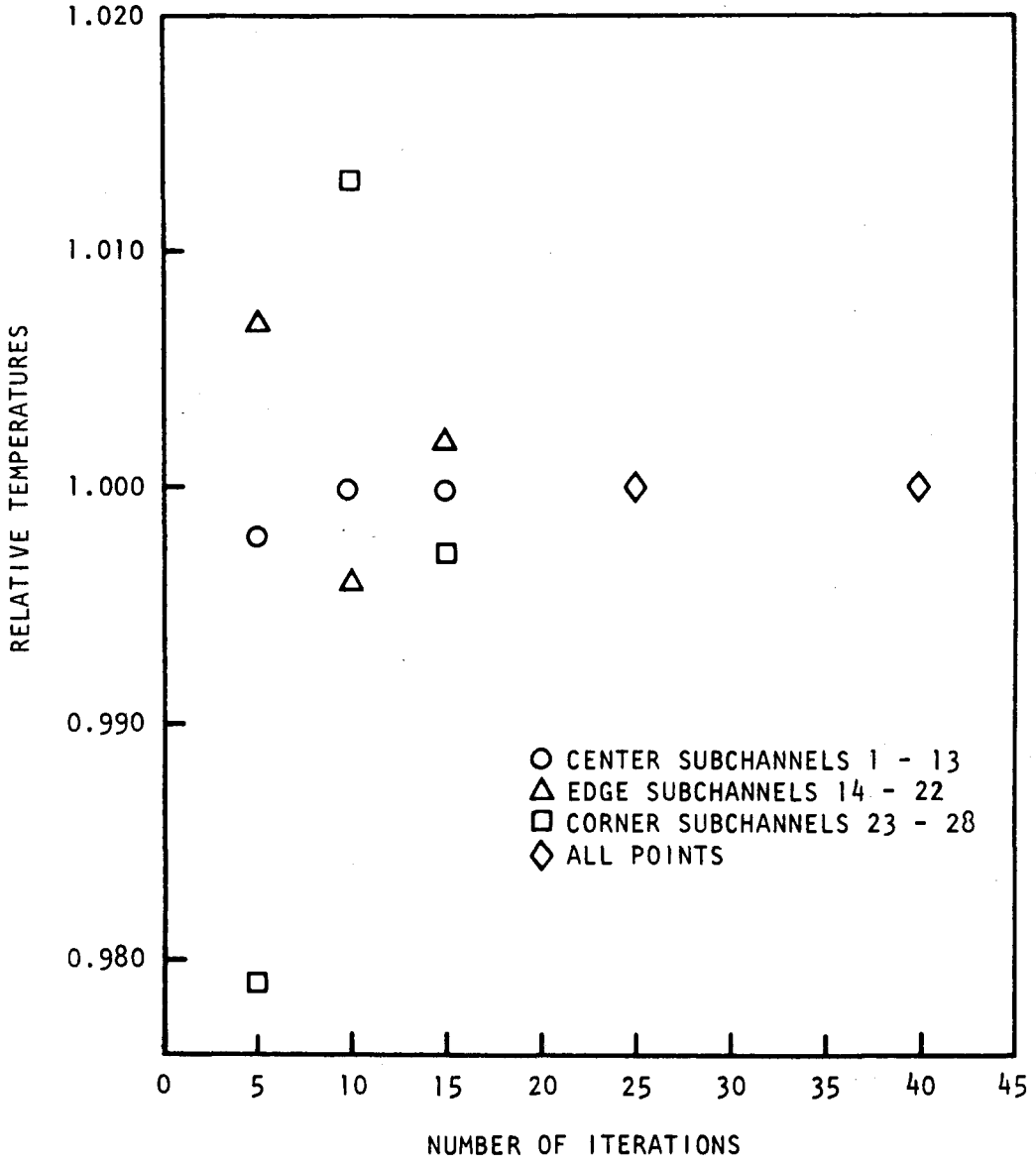

Fig. 2.2 Subchannel temperatures relative to temperatures after 40 iterations

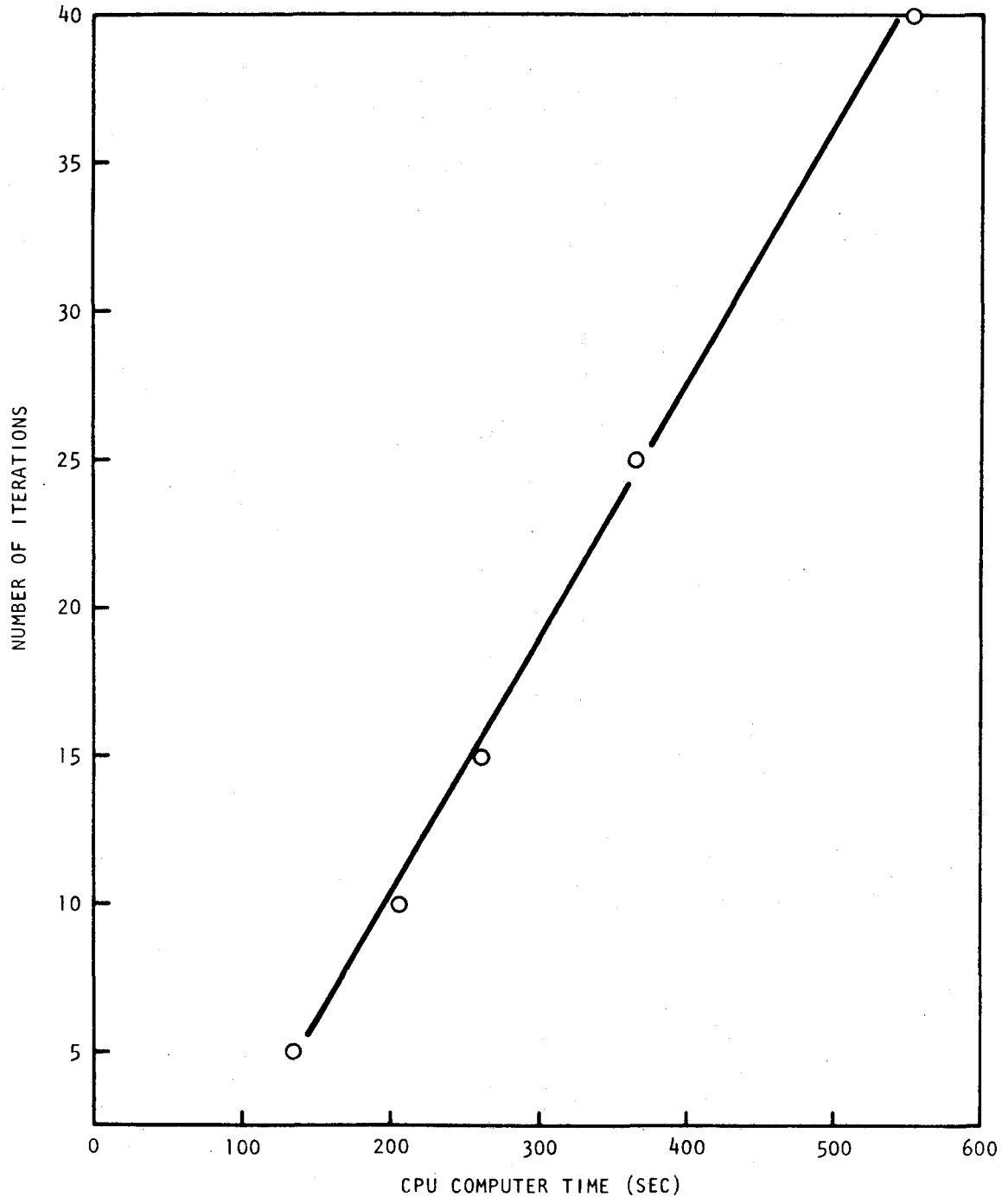

Fig. 2.3 Number of COBRA IV iterations as a function of CPU computer time

execution time on the UNIVAC-1108. Future problems will be limited to fifteen iterations. This is especially important for larger models than the one used in this study because the CPU time per iteration will be larger. Presently, the model shown in Fig. 2.1 is being employed to evaluate the capability of COBRA-IV for transient problems.

The thermal analysis of the fuel assembly was initiated by the modeling of a one-sixth sector of the fuel assembly with COBRA-IV. The model, which is shown in Fig. 2.4, will be used for the initial thermal analysis and for evaluating the computational effectiveness of COBRA-IV for a relatively large problem. Both steady-state and transient analyses are planned. At present, the model is being prepared for computer execution.

2.1.2. Development of the FLOMAX Thermal-analysis Code

The GCFR fuel and blanket assemblies contain a large number of fuel rods and hence a large number of subchannels for heat removal in the assemblies. To account for effects such as power gradients across the assemblies, it is desirable to model the flow and temperature distributions in the complete assemblies, but this cannot be done with the present computers and finite-difference computational methods. Furthermore, finite-difference computations with significant segments of the assemblies will be very costly, especially for transient calculations. Therefore, the development of a new code, FLOMAX, was initiated with the aim to provide a cost-effective analytical tool for the steady-state and transient thermal analysis of the fuel assemblies, with possible extension to analysis of the blanket assemblies.

Presently all rod-bundle thermal-analysis codes use finite-difference computational schemes, which have been found too costly for calculations with large rod bundles. The FLOMAX code will be based on flow analysis by matched asymptotic expansion, as outlined in Ref. 1.* In this method, the governing equations are scaled by the geometry and boundary conditions of the physical problem (i.e., the fuel and blanket assemblies) so that all terms in the equations become dimensionless and are multiplied by parameters of various orders of smallness. To solve the scaled equations,

*References are listed at the end of each section.

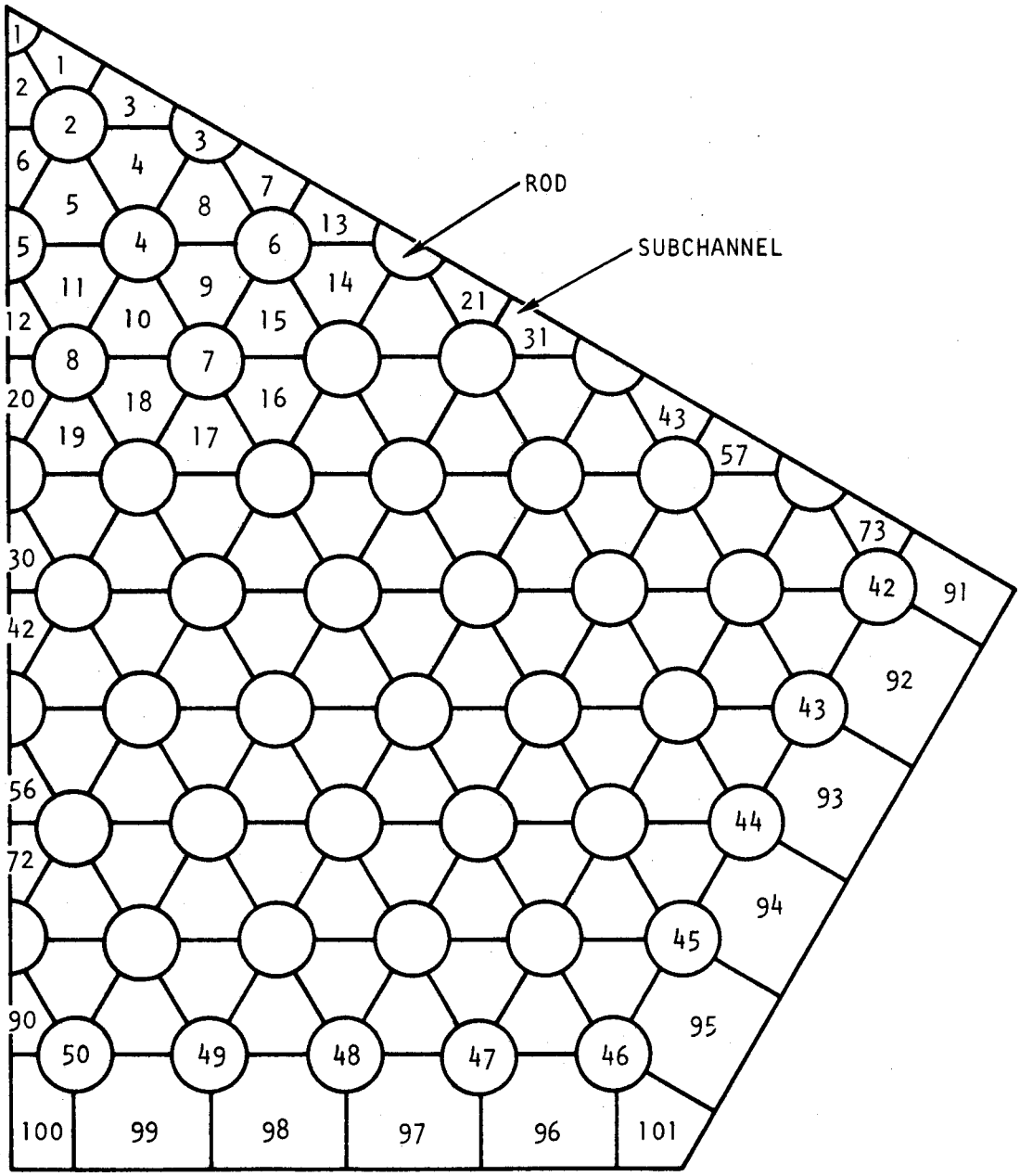

Fig. 2.4 Model for large problem evaluation, 1/6 section of the GCFR fuel assembly (not to scale)

the terms multiplied by small parameters are neglected and a basic lowest-order solution is obtained from the most important terms. Then the lesser-important terms are reintroduced as perturbations to the basic solution, and the higher-order solutions are matched asymptotically to the basic solution. The advantages of this method are that the most important effects are considered first and that higher-order effects can be treated analytically (as opposed to numerically) with linear equations.

The development of FLOMAX was initiated by a study of the equations of motion and of energy transport which govern the compressible turbulent flow of gases. The flows in the GCFR rod bundles are (mildly) compressible or expandable, because of density changes due to heat addition and not because the velocities approach the speed of sound. Based on the time-averaging method of Laufer,[2] the following governing equations were derived:

$$\frac{\partial \rho}{\partial t} + \frac{\partial}{\partial x_k}(\rho u_k) = 0 \quad , \tag{2.1}$$

$$\rho\left(\frac{\partial u_i}{\partial t} + u_k \frac{\partial u_i}{\partial x_k}\right) = -\frac{\partial p}{\partial x_i} + \frac{\partial \tau_{ik}}{\partial x_k} + \rho g_i \quad , \tag{2.2}$$

$$\rho C_p\left(\frac{\partial T}{\partial t} + u_k \frac{\partial T}{\partial x_k}\right) = -\frac{\partial q_k}{\partial x_k} \quad , \tag{2.3}$$

$$p = \rho R T \quad , \tag{2.4}$$

where the repeated subscript implies summation over the coordinate directions, where the (deviatoric) stress, τ_{ik}, is the sum of the laminar and Reynolds stresses, i.e.,

$$\tau_{ik} \equiv \tau^{\ell}_{ik} + \overline{\rho u_i' u_k'} \quad ,$$

and where the heat flux, q_k, is the sum of the fluxes due to molecular conduction and turbulent transport, i.e.,

$$q_k \equiv q^{c}_k + \overline{\rho T' u_k'}$$

Equations (2.1) through (2.3) express the laws of conservation of mass, momentum, and energy and Eq. (2.4) is the equation of state. To apply these equations to the flow in rod bundles, they must be discretized in the transverse coordinates to form a large system of differential equations in time and in the axial coordinate; to use matched asymptotic expansions, they must be scaled as described above. In Ref. 1, discretized equations were derived directly from an integral analysis, and then the equations were scaled. A comparison between asymptotic and finite-difference solutions of a simple two-channel problem is shown in Fig. 2.5. It is preferable, however, to start with the complete field equations, Eqs. (2.1) through (2.4), and then introduce the necessary simplifications to obtain a solution for the given problem. In this way, the effect of neglecting various terms becomes clear. During this reporting period, Eqs.(2.1) through (2.4) were scaled to the GCFR assembly geometries and the general method of solution was determined. Presently, the scaled field equations are being discretized to form the governing subchannel equations.

The FLOMAX boundary-value problem is to solve Eqs. (2.1) through (2.4) subject to the boundary conditions of the fuel assemblies. A schematic of the fuel assembly is shown in Fig. 2.6. The flow and temperature fields in the rod bundle must be distributed such that, for all subchannels, the pressures and temperatures equal p_{in} and T_{in} at $x_1 = 0$, and the pressures equal p_{out} at $x_1 = L$. With Eqs. (2.1) through (2.4), and given the amount of heat added to the fluid, this is a well-defined boundary-value problem. It is elliptic in character because the downstream boundary conditions ($p(L, x_2, x_3, t) = p_{out}(t)$) affect the flow distribution. With matched asymptotic expansions, it is required that the higher-order approximations approach the basic solution smoothly and asymptotically far from the inlet. However, the presence of the grid-type spacers causes nonsmooth, abrupt changes in the flow field, so the asymptotic method must be applied between the spacers (over length ℓ_j in Fig. 2.6), and the solutions for each axial segment ℓ_j must be matched by point collocation. For this reason, the dimensionless x_1-coordinate was defined by

$$x_1' = (x_1 - a_j)/\ell_j \quad .$$

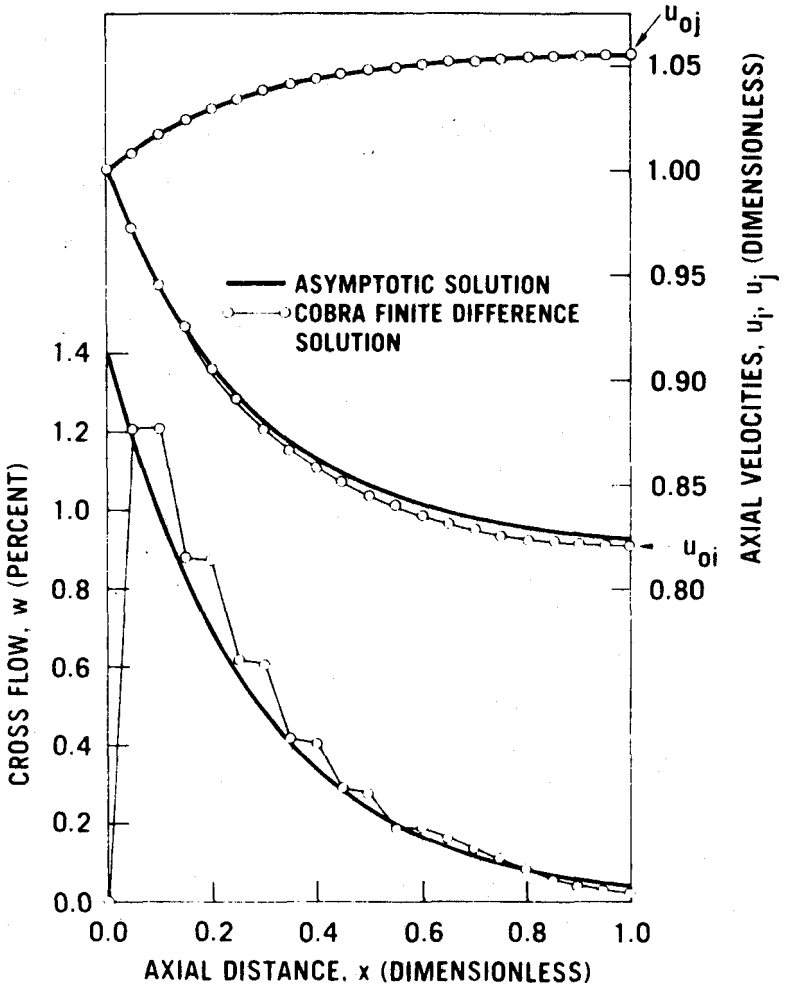

Fig. 2.5 Comparison of asymptotic and finite-difference solutions of a two-channel initial-value problem

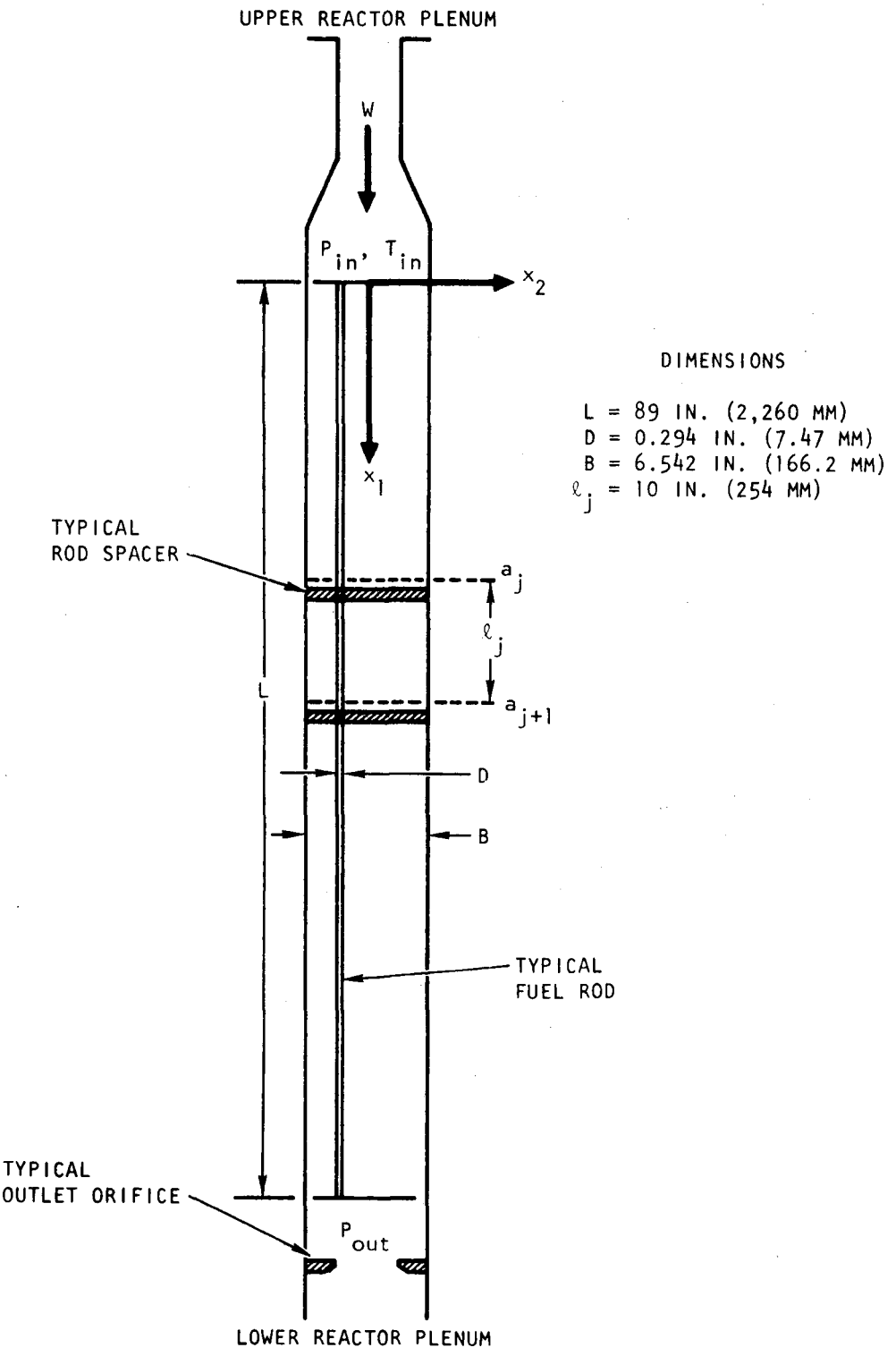

Fig. 2.6 Schematic elevation view of a fuel element

The characteristic transverse dimension is d, approximately equal to the rod diameter, so the dimensionless transverse coordinates are

$$x_2' = x_2/d \qquad \text{and} \qquad x_3' = x_3/d \quad ,$$

and the ratio of the two length scales is

$$\epsilon \equiv d/\ell_j \quad .$$

When two length scales of a problem are very different so that ϵ is small, it is usually possible to use singular perturbation theory and matched asymptotic expansions to obtain a solution to the equations. Based on current designs, a preliminary evaluation showed the following magnitudes for ϵ:

	300 MW(e) GCFR
Fuel assembly	0.037
Blanket assembly	0.116

In all cases, ϵ is a small number, so in the scaled equations the terms multiplied by ϵ will be kept, but the terms multiplied by ϵ^2 or ϵ^3 will be neglected. That is, effects on the order of magnitude of 1% or less will not be considered. The most important effect of neglecting the ϵ^2 terms is that the axial momentum equation, the first of Eqs. (2.2), is changed from an elliptic differential equation to a parabolic differential equation. With the full elliptic equations, the flow disturbances, say due to a spacer, are felt both upstream and downstream of the spacer. With the approximate parabolic equations, disturbances can propagate only downstream. For this reason, the spacer is included at the upstream end of the computational cell represented by ℓ_j in Fig. 2.6. Changes occurring a short distance upstream of the spacer are considered lumped with the spacer. All present rod-bundle codes solve parabolic equations, although this has not been obvious because the equations solved by the codes were not derived from the fundamental field equations.

Similarly, as characteristic length scales were identified to scale the independent coordinate variables, so characteristic scales of velocity,

U, temperature, ΔT, density, ρ_{aj}, pressure, Δp, and stress were identified to scale the dependent variables. Introduction of the scaled variables into Eqs. (2.1) through (2.4) resulted in the following scaled, dimensionless equations:

$$\delta\left(\frac{\partial \rho'}{\partial t'} + \rho' \frac{d\rho_{aj}}{\rho_{aj} dt'}\right) + \frac{\partial}{\partial x_k'}(\rho' u_k') = 0 \quad , \tag{2.5}$$

$$\varepsilon\rho'\left\{\delta\left(\frac{\partial u_1'}{\partial t'} + u_1' \frac{dU}{U dt'}\right) + u_k' \frac{\partial u_1'}{\partial x_k'}\right\} = -\zeta_1 \frac{\partial p'}{\partial x_1'} + \zeta_2\left(\frac{\partial \tau_{12}'}{\partial x_2'} + \frac{\partial \tau_{13}'}{\partial x_3'}\right) + \zeta_3 \rho' \quad , \tag{2.6}$$

$$\varepsilon^3\rho'\left\{\delta\left(\frac{\partial u_2'}{\partial t'} + u_2' \frac{dU}{U dt'}\right) + u_k' \frac{\partial u_2'}{\partial x_k'}\right\} = -\zeta_1 \frac{\partial p'}{\partial x_2'} + \varepsilon^3 \zeta_4\left(\frac{\partial \tau_{22}'}{\partial x_2'} + \frac{\partial \tau_{23}'}{\partial x_3'}\right) \quad , \tag{2.7}$$

$$\delta\rho'\left(\frac{\partial T'}{\partial t'} + T' \frac{d\Delta T}{\Delta T dt'} + \frac{dT_{aj}}{\Delta T dt'}\right) + \rho' u_k' \frac{\partial T'}{\partial x_k'} = -\zeta_5\left(\frac{\partial q_2'}{\partial x_2'} + \frac{\partial q_3'}{\partial x_3'}\right) \quad , \tag{2.8}$$

$$\rho' = \frac{1 + \gamma p'}{1 + \alpha T'} \quad , \tag{2.9}$$

where the primes denote the scaled variables, where ζ_1 to ζ_5 are dimensionless constants, and where ε, δ, γ, and α are perturbation parameters. In Eqs. (2.5) through (2.8) the time was scaled by the characteristic time θ: $t' = t/\theta$.

Several important conclusions were reached from Eqs. (2.5) through (2.9). First, all the transient, or unsteady, terms are multiplied by the parameter δ, which is the ratio of two time scales: $\delta \equiv t_0/\theta$, where t_0 is the transit time between spacers of a fluid particle ($t_0 = \ell_j/U$). With gas-cooled rod bundles, a high axial velocity is required so that the transient time of a particle of fluid, t_0, will generally be very small compared to the smallest time constant of the boundary conditions, θ. In this case, the unsteady terms can be neglected, and a transient problem would be solved as a quasi-steady problem. The δ parameter will be evaluated below. Second, all terms in Eq. (2.7), the transverse momentum equation (in the x_2 direction), are multiplied by ε^3, except the pressure

gradient; thus, the transverse pressure gradient is of the order of magnitude of $\varepsilon^3/\zeta_1 \approx \varepsilon^2$, which is negligible. The implication of this is that the pressures in the subchannels will be nearly equal at any axial position, except in the immediate vicinity of a spacer; this simplifies the solution of the problem. Third, the equation of state, Eq. (2.9) contains two small parameters, $\gamma = \Delta p/p_{aj}$ and $\alpha = \Delta T/T_{aj}$. If these are neglected in the lowest-order solution, then $\rho' = 1$ and the basic solution is the incompressible-flow solution. Thus, the method of solution becomes the construction of a basic incompressible-flow solution, which is then augmented by perturbations due to density changes and flow accelerations at the spacers. To solve transient problems it is still necessary to add the fuel-rod conduction equation to the above system of equations.

A rapid transient condition to be analyzed is the flow reduction following a reactor trip. In this case, the heat generation of the rods changes most rapidly, but, because of the thermal capacitance of the rods, the heat flux, $q_k(t)$, changes only slowly. Therefore, the time constant, θ, should be evaluated from the rate of flow reduction, such as that shown in Fig. 2.7. Another transient condition is the depressurization accident; but, it occurs on a time scale of minutes, which is slow compared to the flow change in Fig. 2.7. If the reduction in reactor flow, F, were an exponential decay ($F = \exp(-t/\theta) \times 100\%$), then the time constant would be given by $\theta = -F/(dF/dt)$. Using this definition of θ, and assuming that the characteristic velocity, U, is proportional to the reactor flow, F, the δ parameter is evaluated as

$$\delta = -\frac{\ell_j/U}{F/(dF/dt)} = \frac{\ell_j\,|dF/dt|}{U(0)F^2} \times 100\% \quad .$$

This parameter is plotted in Fig. 2.8 for the case of the average first-row blanket assemblies ($\bar{U}(0) = 92.5$ ft/sec). As can be seen, δ is a small number for all times. In the case of orificed fuel assemblies with minimum flow ($U_{min}(0) = 204$ ft/sec) and the unorificed fuel assemblies ($U_{max}(0) = 285$ ft/sec), the peak δ values are 0.032 and 0.023, respectively, which are even smaller numbers. Accordingly, it is only necessary to keep terms of order δ; the terms of order $\varepsilon\delta$, etc., can be discarded.

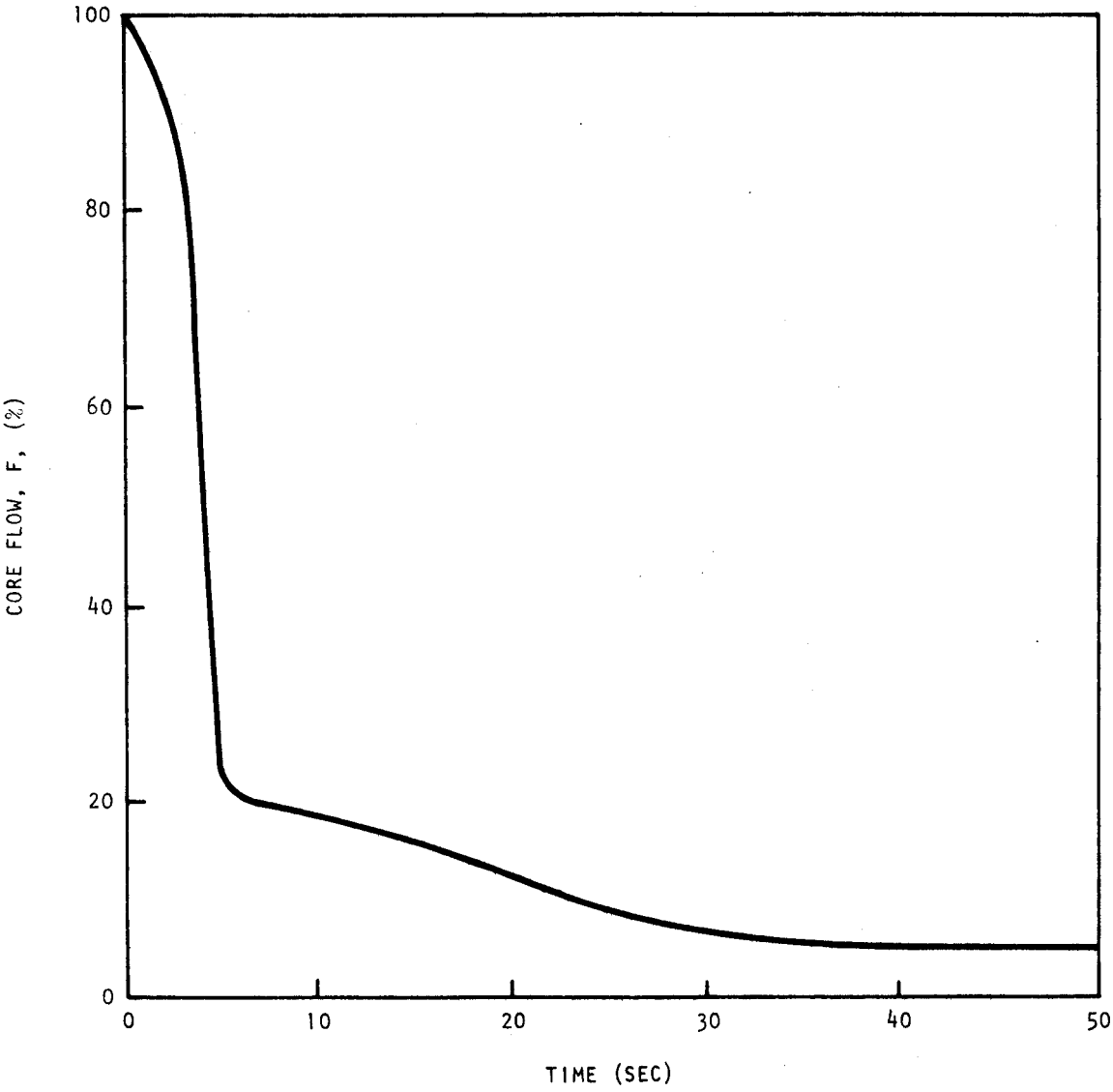

Fig. 2.7 Core flow following reactor trip

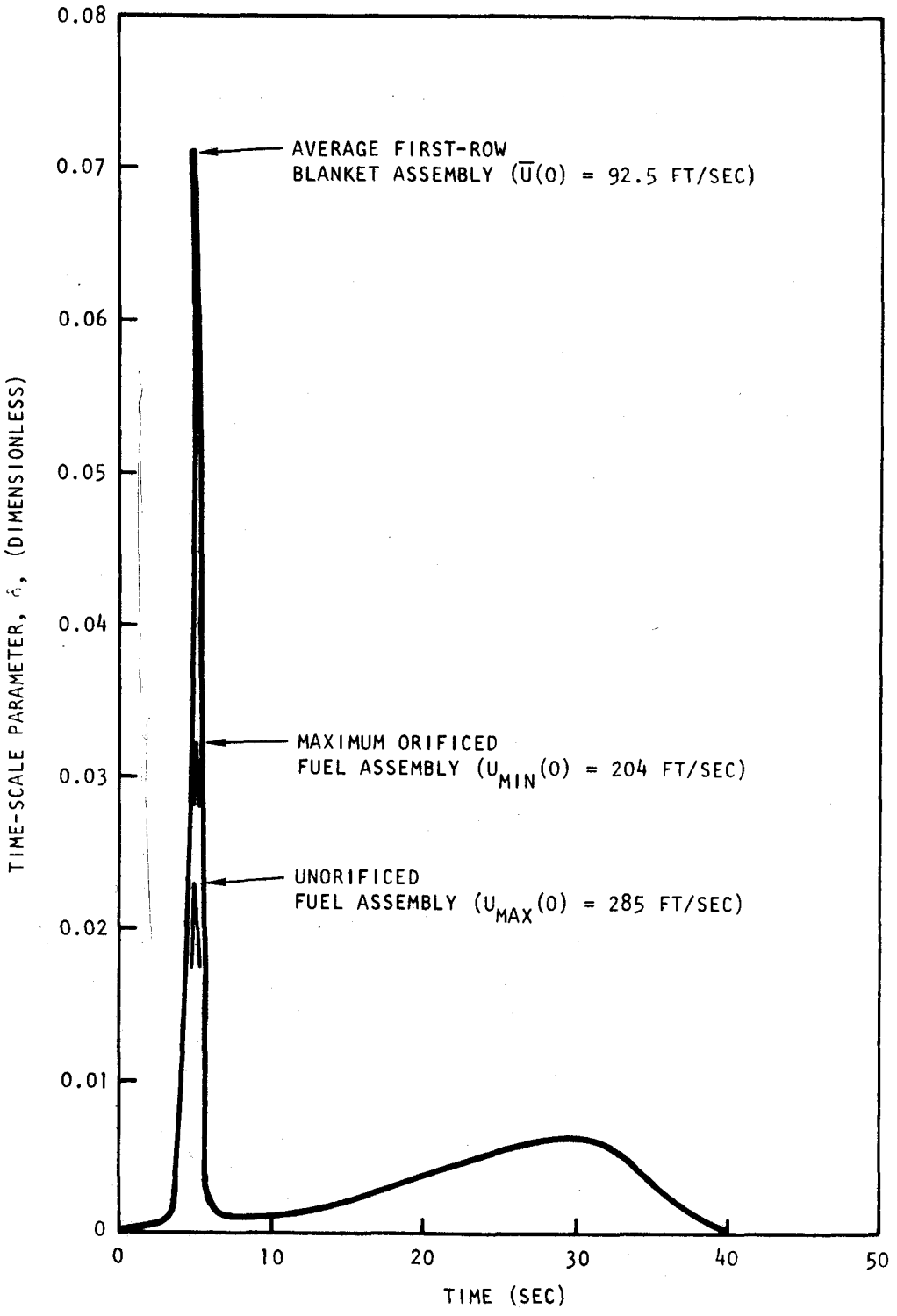

Fig. 2.8 Evaluation of the time scale parameter

The narrowness of the curve for maximum δ suggests that the unsteady terms be neglected completely, without significant error; but, this requires further analysis.

As discussed above, the fuel assembly flow problem is elliptic, since the outlet pressures must all equal P_{out} (see Fig. 2.6). This condition will be met iteratively, as is done by COBRA-IV. Since the equations to be solved are parabolic, they can be solved completely in each cell j, given the inlet conditions of the cell. These considerations led to the flow diagram in Fig. 2.9, which indicates the solution method adopted for FLOMAX. Except for the first cell, the inlet conditions are known from the outlet conditions of the previous cell, as shown by the flow chart. Inlet velocities will be adjusted iteratively to obtain equal outlet pressures.

Presently Eqs. (2.5) through (2.9) are being discretized in the transverse coordinates to form the subchannel equations of FLOMAX. A turbulent mixing model will be selected from correlations in the literature, then the equations will be solved by matched asymptotic expansions. For transient analysis, a conduction model of the fuel rods will be constructed.

2.1.3. Structural Analysis of Fuel Assembly Components

Various finite-element analyses on the fuel-rod spacer grid and the fuel assembly duct were performed by Battelle Pacific Northwest Laboratories (PNL) in FY-74 in three general areas: (1) transverse and axial spacer-grid deflection, (2) spacer-grid hanger buckling, and (3) dilation-distortion of the assembly duct.[3] From these studies it is concluded that there is no major structural problem with the spacer-grid design provided the rods and the spacers do not seize. If seizure occurs, especially near a support point, serious consequences would be expected. A further analysis of this event will be necessary. The following is a summary of the results obtained.

2.1.3.1. Summary of FY-74 PNL Analyses.

1. Spacer-grid Deflection. A quarter segment of the EDM spacer was modeled to investigate the transverse deflection. Each cell was acted upon by a 1-lb axial load simulating differential expansion of the fuel

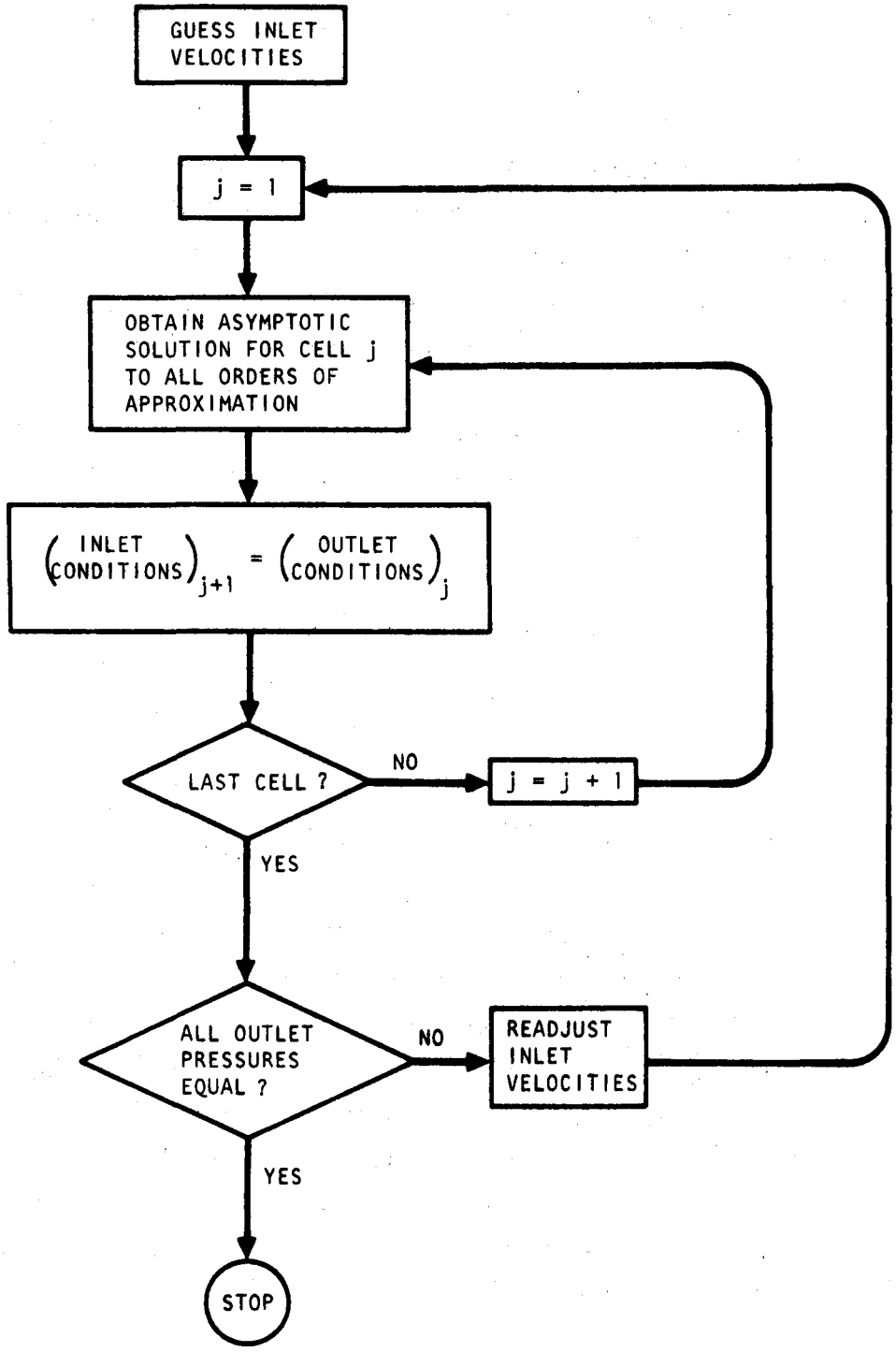

Fig. 2.9 Flow chart of the general computational scheme of FLOMAX for steady-state problems

rods and the spacers. Maximum bending stresses obtained were 4400 psi. The distortions were less than 0.002 in. By incrementally increasing the load, an investigation of peak stress versus displacement was made. For displacements less than 0.025 in., neither buckling nor plastic failure will occur. Assuming an initial design clearance between the fuel rod and the spacer, a limiting load of 20 lb per rod, which yields a peak deflection of 0.030 in., will cause possible locking contact. This is well above any anticipated transverse load.

Lateral spacer distortions were also investigated with a one-half spacer-grid segment (a corner-to-corner model). The loading scheme was a 1-lb load per rod parallel to the longest boundary. Boundary conditions included two adjacent flats fixed and one flat fixed with one displaced 0.005 in. to simulate design clearance closure. Also uniform temperature gradients in both coordinate directions were considered. The results indicated a maximum overall spacer-grid distortion of 0.011 in. and maximum cell distortion of 0.001 in. Localized bending stresses approached 13,000 psi, but the maximum membrane stress, as well as the bending stress for all other elements, were near 2000 psi.

A detailed analysis of an individual cell of the EDM spacer-lattice was also performed. Loading was again a 1-lb lateral load. Peak displacements were 0.6×10^{-4} in. The cell wall stresses of 2400 psi were computed, whereas dimple stresses were 4000 psi or less. Irradiation creep increased the deflection after 18,000 hr to 1.254×10^{-4} in. In all cases, the computed distortion was well within design tolerances.

2. Spacer-grid Hanger. The hanger for the spacer grid was analyzed for the case of transient loading by differential thermal expansion with respect to possible buckling. Various adaptations of the elastic buckling formula were used to obtain allowable loads and stresses. A total of 2-1/2 hr of transients during the 18,000-hr life were considered during which irradiation creep could act. Considering only the fluted section, a maximum load of 114 lb was computed, yielding stresses of 6000 psi. When combined with the flat section, this was reduced to 101 lb, resulting in a stress of 11,200 psi in the nonfluted section.

An additional investigation was made to assess the effect of a 0.035-in. vertical movement of the spacer grid. Axial inelastic buckling deflections of the hanger approached 0.180 in. Consequently, such a spacer movement would result in an unacceptable interaction among the hanger, the fuel rods, and the assembly duct. This area will require further study if such displacements are considered realistic.

3. Assembly-duct Dilation. In this analysis the dilation behavior of the assembly duct was determined using finite-element models. Only elastic and irradiation creep response was considered. For core conditions 5.5 in. below the core centerline and wall thicknesses of 0.100, 0.125, and 0.150 in., outward radial deflections of 0.122, 0.078, and 0.044 in., respectively, after 18,000 hr were computed for elastic and irradiation-induced creep. The irradiation-induced swelling for these conditions ($\phi = 3.66 \times 10^{15}$ n/cm^2/sec, E > 0.1 MeV) is 0.146 in. radially. Conditions 10 in. axially above and below this point were used to investigate the contributions of pressure, temperature, and flux on wall creep distortion. The pressure effect was the most pronounced (4.5 in. above the core centerline), yielding a 0.115-in. radial displacement after 18,000 hr for a 0.125-in.-thick wall. The swelling dilation there is 0.011 in. ($\phi = 3.66 \times 10^{15}$ n/cm^2/sec, E > 0.1 MeV). This indicates that the maximum irradiation-induced creep deflections occur above the core centerline where thermal effects due to flow bypass from the nonuniform creep distortions are less significant. Although the model used is a reasonable approximation for elastic wall behavior, serious uncertainties exist in the irradiation-induced creep and swelling correlations. The resultant swelling is in excess of one-half of the interelement gap (0.250 in.) in the reference design. This may require modification of the gap spacing when the creep and swelling correlations uncertainties are resolved. An alternative from which the GCFR might benefit is the introduction of a nonswelling duct material.

In general, the study proved the design adequacy of the EDM type of spacer grid. The fabricated grid, if chosen, would require an analysis of the type performed for the EDM grid. It would, however, be a more uncertain analysis because of the nature of the fabricated grid. A high

confidence could also be placed in the hanger analysis. However, conclusions relevant to the design adequacy are difficult since little is known about the loading mechanisms or magnitude. The analysis has succeeded in establishing upper bounds but not in ranking the design with respect to the bounds. Additional effort along these lines is required. Further effort is also required in the duct dilation analysis to determine the core conditions for the maximum distortion. Also, a distortion map of the core cross section at several axial positions must be constructed to assess element clearance reduction and possible interference. These analyses will include irradiation-induced creep and swelling. The results obtained thus far indicate some duct redesign may be required to reduce the dilation and prevent element interference.

2.1.3.2. Spacer-grid Deflection. One item of analysis by PNL was carried over to FY-75 and was completed. This was a further investigation of the lateral deflection of the spacer grid using a flat-to-flat model and loading scheme. This analysis, in conjunction with the peak-to-peak analysis previously performed, was intended to identify differences in the deflection caused by orientation of the spacer grid.

The analytical model consisted of a flat-to-flat one-half spacer-grid segment composed of 310 nodes and 440 elements. The nodal points along the lower boundary were allowed to translate only along the abscissa in Fig. 2.10. Nodes 306 through 310 were fixed horizontally but were allowed to translate vertically. The slanting boundary defined by nodes 165, 185, 203, 293, and 305 were rotated to allow translation parallel to the surface and to be fixed perpendicular to the surface. The loading conditions were restricted to a uniform temperature condition with a 1.0 lb/rod force in the X direction. The boundary displacement conditions were established to simulate the reaction of one side of the duct wall on the adjacent grid boundary due to a transverse fuel-rod load.

The distorted geometry is shown in Fig. 2.11. Because of the limitations of the ANSYS code, the rotated geometry causes the distorted positions of nodes 165, 185, 203, 221, 293, and 305 to be plotted incorrectly. The computation is done correctly, but the results are not transformed into the correct coordinates for the plotter. The maximum displacement

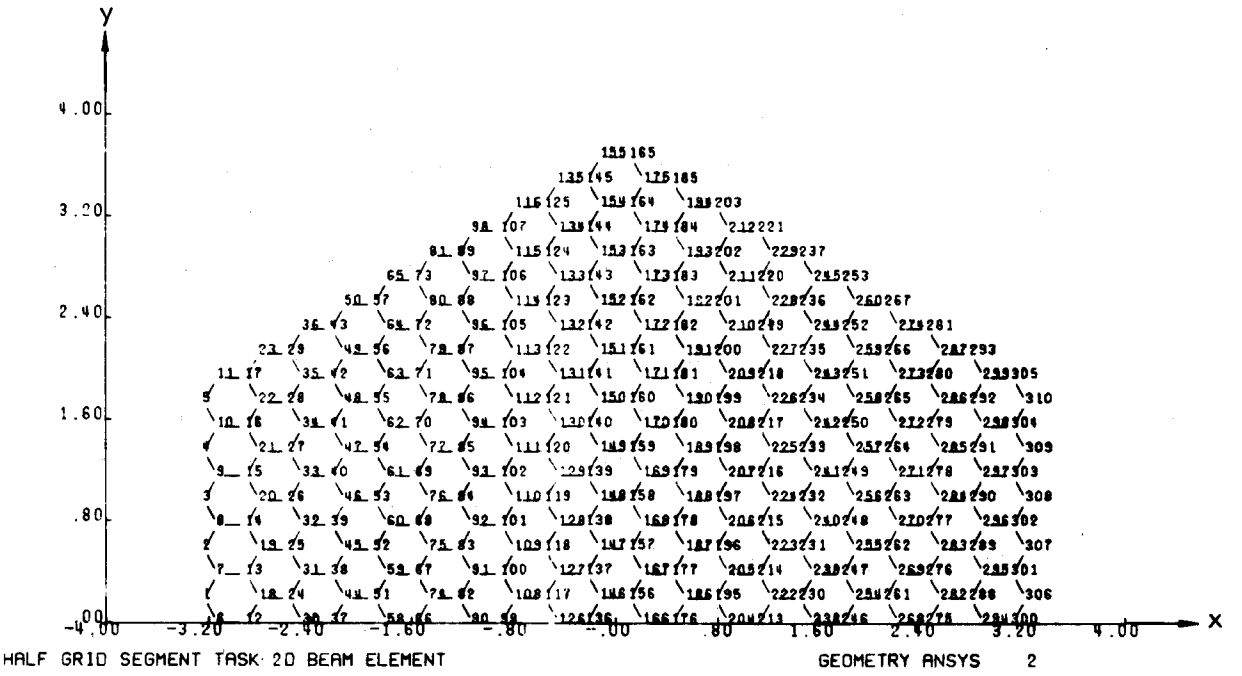

Fig. 2.10 Flat-to-flat spacer-grid model (loads are applied in the positive x direction and are adjusted to simulate a 1 lb/rod load)

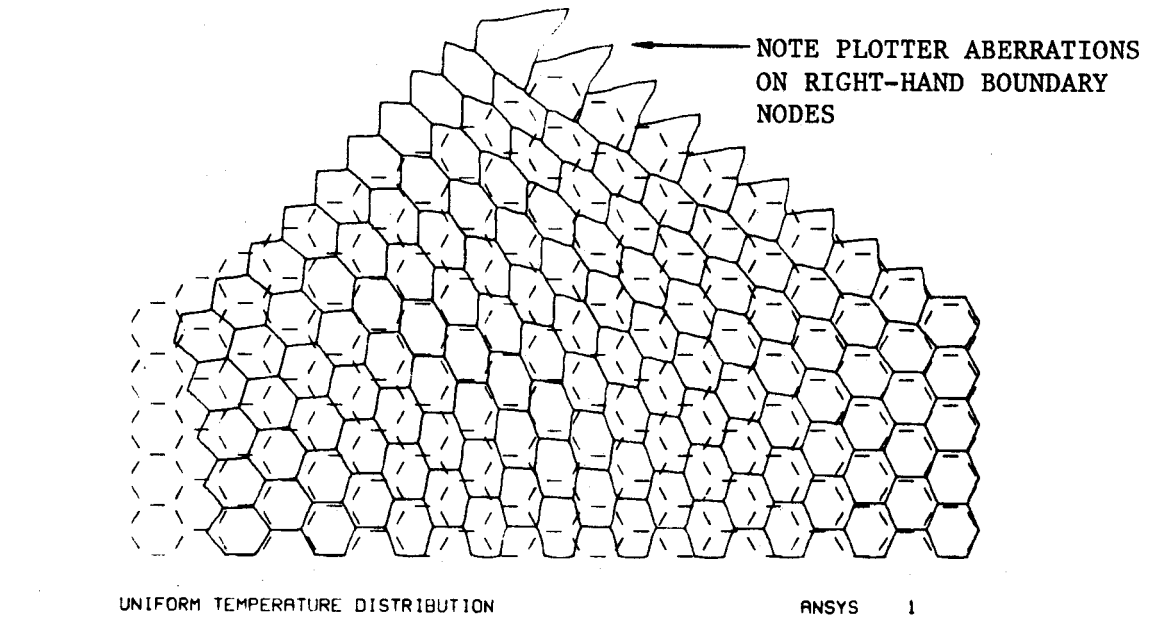

Fig. 2.11 Distortion plot of the geometry shown in Fig. 2.10 (distortions in the y direction are limited to zero on the abscissa; the right boundary is fixed)

is shown by node 1 to be 0.0105 in. The maximum individual cell distortion occurs around elements 146 to 155 and is ∿0.002 in. The bending stresses are at a maximum of 27,000 psi around node 225. The associated direct, or axial, stress was only -527 psi. The magnitude of the bending stress decreases down to 15,000 psi around node 160, whereas the direct stress changed to -973 psi. The decrease in bending stresses appears to be quite similar in all radial directions from node 225.

2.1.3.3. Assembly Duct Dilation. Numerous duct dilation calculations will have to be performed for the GCFR assemblies. Therefore, an analytical viscoelastic dilation model was developed that will reduce the cost of these calculations considerably. The dilation of the duct under internal pressure is due almost entirely to irradiation creep of the duct material. In terms of fast flux ($\phi = 0.588\ \bar{\phi}$, E > 0.1 MeV), and with a mean neutron energy of $\bar{E} = 0.455$ MeV, the irradiation-creep correlation (from the LMFBR Handbook, HEDL-TME-71-32) was written as follows:

$$J \equiv \frac{\varepsilon}{\sigma} = 1.316 \times 10^{-23}\phi[1 - \exp(-\phi t/2.56 \times 10^{20})] + 5.8 \times 10^{-30}\phi t \quad , \qquad (2.11)$$

where ε = strain (in./in.),

σ = stress (psi),

ϕ = fast flux (n/cm^2-sec),

t = time (sec).

Equation (2.11) is the same creep correlation used by PNL in the numerical dilation calculations. The variable J in the above equation is the creep compliance function as defined by Flügge[4] in the theory of linear viscoelasticity. Equation (2.11) is applicable to the linear theory because the stress and the strain are proportional, although the proportionality factor changes with time or fluence.

Application of the linear theory also requires a geometrically linear dilation model, such as the model in Fig. 2.12(a). The complete dilation problem is represented by Fig. 2.12(b) where symmetry dictates that the duct has zero rotation at the corners and at the centerline of the flats. Considering the outward deflection of the corner to be small, the right end of the symmetry sector was fixed, giving the beam deflection problem

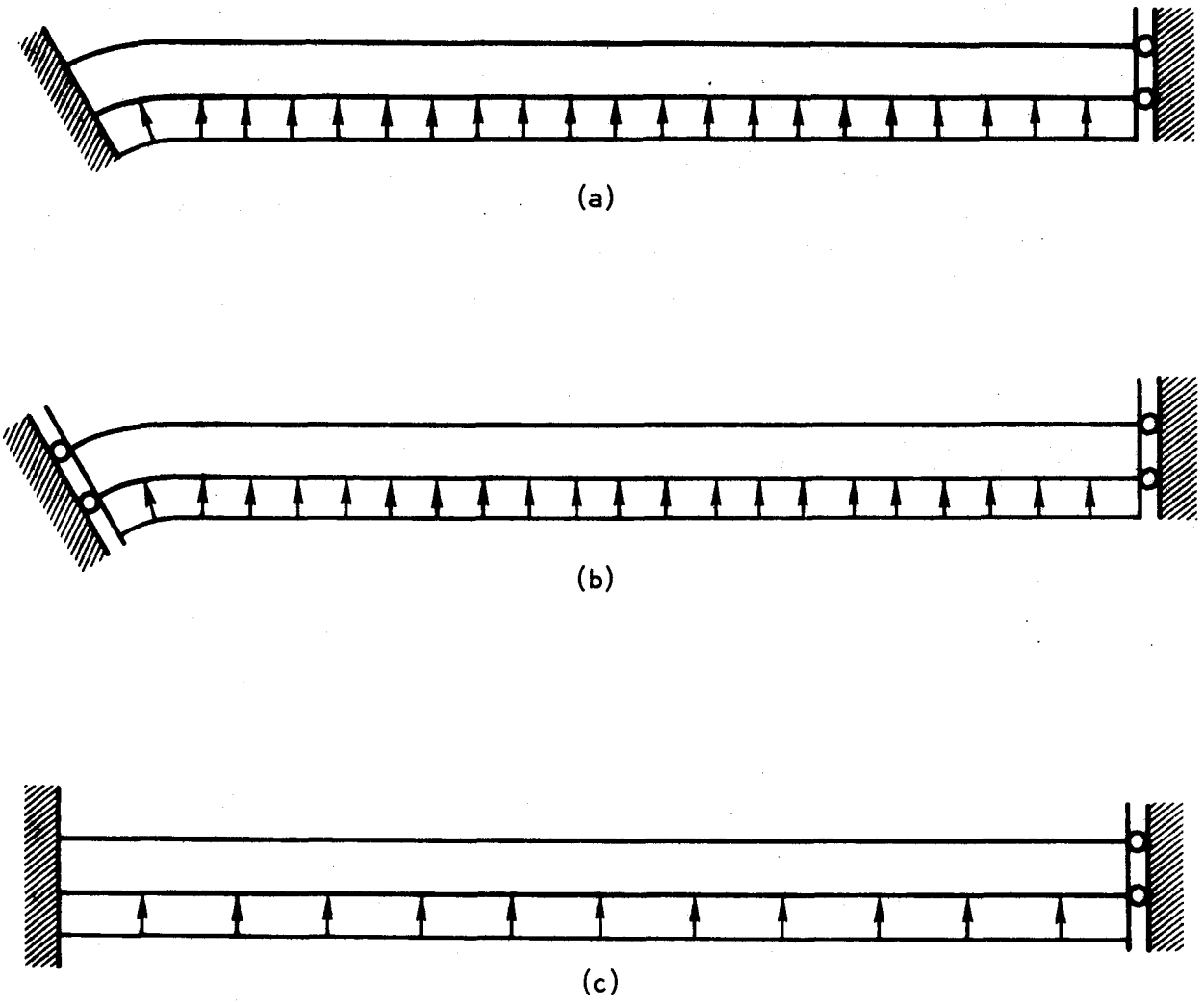

Fig. 2.12 Duct dilation models for application of linear viscoelastic theory

of Fig. 2.12(a). As discussed by Flügge, for the type of problem of Fig. 2.12(a), a correspondence principle exists between the elastic solution and the viscoelastic solution; the latter is obtained by replacing 1/E in the elastic solution by J, where E is Young's modulus. Although the analytical elastic solution of the problem in Fig. 2.12(a) can be obtained, the problem was further simplified by omitting the curvature of the beam at the corner, thus yielding the ordinary, double-fixed-end-beam problem (see Fig. 2.12(c)). The models in Fig. 2.12 were drawn to a scale of about 3:1, so it can be seen that the approximation of neglecting the curvature at the corner will have negligible effect on the deflection of the beam at the centerline of the flat. For a wide beam, the elastic deflection at the centerline is given by

$$\delta_e = \left(\frac{1 - \nu^2}{384}\right)\left(\frac{w\ell^4}{EI}\right) = \frac{K}{E} \quad ,$$

where ν = Poisson's ratio,

w = load intensity (pressure),

ℓ = corner-to-corner length,

I = moment of inertia.

The total deflection is the sum of the elastic and the creep deflections:

$$\delta = K\left(\frac{1}{E} + J\right) \quad . \tag{2.12}$$

A comparison of the viscoelastic creep deflections with the finite-element deflections is shown in Fig. 2.13. The agreement is excellent. The effect of fixing the corner of the duct is to make the stresses constant in time for a constant pressure. Calculations by PNL showed the stresses to be very nearly invariant with time, as reported in the previous quarterly report,[3] so a good agreement between the deflections should be expected. For comparison, a range of deflections are also shown in Fig. 2.13, which were based on the LIFE-III creep correlation:

$$J = A[1 - \exp(-\phi t/B)] + C\phi t \quad , \tag{2.13}$$

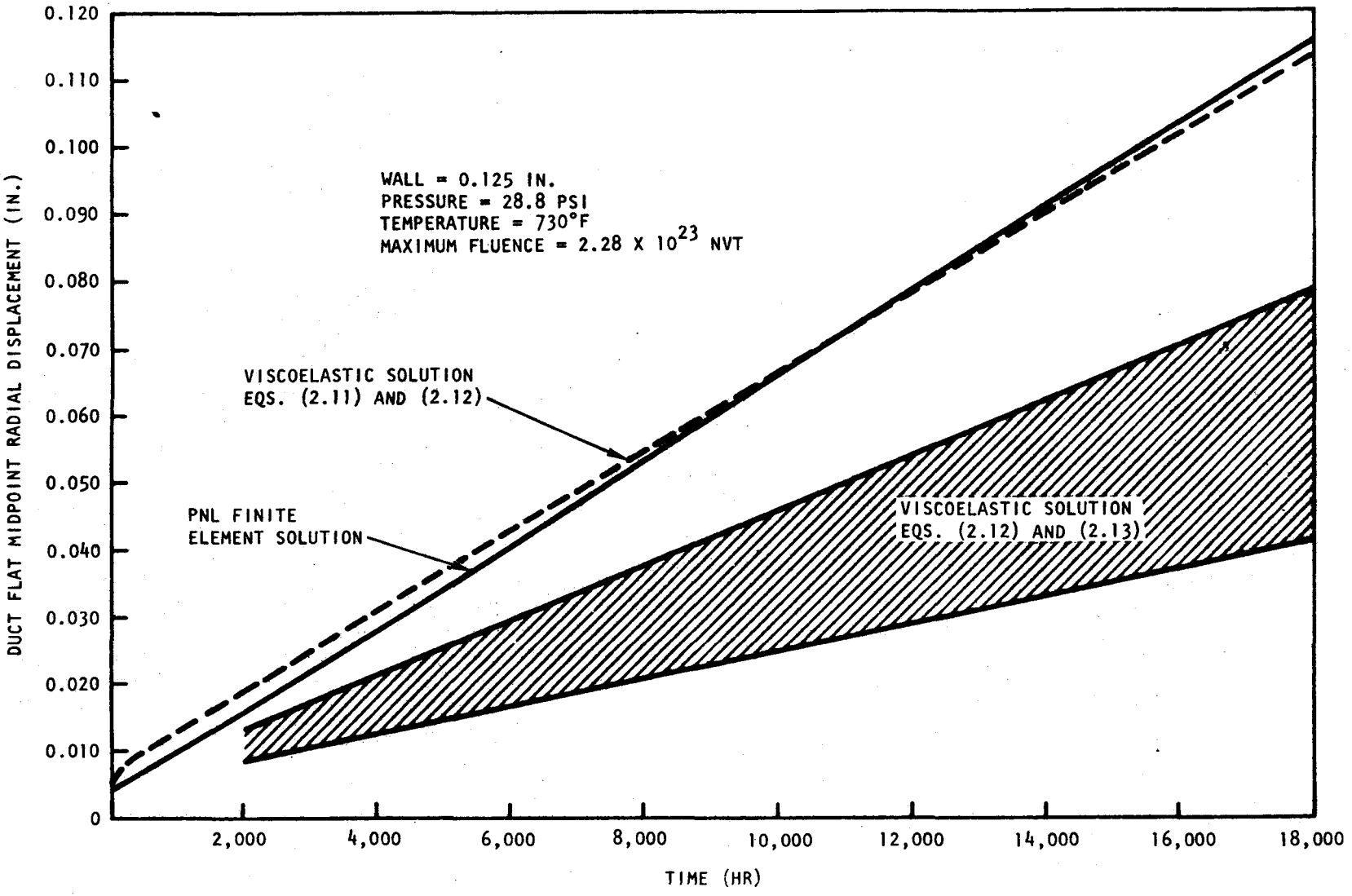

Fig. 2.13 Duct radial deflection vs irradiation time

where $A = (1.3 \pm 0.3) \times 10^{-8}$,

$B = 5 \times 10^{20}$,

$C = (3 \pm 1) \times 10^{-30}$.

Considering the uncertainty of the irradiation-induced creep correlation, the accuracy of the viscoelastic dilation model presented above is more than adequate for future calculations. The effects of thermal creep and swelling appear to be negligible.

The above viscoelastic dilation model will be used in the evaluation of the effect of dilation on the thermal performance of the fuel assembly and in designing an adequate assembly duct. For example, the effect on dilation of varying the wall thickness of the duct is shown in Fig. 2.14, in comparison with PNL numerical data. Duct dilation may cause overcooling of the edge subchannels of the assembly unless relatively thick duct walls are used.

2.1.4. Core Element Development Plan

Descriptions for the various tasks, subtasks, and work items to be included in the overall core development plan have been completed and are now in review.

2.2. BLANKET ASSEMBLY ANALYSIS

The purpose of this task is to develop analytical methods for the thermal-hydraulic analysis of the GCFR radial blanket element. The methods should be capable of analyzing the geometry (closely spaced rods and flow baffles) and the large thermal gradients to which the radial blanket is subjected. This task was initiated during this quarter.

2.2.1. Review of Methods for Steady-state Thermal-hydraulic Analysis

Various available methods for steady-state thermal-hydraulic analysis of the radial blanket assembly were reviewed. The acceptable method has to be capable of modeling the baffled geometry of the blanket assembly with power gradients in the axial as well as the radial direction. The methods reviewed included heat-exchanger codes, the COBRA-IV code, and network analysis methods. Heat-exchanger methods were found inadequate for analysis of the GCFR blanket assembly as those codes are designed

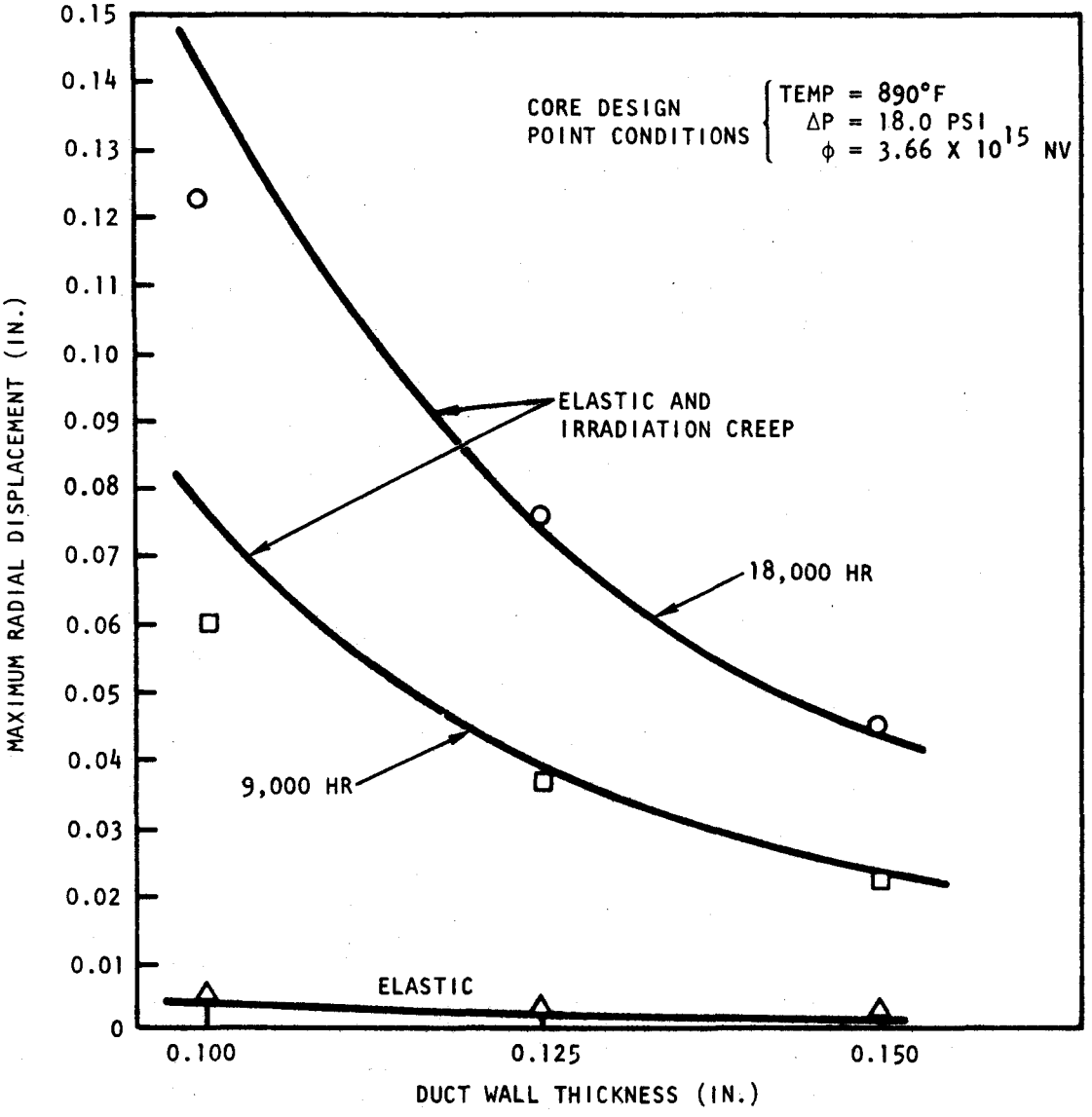

Fig. 2.14 Displacement at the centerline of the duct flat as a function of duct wall thickness (solid lines are the viscoelastic solutions, data points from PNL finite element calculations)

to evaluate the overall heat transfer and pressure drop rather than analysis of local effects. Application of COBRA-IV for the blanket geometry is uncertain at the present time because its capacity to accurately handle the baffled geometry has not been determined. Compared with other methods, the network analysis method was considered to be the most suitable for steady-state thermal-hydraulic analysis of the blanket assembly.

2.2.2. Comparison of Network Analysis with Experiments

To evaluate the feasibility of network methods for thermal-hydraulic analysis of the blanket assembly, the results of the blanket-assembly experiments being carried out under private funding at the University of California, Santa Barbara, were compared with the network analysis results. A network model of the blanket-assembly geometry between two baffles was prepared. The network consisted of 60 nodes and 105 branches and represented the three-dimensional character of the flow in the blanket assembly. The correlations used for loss coefficients in a single baffle hole and single window flow channel were experimentally obtained values. The values for the cross-flow resistances were obtained from the literature.

The excellent agreement for overall pressure drop versus flow relation between experiments and analysis is shown in Fig. 2.15. Another quantity compared was the flow distribution between the baffle zone and window zone at two flow rates, as shown below. (Because the experiments are being conducted with water, the network simulation was done using water properties.)

Water Flow Rate (gpm)	% Flow Through Window		% Flow Through Baffle	
	Analysis	Experiment	Analysis	Experiment
200	45.0	44.3	55	55.7
300	44.5	44	55.5	56.0

2.3. ASSEMBLY MECHANICAL TESTING

The objective of this subtask is to conduct mechanical testing of components and core element assemblies. Fuel-rod–spacer-grid interaction

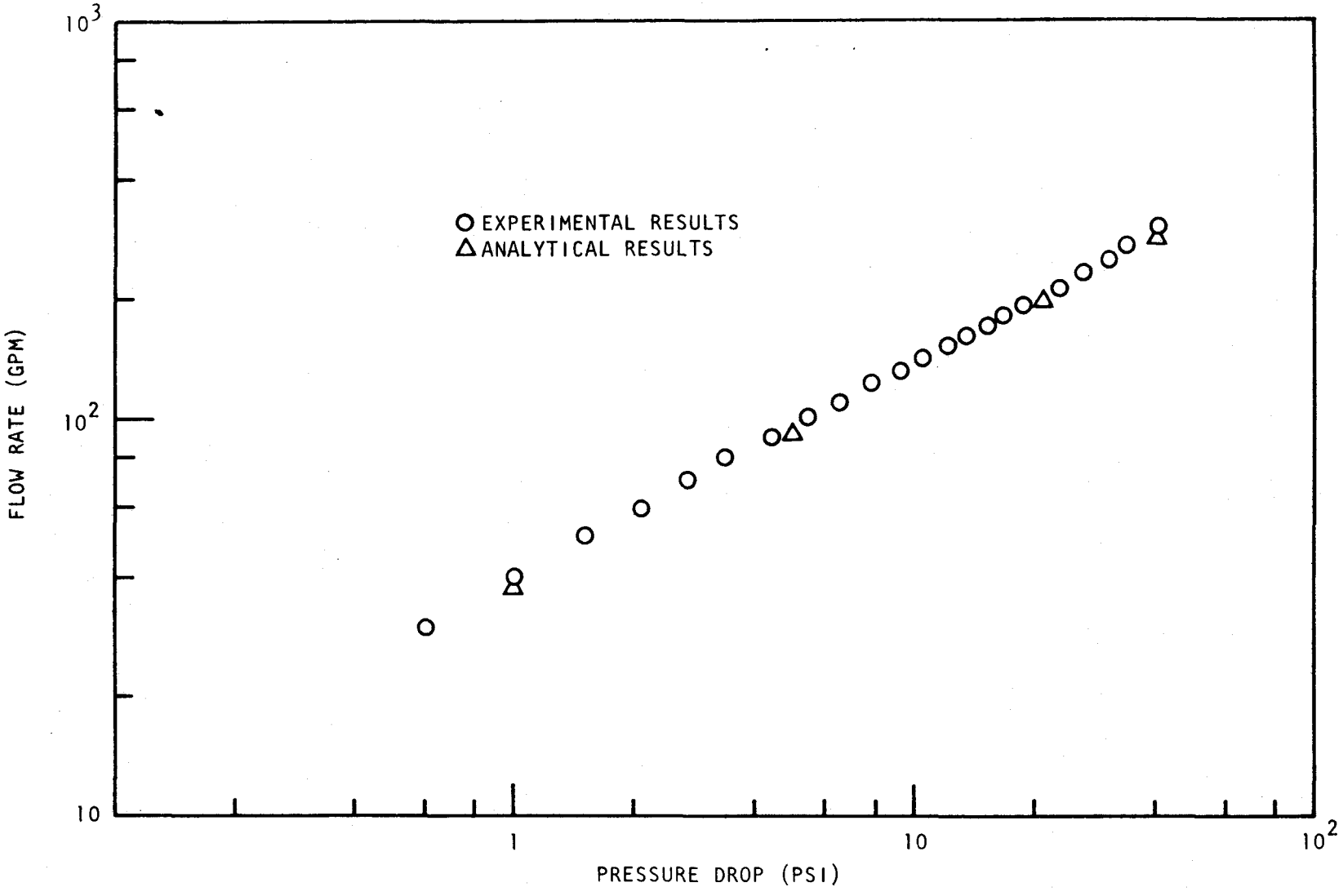

Fig. 2.15 Comparison of experimental results and analytical results obtained by network model for GCFR blanket

tests are currently being conducted and planning of seismic and flow-induced vibration tests have been initiated. In the rod-spacer interaction tests, the friction wear and adhesion between the fuel-rod cladding and the hexagonal spacer grids are being evaluated. The current effort on seismic and flow-induced vibration is directed toward preparation of a test program plan.

2.3.1. Rod-spacer Interaction Tests

The rod-spacer interaction test is to evaluate the interaction between the rod and the spacer in the range of impurity levels (primarily hydrogen and water) expected in the GCFR helium coolant. These interactions arise from the relative motion between the rod and the spacer due to a normal operating load and to various reactor transients that cause contact of the rod and spacer. This results in friction, wear, and possibly adhesion between the rod and the spacer.

The initial investigation was on pressed spacers with convex contact surfaces, or dimples, and smooth or ribbed rods. Both spacers and rods were of Type 316 stainless steel. Adhesion was observed in tests on smooth rods in an environment containing 90 μatm of H_2O at a H_2/H_2O ratio of 10 in helium. When the H_2/H_2O ratio was changed to 100 at the same absolute H_2O level, no adhesion was observed. Additional tests were conducted on spacers machined by electrodischarge machining (EDM). These spacers had a flat or concave contact surface and a somewhat rougher surface. No adhesion has been observed with these spacers under the same conditions that adhesion was observed with the pressed spacers. Also, pressed spacers made from Inconel 718 and Inconel 625 did not adhere when tested at a H_2/H_2O level of 10 against Type 316 stainless steel tubes. Dissimilar material combinations, in general, showed lower coefficients of friction.

The tests conducted during the current quarterly reporting period included the evaluation of EDM spacers with concave contact surfaces made from 20% cold-worked Type 316 stainless steel rod at GA. These were tested against both ribbed and smooth rods of 20% cold-worked Type 316 stainless steel. No adhesion has been observed; the test conditions and the resulting coefficients of friction are tabulated below.

Tube	Temp. (°C)	Linear Travel (in.)	H_2/H_2O (μatm)	Coefficient of Friction	Remarks
Ribbed and smooth	525° and 750°C	15 and 120	900/90	0.4 to 0.7	No adhesion

All of the possible combinations listed above, except smooth tubes at 750°C, were tested. The frictional behavior is very similar to that previously reported for similar tests with EDM spacers with flat contact surfaces. The lowest value for the coefficient of friction was observed for a smooth tube at 525°C. The maximum depth of the wear grooves on the ribs was about one-fourth the rib height. Some tests show pileup, or deposition, of material on one or two ribs, the rest show wear grooves. Spacers from all tests show a small number of long scratches, indicating contact only at certain locations. A typical wear track on a smooth tube is shown in the scanning electron micrograph in Fig. 2.16. Material pile-up at the end of the wear track is typical of the interaction with smooth tubes. The area near the end of the wear track is magnified in Fig. 2.17. Further characterization of the wear will be determined during the next reporting period.

Other rod-spacer tests have been made in connection with the BR-2 helium loop experiments. These tests (which are privately funded) were conducted on ground 20% cold-worked stainless steel tubes and 4981 EDM spacers from Kraftwerke Union (KWU), the hydrogen-to-water level used was 30,000/300 μatm. Only long stroke tests are complete. No adhesion has been observed and the maximum depth of the grooves is about one-third of the rib height. One of the tests showed a considerable number of wear particles deposited between the ribs. The maximum dimension of the particles is about 2 mils.

The parts for the third test-rig were completed by the vendor and inspected at GA. The inspection showed variances in 16 parts, of which about 9 were acceptable as is. The other 7 parts were returned to the vendor for rework.

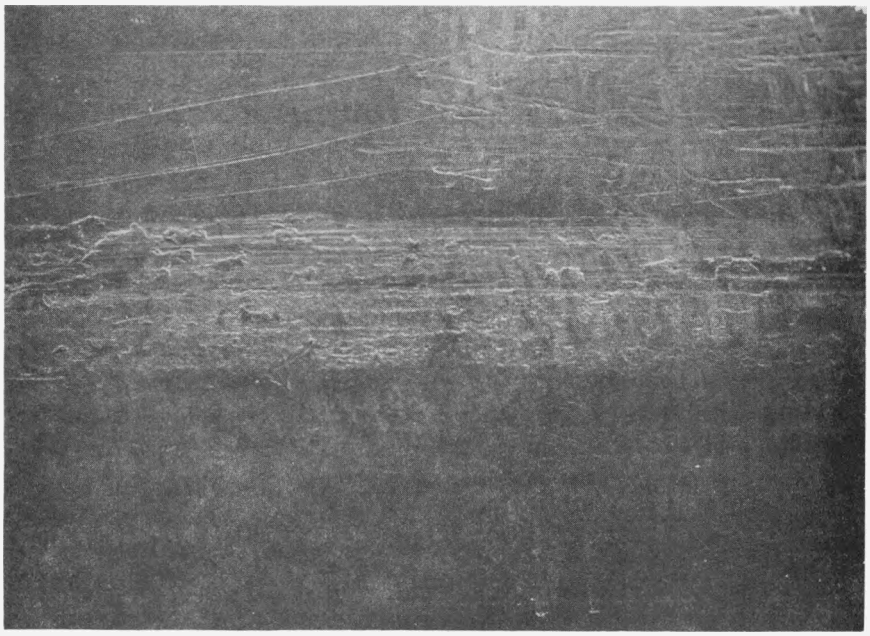

Fig. 2.16 Wear track on smooth tube (total linear travel 120 in. at 525°C; H_2/H_2O = 900/90 μatm)

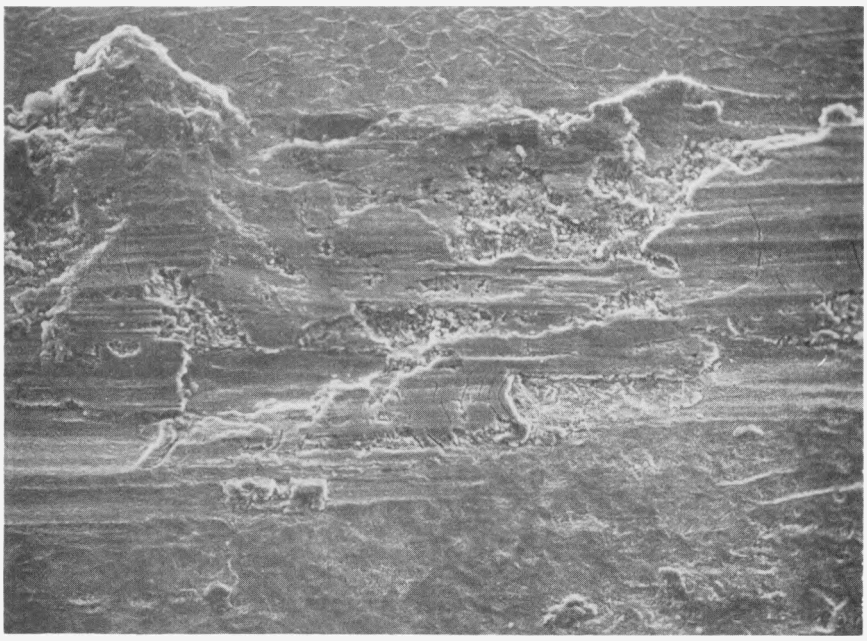

Fig. 2.17 Area near the end of wear track (center left in microphotograph in Fig. 2.16)

The failure of one load cell in each of the two test rigs occurred and these load cells were returned to the vendor for repairs. The remaining two load cells were mounted in one test rig and testing continued. At the conclusion of the BR-2 support tests, it was decided to move both rigs to a new laboratory location where more space is available. This relocation is now in progress.

2.3.2. Seismic and Vibration Test Support

2.3.2.1. Flow-induced Vibration Analysis. The study of the potential for flow-induced vibration in core elements continued during the quarter with a thorough review of the literature available on the subject of instabilities due to axial flows. This is the type of flow found in the GCFR standard fuel assemblies and control fuel assemblies.

The literature surveyed included work by Paidoussis, Ohlmer, S.S. Chen, Y.N. Chen, Wambsganss, Reavis, and others. Most of the authors formulate analytic or semianalytic models of the flow-induced vibration problem, and then modify them as necessary to correlate with experimental data. The experimental data exhibit considerable scatter, due perhaps to anomalies in the test chambers, so that agreement only to within an order of magnitude may be expected.

An example of the correlations used is one given by Paidoussis[4]:

$$\frac{\delta}{D} = 5K\alpha_1^{-4}\left[\frac{u^{1.6}\,\varepsilon^{1.8}\,Re^{0.25}}{1+u^2}\right]\left[\left(\frac{D_h}{D}\right)^{0.4}\right]\left[\frac{\beta^{2/3}}{1+4\beta}\right] \times 10^{-4} ,$$

where δ = maximum amplitude,

D = rod diameter,

K = noise factor, which varies between 1 and 5,

α_1 = dimensionless first code eigenvalue of the cylinder,

u = dimensionless flow velocity,

ε = ratio of tube length to tube diameter,

Re = Reynold's number based on hydraulic diameter,

D_h = hydraulic diameter,

β = mass ratio (essentially equals the ratio of coolant virtual mass to rod mass for the GCFR).

Allowing for the scatter of the data and assuming "worst" conditions (i.e., noisy flow and maximum velocity) this and all other correlations indicate that the rods will vibrate at a frequency of approximately 120 Hz with a maximum amplitude of less than 0.01 mm. The extreme smallness of this amplitude is due primarily to the very low density of the helium coolant used ($\sim$ 6 kg/m^3), which more than makes up for the relatively high velocities used ($\sim$ 85 m/sec max.). This results in a relatively modest dynamic head ($\sim$ 2 x 10^{-4} n/m^2) and means that the ratio of fluid virtual mass to rod mass is very low (7 x 10^{-4}).

The flow-induced vibrations of a whole fuel assembly were also analyzed. It was found that the velocity of the coolant is far below that needed to cause fluid-elastic instability, so flutter of the ducts will not occur. Other flow-induced vibrations should have very small amplitudes because the assembly is quite massive and stiff and because of the low-density coolant used. Possible resonance of the assembly with the vibrating fuel rods is unlikely because the assembly and the rods have widely different frequencies (assembly = 9.5 Hz, rod = 120 Hz) and hence should not couple.

It thus appears that flow-induced vibrations pose no significant problems for the GCFR. This will be confirmed by tests. Future work in this area will be to further refine the analysis of fuel element vibrations and to analyze the flow-induced vibrations due to the mixed cross and parallel flow in the blanket assemblies.

2.3.2.2. Seismic Analysis. The seismic analysis of the GCFR core elements continued. Work centered primarily on converting the mathematical model of the GCFR from the previously used dynamic-response code to the Structural Analysis Program (SAP) IV code. SAP IV is a modern (June 1973) finite-element code for the static and dynamic analysis of linear systems. Its dynamic analysis capabilities include fully three-dimensional response-spectrum and time-history analyses.

At present, the GCFR is modeled as a two dimensional assemblage of beams and concentrated masses. This has been analyzed by both the response-spectrum and the time-history methods. The earthquake response spectrum

was that given in AEC Regulatory Guide 1.60, scaled to represent a 0.33 g maximum horizontal acceleration earthquake; damping values were taken in accordance with AEC Regulatory Guide 1.61. A time-history analysis has also been done using an earthquake time history developed by GA from the response spectrum given in Regulatory Guide 1.60. The results are in reasonable agreement, and also agree favorably with the results of a previous analysis using the older dynamic-response code. Some isolated problems still exist, so further work is necessary before results can be finalized. Future work will include modeling the structure as a fully three-dimensional structure, improved modeling of the fuel elements, and modeling of the blanket and control fuel elements.

2.3.3. PNL Seismic and Vibration Studies

Work continued at GA and at PNL on the preparation of a test program and analysis to evaluate the dynamic effects of flow-induced vibration and seismic events on the GCFR core element assemblies. A test program was prepared by PNL for the proposed flow-induced vibration testing and seismic testing. These program plans were reviewed at GA and were followed by a meeting with PNL personnel to discuss proposed changes. The test plans are now being finalized.

The equipment available at the PNL test site for performing dynamic testing is as follows:

1. An air compressor that is capable of supplying air at the rate of 100 STP ft^3/hr at 5300 psi. The compressor is derated by at least a factor of 3; by using a larger-size motor it is capable of 300 STP ft^3/hr.
2. Helium storage tanks of 500-ft^3 capacity at 2500 psi that can be assembled in parallel storage for a blowdown test.
3. Two vertical vibration facilities used for the FFTF vibration testing.

This equipment will provide the capability for doing at least part of the flow-induced vibration testing. The compressor and storage tanks

can be combined for a blowdown test of 1-hr duration or more. The equipment is in excellent condition and represents a considerable savings in required test facility funds.

The single-rod and 19-rod flow-induced vibration tests are proposed to be continuous flow tests so that some fretting and wear data can be obtained. The seismic testing would be done at a testing laboratory that has the dynamic equipment capability for simulation of seismic events.

2.4. ASSEMBLY FABRICATION DEVELOPMENT

The GCFR reference core element designs are being evaluated to determine the fabricability and feasibility of assembly of the element components. This task was initiated by a review of the design for component fabricability, including contacting outside vendors that might be potential fabricators of components. Whenever the design review or vendor survey indicate a potential problem of feasibility of fabrication or assembly, then conceptual design layouts will be conducted. The areas where fabrication and assembly problems appear to exist are

1. Fuel and rod assembly,
2. Bottom fuel-rod grid design,
3. Fuel-rod spacer grids and grid supports (hangers),
4. Grid-plate shielding above active core,
5. Element annular fission-product trap.

As a result, alternative conceptual designs are being considered for these areas.

In parallel with the review of the design, contacts were made with several potential vendors and fabricators to discuss the element assembly components. The discussions included possible design changes or alternate concepts to facilitate fabrication of components. The following vendors were contacted:

1. ACE Industries, Santa Fe Springs, Calif., to discuss fuel-rod support and spacer-grid fabrication using EDM machining.

2. Clark-Wheeler, Paramount, Calif., to discuss gun-barrel drilling of the fission-product manifold vent holes and fabrication of the element hexagonal ducts.

3. Peerless Industries, Los Angeles, Calif., to discuss EDM machining of rod support and spacer-grid fabrication.

4. Mechanical Seals Corporation, Irvine, Calif., to discuss the application of the MS lockring tube joint to the fuel-rod grid manifold.

5. Sealectro Corporation, New Jersey (Los Angeles Division), to discuss miniature coaxial thermocouple connectors.

ACE Industries were early pioneers in electrodischarge machining and are more production oriented. They were thus reluctant to do small quantity parts fabrication that require tooling and technique development.

Clark-Wheeler does a major portion of the fabrication of the hexagonal duct for the FTR core elements. They thought that our single-step duct tube would be considerably easier to draw. They do not use the Turks Head roller forming technique as CARTECH does for hexagonal tubes. Clark-Wheeler does subcontract business with CARTECH, including gun-barrel drilling of tubes, trepanning, and final drawing.

Clark-Wheeler has very extensive capabilities in the gun-barrel drilling of long holes, which resulted from their aircraft hydraulic systems business. They can do drilling of holes from 0.120 in. in diameter and several inches in length to 6 in. in diameter and a 45 ft length. The vent-hole requirement for the fission-product manifold was discussed. They feel that the technology of hole drilling tools limits them to a 0.120-in. diameter. Although tools could be developed for a 0.090-in.-diam hole for a 4 in. length, there is presently no incentive to do this in the U.S. gun-barrel-drilling industry.

Peerless Industries specializes in the EDM drilling of small-diameter long holes. They could easily do the 0.040-in. diam by 6-in.-long vent holes. However, they were not enthusiastic about EDM machining of the fuel-rod support grid or the spacer grids. They suggested a redesign

of the rod support grid to make it amenable to fabrication by numerically controlled milling machines. This was studied conceptually and the preliminary conclusion is that it is a feasible alternative fabrication technique.

The MS lockring tube joint is an invention of the Mechanical Seals Corporation. It has been successfully used on tubesheet-type joints. It makes a lap joint between a tube and a header by a ring which swages the parts together. The tube material is usually inelastically deformed. Methods of applying this joint to the fuel rod to vent manifold seal were discussed. There are two design problems in this application: (1) the clearance necessary to clamp the ring around the fuel rod and (2) to replace a fuel rod in a vent manifold, the connection would have to be reformed. Further design studies were proposed to be done by GA and Mechanical Seals Corporation to consider what design changes are feasible.

The Sealectro Corporation markets a line of miniature coaxial radio-frequency (RF) connectors that have been proposed for thermocouple connector applications. One miniature size was selected for further design studies. It has a maximum diameter of 0.190 in., which would be reduced to 0.167 in. for insertion into a tube in the GCFR fuel assembly. The temperature limit of the current design is 200°C, which is apparently a limit of their Teflon insulating material. Several connectors were procured to study their possible application as a connector to a standard chromel-alumel thermocouple.

REFERENCES

1. Lund, K. O., "A Solution to the Steady, Isothermal Flow in Rod Bundles using Matched Asymptotic Expansions," ASME Winter Annual Meeting, New York, November 1974, Paper No. 74-WA/HT-4.

2. Laufer, J., "Turbulent Shear Flows of Variable Density," AIAA Journal, Vol. 7, No. 4, April 1969.

3. "Gas-Cooled Fast Breeder Reactor Quarterly Progress Report for the Period May 1, 1974 through July 31, 1974," USAEC, Report GA-A13148, Gulf General Atomic, September 26, 1974.

4. Flügge, W., Viscoelasticity, Blaisdell Publishing Co., Waltham, Mass., 1967.

5. Paidoussis, M. P., "The Dynamical Behavior of Cylindrical Structures in Axial Flow," Annals of Nuc. Sci. and Engng., Vol I, 1974, p. 94.

III. FUELS AND MATERIALS DEVELOPMENT (189a No. 13126)

The scope of the GCFR fuels and materials task is to extend the LMFBR fuel and materials technology to conditions and design features that are specific to the GCFR, such as the use of vented fuel, fission-product traps, and surface-roughened cladding. A thorough surveillance and analysis of the LMFBR irradiation testing and fuels and materials program are maintained because of the similarity between GCFR fuel rods and other core materials. A detailed fuel, blanket, and control-rod development plan will be used to guide the selection of tests to be performed.

An irradiation program for the development of fuel elements for the GCFR is being conducted using the Oak Ridge Research Reactor (ORR) for thermal-flux irradiation of vented fuel rods and the EBR-II for fast-flux irradiation of sealed rods. The irradiation program is a cooperative effort among GA, ANL, HEDL, and ORNL. Parametric tests followed by statistical tests will be performed to establish fuel-rod designs. Tests to determine operational margins and tests to failure will be performed as needed to complement similar tests performed under the LMFBR program. Out-of-pile experiments to determine the effect of impurities in flowing helium on the mechanical properties of surface-roughened cladding will be performed at PNL.

The measurements of tritium yield, venting fraction, and diffusion through fuel-rod cladding are planned.

3.1. FISSION-PRODUCT RELEASE AND TRANSPORT

The release and transport of fission products in GCFR fuel are being measured and studied in capsule GB-10, which is being irradiated in the ORR. The burnup of the pressure-equalized and vented fuel rod in GB-10 reached 56,200 MWd/Te on October 26, 1974, of an exposure goal 75,000 MWd/Te. The first 27,000 MWd/Te was accumulated at 12 kW/ft at a cladding outside surface temperature of 565°C and the remainder has been accumulated at

13.5 kW/ft at a cladding outside surface temperature of 630°C. Irradiation of GB-10 is continuing.

The development of tritium-monitoring instrumentation to be installed on the sweep-gas sampling line of capsule GB-10 continued during this quarterly period. The changes in the flow resistance of the fuel rod, presumably as the result of transport and deposition of fission products and perhaps fuel, are reported. Also reported are the results and analysis of the radioactivity vented through the sweep-gas line at different operating pressure levels. Finally, an analysis of the venting of gaseous fission products from the fuel rod in capsule GB-10 as a consequence of power cycling is reviewed.

3.1.1. Tritium-monitoring Instrumentation

The conceptual design of the tritium-monitoring system being developed for the GB-10 experiment was described in the previous quarterly report.[1] The conceptual design for the system was developed in consultation with ORNL and with the General Atomic HTGR project, the latter having developed and placed into operation a tritium-monitoring system for the Peach Bottom Atomic Power Station. The system is designed to

1. Separate tritium (and hydrogen) from other impurities using either a chromatographic sorption on liquid-nitrogen-cooled charcoal or the permeation of tritium (and hydrogen) through a palladium-silver membrane.
2. Oxidize HT to HTO or, conversely, reduce HTO to HT so that the chemical state of the fission-produced tritium vented from GB-10 can be determined.

Studies during this quarterly reporting period have been directed primarily toward obtaining basic data applicable to the permeation of tritium and hydrogen through the silver-palladium membrane. A schematic of the calibration apparatus being used with the diffusion membrane is shown in Fig. 3.1, which is prototypic for the GB-10 fission-gas venting system except for the pressure (nominally 1 atm rather than 65 atm).

The studies have shown that tritium permeation is essentially insensitive to temperature in the range 350° to 525°C. This result was totally

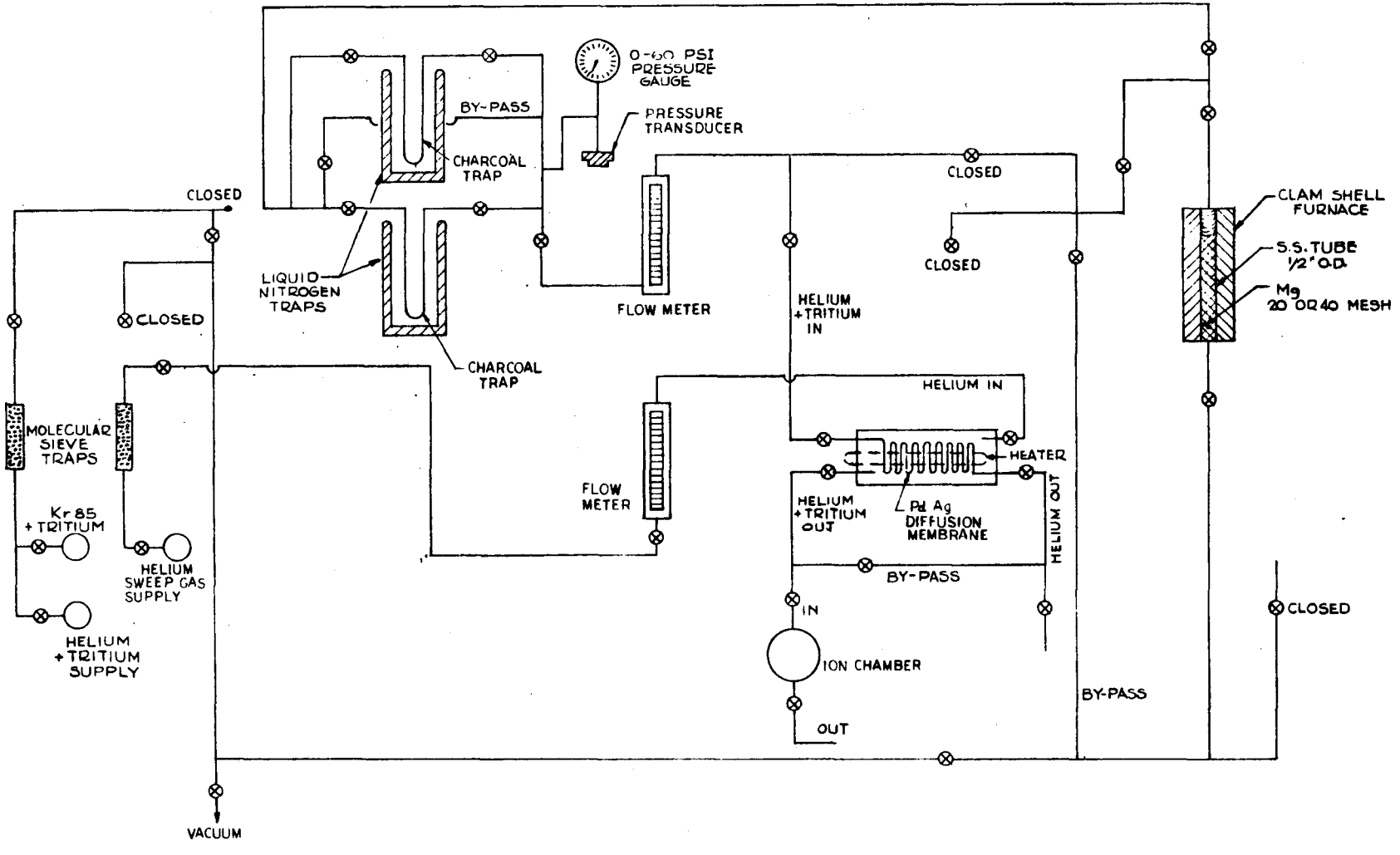

Fig. 3.1 Instrument calibration system for tritium monitoring

unexpected, but it indicates that surface or other phenomena, other than mass transport through metal, are the rate-determining step in the permeation process.

Tritium permeation is, however, pressure and flow-rate dependent, as expected. The fractional permeation increases (1) when the tritium concentration on the inlet side of the membrane increases or (2) when the tritium concentration on the permeate (sweep) side of the membrane decreases.

The inlet tritium concentration can be increased by either increasing the inlet pressure at constant permeate pressure or by increasing the inlet flow rate at constant pressure. Conversely, the tritium concentration on the permeate side can be decreased by increasing the helium sweep pressure (thereby diluting the tritium) at constant flow rate or by increasing the permeate helium sweep rate at constant pressure. The effect of variations in inlet and permeate pressure is shown in Fig. 3.2. The data indicate that the maximum tritium permeation of $\sim$94% can be attained. This permeation fraction is considered quite satisfactory so long as it remains constant with time.

The effect of flow rate on the fractional permeation at constant pressure is smaller than the effect of pressure at constant flow rate over the range of the experiments (flow rates in the range of 100 cm^3/min to 1000 cm^3/min).

Some preliminary experiments carried out to determine the effects of micro (43 ppm) and macro (1.5%) amounts of H_2 in the helium carrier gas gave puzzling results and tritium and hydrogen mass balances could not be maintained. Since rather extended investigations would be required to determine the cause of these effects and the time available for the experiments was short, this approach was temporarily set aside in favor of an effort to confirm the dynamic behavior of tritium and argon (the most likely contaminant of the tritium in GB-10) in liquid-nitrogen-cooled charcoal traps. These experiments, which are for determining the delay times for the two species as a function of trap size, geometry, and flow rate, are currently under way.

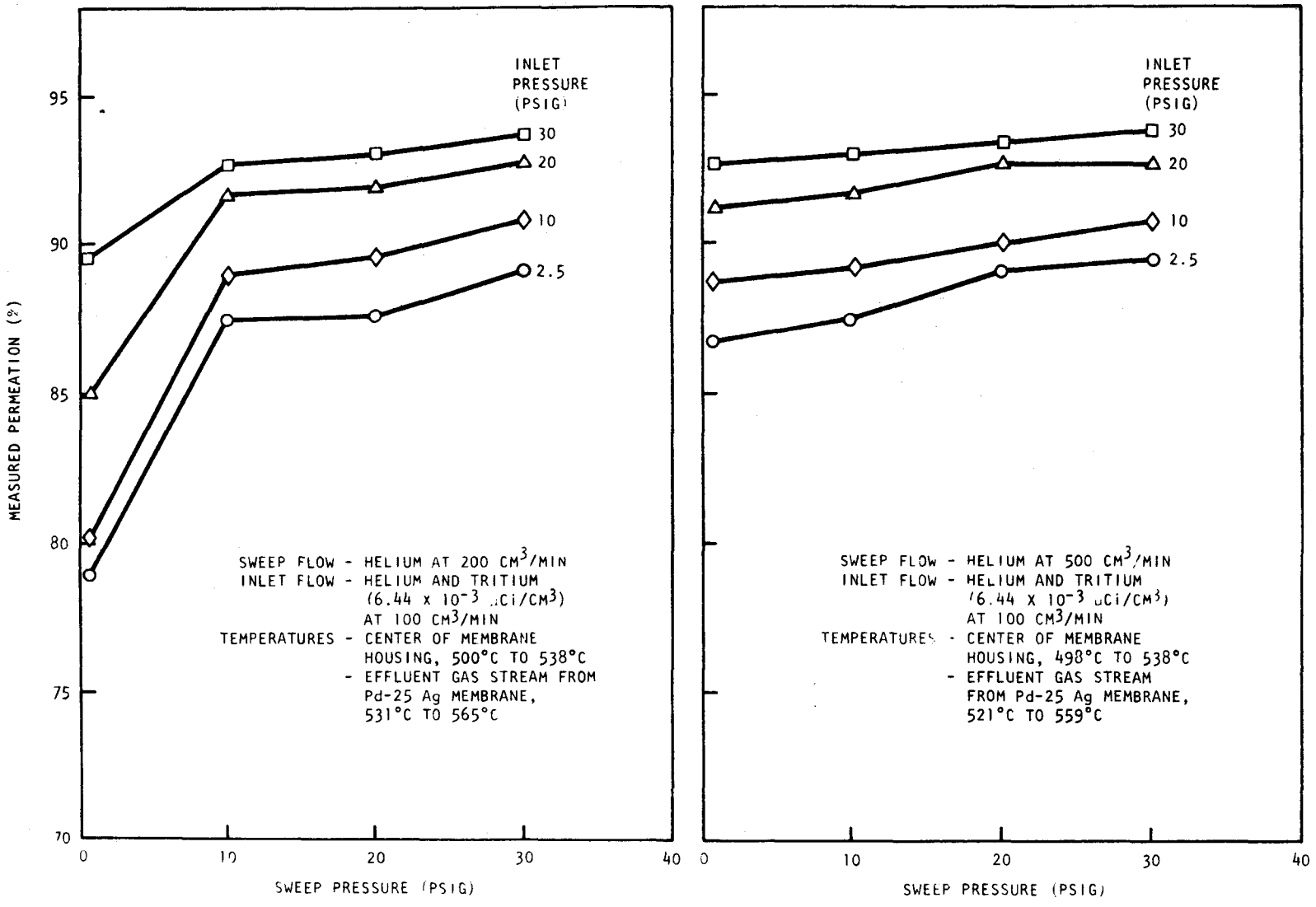

Fig. 3.2 Effect of inlet and sweep pressure on tritium permeation

3.1.2. Flow-resistance Changes

Toward the end of the previous quarterly period, an increase in the flow resistance of the fuel rod was noted. By testing in the various flow modes, the increasing resistance was found to be occurring in the fueled region of the fuel rod. In situ measurements were made in the flow mode in at the bottom of the fuel and out at the top of the charcoal trap (BF-TT). The flow and instrumentation arrangements are shown in Fig. 3.3. The inlet line to the bottom of the fuel rod is approximately 80 ft long and 0.027 in. in diameter. At the pressure, temperature, and flow-rate conditions of the tests, the line pressure losses are only a few psi; i.e., the flow resistance of the line is only a small part of the total resistance at operating conditions. Flow through the lines and the fuel rod is laminar except perhaps locally in some of the small passages in the interstices of the fuel. The flow resistance of the rod and sweep-gas line between the two pressure gauges has been calculated and normalized to the preirradiation resistance. The normalized resistance is

$$R = \Delta P(1000)/Q(14.7)\ r \quad ,$$

where ΔP = measured pressure drop (psi),

Q = volumetric flow rate at temperature and pressure (cm^3/min),

r = normalization factor ($r = R$ at the preirradiation condition, 2.583 psi-min/cm^3).

The data and the normalized flow resistance over the irradiation period of more than two years and a burnup of 50,000 MWd/Te are given in Table 3.1. The results show a slow, gradual buildup in the flow resistance of the fuel rod up to about 45,000 MWd/Te. The flow resistance then began to increase rapidly, reaching a peak value of 14.6 times the preirradiation value and then began decreasing again. Currently, the normalized flow resistance is about 7.6 times the preirradiation value and is continuing to decrease. It is noted that the resistance in the "cold" condition when the capsule is shut down is essentially unchanged.

The reasons for the rise and fall of the flow resistance are unknown at this time and can only be speculated. Since the shutdown resistance

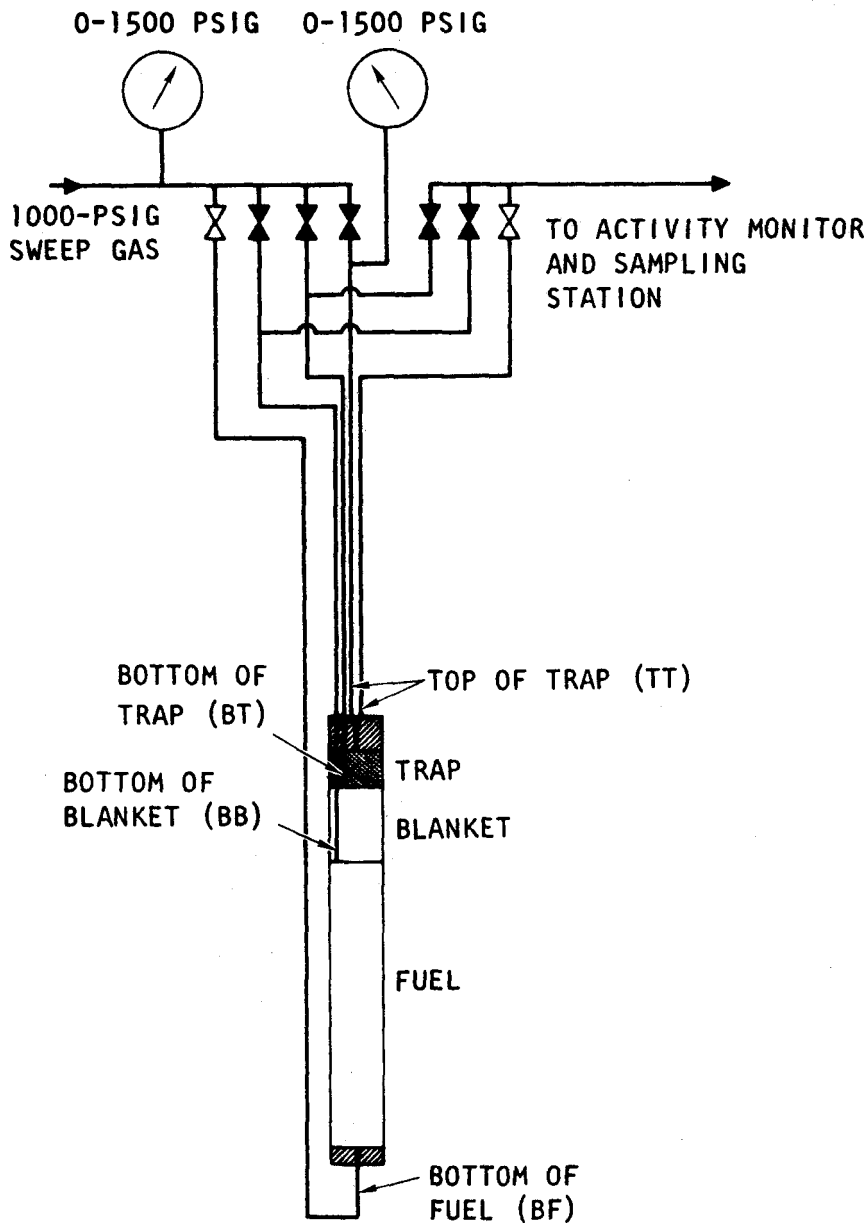

Fig. 3.3 Schematic of capsule GB-10 sweep gas system for in situ flow resistance measurements

Table 3.1

FLOW RESISTANCE OF GCFR FUEL ROD IN CAPSULE GB-10

Date Taken	Operating Conditions	ΔP (psi)	Volumetric Flow Rate (cm^3 STP/min)	Flow Resistance, r	Normalized Resistance
8/27/72	Preirradiation	45	1185	2.583	1.0
8/29/72	Initial startup	77	949	2.583	2.1
	Typical long time at low burnup	20	1000	2.583	0.53
5/16/74	Low pressure (300 psi)	73	240	2.583	2.4
6/13/74	Low pressure (300 psi)	73	230	2.583	2.5
6/26/74		109	1000	2.583	2.9
7/2/74	Burnup at 50,000 MWd/Te	155	980	2.583	4.2
7/11/74		121	610	2.583	5.2
8/1/74		235	740	2.583	8.4
8/11/74		175	315	2.583	14.6
8/22/74	Shutdown	47	1005	2.583	1.2
9/3/74	Return to power (13.5 kW/ft)	210	480	2.583	11.5
9/10/74		159	397	2.583	9.55
9/12/74	Shutdown	22	530	2.583	0.99
9/12/74	Full power (13.5 kW/ft)	167	425	2.583	7.60

has not changed significantly and the resistance upon return to power is many times the shutdown value, it appears that differential expansion between the fuel and the cladding and within the fuel itself results in constriction of the flow passages at operating power levels. Second, reduced resistance is observed following shutdowns, suggesting that new passages or perhaps enlarged passages have been opened, for example, by fuel recracking. It is also noted that the large increase in resistance occurred after the power level had been raised from 12 to 13.5 kW/ft, although it did not rise steeply until after about 20,000 MWd/Te had been

accumulated at the higher power level. The effect of operation for 10,000 MWd/Te at 200 and 300 psi just prior to the peaking of the flow resistance is not known. However, fuel and volatile fission-product transport to the fuel-blanket interface observed in other fuel-rod irradiations would be accelerated at the lower pressures relative to the normal operating pressure of 1000 psi. We can only speculate about the significance of the fact that the resistance began going down again shortly after operation at 1000 psi was resumed.

Monitoring of the flow resistance of the fuel rod will continue as the irradiation proceeds.

3.1.3. Pressure Effect on Venting

Irradiation capsule GB-10 has been operated at sweep-gas and internal fuel rod pressures of 200 and 300 psig for about 5,000 MWd/Te, or 50 effective full power days, at each pressure level in addition to normal operation at 1000 psig. The effect of pressure not only on the release of gaseous and volatile fission products from the solid phase in the fuel to the gas phase in the interstices of the fueled region of the rod, but also on their being vented from the fuel rod has been measured. The radioactivity in the sweep gas flowing in the sampling line was measured with a calibrated ion chamber. Also, the isotopic content of the fission gases has been measured both by an on-line Ge(Li) gamma spectrometer and by vial samples taken and analyzed in the laboratory with a Ge(Li) gamma spectrometer. The results of the ion chamber measurements have been analyzed and are presented below. The fission-gas isotope measurements will be analyzed and reported subsequently.

The data taken during the low-pressure operation of capsule GB-10 is tabulated in Table 3.2. The flow mode where the sweep gas enters at the bottom of the fuel and exits at the top of the trap (BF-TT) is used to measure the radioactivity released from the fuel. The flow mode where the sweep gas enters at the top of the trap and exits from the same point (TT-TT) is used to measure the radioactivity that is first released from the fuel and then vented from the rod. In either flow mode, decay during transport from the fuel to the ion chamber and dilution by the sweep gas affect the ion chamber readings. Corrections for the dilution were made

Table 3.2

EFFECT OF INTERNAL FUEL-ROD GAS PRESSURE ON RELEASE AND VENTING OF GASEOUS FISSION PRODUCTS

Time[a] (days)	Flow Mode	Pressure (psig)	Pressure at Ion Chamber (psig)	Flow (cm^3 STP/min)	Actual Flow (cm^3/min)	High-pressure Activity (mR/hr)	High-pressure Activity Normalized to 20 cm^3/min (mR/hr)
0	TT-TT	999	995	1215	19.3	6.8	6.6
16	TT-TT	999	995	1200	19.1	18	17.2
50	TT-TT	995	991	1180	18.8	9	8.5
59	TT-TT	982	978	1170	18.9	10.5	9.9
73	TT-TT	201	197	275	20.8	68	70.7
80	TT-TT	201	197	280	21.2	54	57.2
98	TT-TT	198	194	290	22.3	33	36.8
108	TT-TT	197	193	280	21.6	34	36.7
114	TT-TT	195	191	820	63.9	13	41.5
114	TT-TT	197	193	190	14.9	42	31.3
150	TT-TT	304	300	390	19.9	12.6	12.5
154	TT-TT	303	299	385	19.7	19.5	19.2
158	TT-TT	305	301	385	19.6	19.5	19.1
163	TT-TT	303	299	385	19.7	20	19.7
171	TT-TT	303	299	380	19.4	29.5	28.6
16	BF-TT	935	931	1130	19.2	3150	3024
50	BF-TT	940	936	1120	18.9	2670	2523
74	BF-TT	158	154	175	16.6	5000	4150
80	BF-TT	163	159	185	17.1	2550	2180
98	BF-TT	155	151	175	16.9	1550	1310
108	BF-TT	158	154	175	16.6	1730	1436
114	BF-TT	154	150	175	17.0	1250	1063
150	BF-TT	248	244	290	18.0	750	675
154	BF-TT	231	227	245	16.3	1610	1312
158	BF-TT	239	235	255	16.4	1350	1107
163	BF-TT	238	234	275	17.7	900	797
171	BF-TT	229	225	240	16.1	1395	1123

[a]Time after raising the power level from 12 kW/ft to 13.5 kW/ft.

and the results are listed in the last column of Table 3.2. However, it is not possible to correct for decay in transit because the activity comes from a complex mixture of fission-product gases, which is not known.

Analyses of the conditions in capsule GB-10 during the low-pressure operations[2] have shown that dilution is the dominant effect in the TT-TT flow mode and that decay in transport is negligible. In the BF-TT flow mode, dilution is also the dominant process for all of the fission-gas isotopes except Kr^{89} and Xe^{139}. For those two isotopes, dilution and decay are competing on an equal basis so that the radioactivity in the gas at the ion chamber is not sensitive to either correction. Thus, the results in Table 3.2 are believed to be valid with only the dilution corrections.

The corrected dose-rate data are plotted in Fig. 3.4. At the top of the figure are the curves resulting from the radioactive gases released from the fuel, i.e., swept to the ion chamber by gas flowing over the fuel while operating in the BF-TT flow mode. These curves show decreasing dose rate regardless of the direction in which the pressure is changed. The decreasing dose rate is part of a superimposed transient in the release that is still in progress following a change in the power level in the rod from 12 to 13.5 kW/ft. The transient isotopic release measured at 1000 psig and reported previously[2] showed an initially high release rate following the step change in power level and then a gradual decay in rate toward a new but higher equilibrium level than had prevailed at 12 kW/ft. The decreasing dose rate thus appears to fit into the transient release pattern.

At the bottom of Fig. 3.4 are the curves that resulted from the radioactivity vented from the fuel rod, i.e., swept to the ion chamber by gas flowing across the vented end of the fuel rod while operating in the TT-TT flow mode. The strong effect of the pressure on the dose rate is apparent. At about 1000 psig, the ratio of the dose rate from released activity to vented activity is 261. The ratios of the released to vented activity at 200 and 300 psi are 30 and 51, respectively. Thus, the dose rate from the vented activity is 8.7 times greater at 200 psig and 5.1 times greater at 300 psig than it was at 1000 psig. It is concluded that the helium

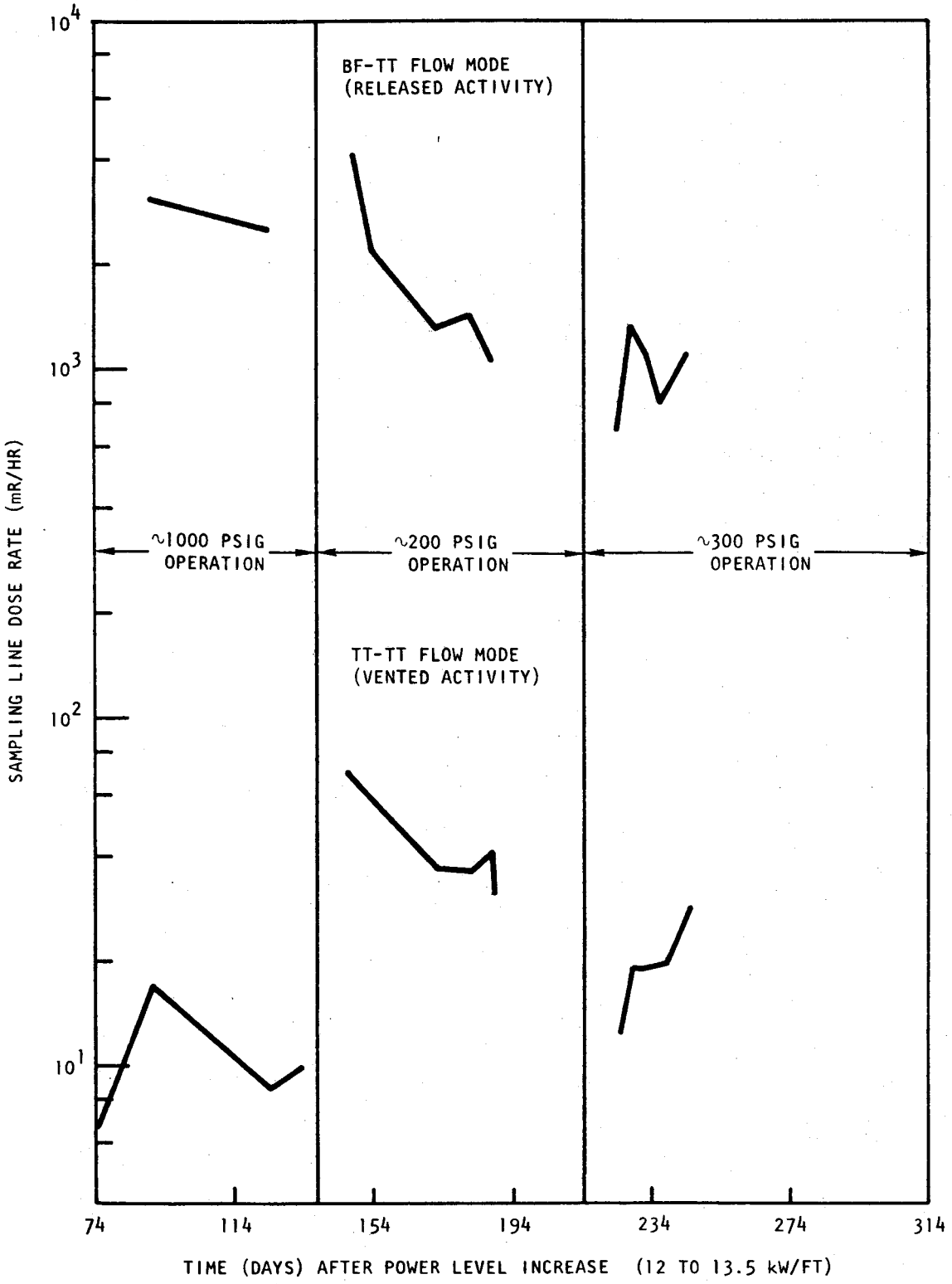

Fig. 3.4 Effect of internal fuel-rod gas pressure on release and venting of gaseous fission products

gas pressure in the GCFR is very effective in the control of radioactivity being vented from the fuel rod in the process of maintaining pressure equalization and that the ion chamber can be used at least as a crude but simple instrument to indicate the onset of a cladding leak, which would have the same effect as switching from the TT-TT flow mode to the BF-TT flow mode.

3.1.4. Power-cycling Analysis

Analysis of the expected release and venting of gaseous fission products during power cycling was performed for capsule GB-10. The results have been used as a basis for specifications for the power-cycling tests to be conducted.

The calculations given below describe the behavior of the fission-gas content within a defined volume in a fuel rod as a function of power cycling. The input data are based on known or approximated conditions in capsule GB-10. The assumptions made are that (1) there is complete mixing between the fission gas and diluent gas, (2) no fission gas is expelled from the volume during the power decrease via back diffusion, and (3) the diluent gas that enters the volume during power decrease contains no fission gases.

3.1.4.1. Power Decrease Half-cycle. Initially, the rod is at full power, P_f. The power then linearly decreases with time according as

$$P = P_f - kt \quad . \tag{3.1}$$

The rate of power change, k, is 3% of P_f per minute (5×10^{-4} P_f/sec). The rate of change of N, i.e., the number of fission-gas atoms contained in the fixed volume, is given by

$$\frac{dN}{dt} = R_p - \lambda N \quad , \tag{3.2}$$

where R_p is the release rate (atoms/sec) and λ is the decay constant (sec^{-1}) for the particular isotope that is being studied. R_p is dependent on the power and the temperature of the fuel, which in this case are

both dependent on time, and

$$R_p = \frac{3CP}{a}\sqrt{\frac{D}{\lambda}}\, e^{-\Delta H/2RT} \quad , \tag{3.3}$$

where C is a constant that is the product of the fission yield for a particular isotope and the number of fissions per second per kilowatt, D is the diffusion coefficient (in the fuel matrix) (cm^2/sec) for the isotope being studied, a is the grain size (cm), ΔH is the activation energy (J/mole), R is the universal gas constant (J/mole-K), and T is the absolute temperature (K).

The variation of temperature with power or time is given by

$$T = T_s + \frac{\Delta T_f}{P_f} P = T_s + \Delta T_f - \frac{\Delta T_f}{P_f} kt \quad , \tag{3.4}$$

where T_s is the temperature of the heat sink and ΔT_f is the temperature drop from fuel to heat sink at full power. Consequently, $T_s + \Delta T_f$ is the temperature at full power, T_f. Substituting this value into Eq. (3.4), we have

$$T = T_f - \frac{\Delta T_f}{P_f} kt \quad . \tag{3.5}$$

Substituting Eqs. (3.5) and (3.1) into Eq. (3.3), R_p becomes

$$R_p = \frac{3C}{a}\sqrt{\frac{D}{\lambda}} \exp\left[-\Delta H/2R\left(T_f - \frac{\Delta T_f}{P_f} kt\right)\right] (P_f - kt) \quad . \tag{3.6}$$

The occurrence of the t term in the denominator of the exponent in Eq. (3.6) makes the analytical solution of Eq. (3.2) extremely difficult.

A reasonable approximation of R_p, over the time range of interest here, was obtained by plotting ln R_p versus t. The function can then be estimated by a straight line, whose equation is given by

$$R_p = C_1 e^{-C_2 t} \quad , \tag{3.7}$$

where C_1 and C_2 depend on the isotope being studied. The solution of

Eq. (3.2) then becomes

$$N = \frac{C_1}{\lambda - C_2} e^{-C_2 t} + e^{-\lambda t}\left(N_0 - \frac{C_1}{\lambda - C_2}\right) \quad , \tag{3.8}$$

where N_0 is the number of fission-gas atoms in the volume at the beginning of the power decrease. At $t = 0$, this value is R_p/λ.

3.1.4.2. Power Increase Half-cycle. When the power is increased from its low point back to full power, the differential equation becomes

$$\frac{dN}{dt} = R_p - \lambda N - \frac{N}{n}\left(\frac{dn}{dt}\right) \quad , \tag{3.9}$$

where n is the number of diluent atoms in the volume and dn/dt is the rate of efflux of diluent atoms. From the ideal gas law, we have

$$n = \frac{P_r V}{Rt} \quad , \tag{3.10}$$

where P_r is the total pressure (which is a constant). By differentiation and substitution, we obtain

$$\frac{1}{n}\left(\frac{dn}{dt}\right) = \frac{1}{T}\frac{dT}{dt} \quad . \tag{3.11}$$

For the case in which the power is increasing, the temperature can be described by

$$T = T_f + \frac{\Delta T_f k}{P_f}(t - t_1) \quad , \tag{3.12}$$

where t_1 is the time required to reach the power minimum during the transient and t is the time measured from the beginning of the power increase half-cycle. Substituting Eq. (3.12) into Eq. (3.11) and differentiating, we obtain

$$\frac{1}{n}\left(\frac{dn}{dt}\right) = \frac{1}{\frac{T_f P_f}{\Delta T_f k} + t - t_1} \quad . \tag{3.13}$$

The variation of release rate with time can also be approximated in much the same way as described above, yielding a value of R_p equal to

$$R_p = C_1 e^{-C_2(t_1-t)} . \tag{3.14}$$

Substituting Eqs. (3.13) and (3.14) into Eq. (3.9) and solving the differential equation, we obtain

$$N = \left(\frac{1}{\frac{T_f P_f}{\Delta T_f k} + t - t_1}\right)\left\{\left(\frac{e^{-C_2(t-t_1)}}{C_2 + \lambda}\right)\left[\frac{T_f P_f}{\Delta T_f k} - t_1 + \frac{(C_2 + \lambda)\, t - 1}{C_2 + \lambda}\right]\right.$$

$$\left. + e^{-\lambda t}\left[N_1\left(\frac{T_f P_f}{\Delta T_f k} - t_1\right) + \frac{e^{-C_2 t_1}}{C_2 + \lambda}\left(t_1 + \frac{1}{C_2 + \lambda} - \frac{T_f P_f}{\Delta T_f k}\right)\right]\right\} . \tag{3.15}$$

The value of N_1 is obtained from the previous half-cycle, at $t = t_1$, from Eq. (3.8). For a number of cycles, the value for N_0 in Eq. (3.8) becomes the previous value of N calculated upon return to full power.

3.1.4.3. Computer Program. A basic program, BEAR, has been written to evaluate N during power transients. The program is intended for use on an interactive terminal and prompts the user for input. The data used for input is given below.

T_f = 1,700°F = 1,200°K,
T_s = 48°C = 321°K,
ΔT_f = 879°K,
P_f = 10.13 kW,
$D^{1/2}$(Kr) = 5.10×10^{-5} cm/sec$^{1/2}$,
λ(85m) = 4.38×10^{-5} sec^{-1},
λ(89) = 3.66×10^{-3} sec^{-1},
ΔH(Kr) = 1.62 eV = 37.4°K cal/mole,
R = 1.987×10^{-3}°K cal/deg-mole,
a = 8,000 μm = 0.8 cm,
C(85m) = 2.492×10^{11} atoms/kW-sec,

$C(89) = 7.038 \times 10^{11}$ atoms/kW-sec,

$k = 5.065 \times 10^{-3}$ kW/sec.

For approximations to $R_p = C_1 e^{-C_2 t}$,

C_1 (Kr-85m) $= 3.10 \times 10^7$ atoms/sec, C_2 (Kr-85m) $= 4.30 \times 10^{-3}$ sec^{-1},

C_1 (Kr-89) $= 9.30 \times 10^6$ atoms/sec, C_2 (Kr-89) $= 4.278 \times 10^{-3}$ sec^{-1},

The variation of N with cycle length and number of cycles has been evaluated for Kr^{85m} (4.4 h) and Kr^{89} (3.16 m) and the data are given in Table 3.3. The power changes used—10%, 20%, and 30%—correspond to half-cycle times of 200, 400, and 600 sec. It can be readily seen that when the half life is comparable to the half-cycle time, equilibrium is reached fairly quickly. On the other hand, when the half life is very much larger than the half-cycle time, equilibrium is not reached even after 25 cycles.

Table 3.3

VALUES OF N AT END OF EACH HALF CYCLE

	Kr^{85m}		Kr^{89}	
Cycle No.	Power Decrease N x 10^{11}	Power Increase N x 10^{11}	Power Decrease N x 10^9	Power Increase N x 10^9
	10% Power Change			
0	---	7.08	---	2.54
1	7.06	6.48	2.06	0.920
2	6.47	5.94	1.28	0.572
3	5.93	5.45	1.12	0.498
4	5.44	5.00	1.08	0.482
5	5.00	4.59	1.07	0.478
6	4.59	4.22	1.07	0.478
7	4.22	3.88	1.07	0.477
8	3.89	3.57	1.07	0.477
9	3.58	3.29	1.07	0.477
10	3.30	3.03	1.07	0.477
11	3.05	2.80	1.07	0.477
12	2.82	2.59	1.07	0.477
13	2.61	2.39	1.07	0.477
14	2.42	2.22	1.07	0.477
15	2.24	2.06	1.07	0.477

Table 3.3 (Continued)

Cycle No.	Kr^{85m} Power Decrease $N \times 10^{11}$	Kr^{85m} Power Increase $N \times 10^{11}$	Kr^{89} Power Decrease $N \times 10^{9}$	Kr^{89} Power Increase $N \times 10^{9}$
20% Power Change				
0	---	7.08	---	2.54
1	7.01	5.88	1.35	0.267
2	5.84	4.90	0.824	0.163
3	4.87	4.08	0.800	0.158
4	4.07	3.41	0.799	0.158
5	3.41	2.86	0.799	0.158
6	2.87	2.41	0.799	0.158
7	2.43	2.03	0.799	0.158
8	2.06	1.73	0.799	0.158
9	1.75	1.47	0.799	0.158
10	1.50	1.26	0.799	0.158
11	1.30	1.09	0.799	0.158
12	1.13	0.946	0.799	0.158
13	0.988	0.829	0.799	0.158
14	0.873	0.732	0.799	0.158
15	0.778	0.652	0.799	0.158
30% Power Change				
0	---	7.08	---	2.54
1	6.96	5.29	0.801	0.0696
2	5.22	3.97	0.526	0.0457
3	3.93	2.99	0.524	0.0455
4	2.97	2.26	0.524	0.0455
5	2.27	1.72	0.524	0.0455
6	1.74	1.32	0.524	0.0455
7	1.36	1.03	0.524	0.0455
8	1.07	0.813	0.524	0.0455
9	0.857	0.651	0.524	0.0455
10	0.700	0.532	0.524	0.0455
11	0.584	0.444	0.524	0.0455
12	0.497	0.378	0.524	0.0455
13	0.434	0.330	0.524	0.0455
14	0.386	0.294	0.524	0.0455
15	0.352	0.267	0.524	0.0455

The analysis was extended to calculate the number of cycles required to approach equilibrium for the Kr^{85m} case. The computer program was revised to test for equilibrium by calculating the fractional change of

the fission-gas content from end-of-cycle to end-of-cycle and comparing the result to a change indicator value. Three values of the indicator were chosen for current purposes: 0.01, 0.005, 0.0001. The same input data were used as in the previous calculation. The results are given below.

% Power Change	Indicator	N x 10^{10} (atoms)	Number of Cycles
10	0.01	4.72	53
10	0.005	4.48	61
10	0.0001	4.26	103
20	0.01	2.91	33
20	0.005	2.85	36
20	0.0001	2.79	57
30	0.01	1.97	24
30	0.005	1.94	27
30	0.0001	1.92	40

Two-volume Model. Previous analysis indicated that the "fresh" fission gases from the fuel region are not vented; they move back and forth in the upper blanket and shield region of GCFR fuel rods except under deep (power cycling) breathing conditions (changes > 30% of full power). The "front" between the "fresh" and "stale" gases is restricted to very short mixing lengths by the narrow gap between the pellets and the cladding and the very large length-to-gap ratio. A two-volume model, as described below, has been used to evaluate conditions to be expected in capsule GB-10.

In calculating the venting fractions for the power cycling experiment in capsule GB-10, the following model was assumed:

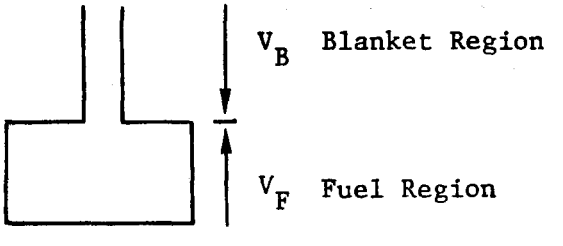

in which V_F is the free volume of the fuel region and V_B is the free volume of the blanket region. We will examine the relative magnitudes of these two volumes later. The length-to-diameter ratio, 1/D, in the blanket region is sufficiently large so that the frontal edge of gas coming from the fuel region is kept sharp. Complete mixing is assumed in the fuel region.

We will first consider the isothermal case, where the gas in the two regions is at the same temperature. At the end of the power decrease half-cycle, the temperature is a minimum and the number of moles of diluent gas (helium) in V_F is at a maximum. Thus, the expression for the total volume, V_T, of n moles of diluent gas becomes

$$V_T = \frac{nRT}{P_r} \quad , \tag{3.16}$$

where P_r is the total gas pressure, n is the total number of moles of helium in the free volume (V_F) of the fuel region at the lowest temperature of the power cycle, R is the gas constant, and T is the absolute temperature of the gas in the fuel region. The expressions for n and T are

$$n = \frac{P_r V_F}{R\left(T_F - \frac{\Delta T_F k t_1}{P_F}\right)} \quad , \tag{3.17}$$

$$T = T_F - \frac{\Delta T_F k (t_1 - t)}{P_F} \quad , \tag{3.18}$$

where T_F is the gas temperature at full power, ΔT_F is the temperature difference between the reactor pool water and the gas at full power, P_F is the full power, k is the rate of power change, and t_1 is the half-cycle time.

Substituting Eqs. (3.17) and (3.18) into Eq. (3.16), we obtain

$$V_T = V_F + \frac{V_F t}{\frac{P_F T_F}{\Delta T_F k} - t_1} \quad . \tag{3.19}$$

But the volume expanded out of the fuel region, V_E, is equal to $V_T - V_F$, so that

$$V_E = \frac{V_F t}{\frac{P_F T_F}{\Delta T_F k} - t_1} \quad . \tag{3.20}$$

Thus, the volume vented from the top of the blanket region, V_V, would be

$$V_V = \frac{V_F t}{\frac{P_F T_F}{\Delta T_F k} - t_1} - V_B \tag{3.21}$$

for values of $V_V > 0$. The relationship of V_F to V_B for the point at which $V_V = 0$ is given below for the end of the power increase half-cycle at various levels of power change.

% Power Change	V_F/V_B
10	12.7
20	5.8
30	3.6

This indicates that V_F must be at least 12.7 times V_B for any gas to be vented from the blanket region during a 10% power change (assuming that the gas in the blanket region is isothermal with the gas in the fuel region).

For the nonisothermal case, the displaced volume becomes

$$V_E = \frac{V_F t}{\frac{P_F T_F}{\Delta T_F k} - t_1} \left(\frac{T_B}{T}\right) \quad , \tag{3.22}$$

where T_B is the temperature of the blanket region and T is the temperature of the fuel region. The vented volume for the nonisothermal condition is $V_E - V_B$. From our interpretation of the data in the planning document for the GB-10 experiment,[3] $T_B \approx 350° = 623°K$. When full power

is reached, $T - T_F$ and $t = t_1$. We can then calculate the ratio of V_F/V_B to obtain a value of $V_V = 0$ at this point, which results in

% Power Change	V_F/V_B
10	24.4
20	11.2
30	6.85

The following calculations were made to estimate the free volumes in the fuel, blanket, and trap regions in the unirradiated state:

Region	Region Volume (cm^3)	Cladding Volume (cm^3)	Free Volume (cm^3)
Fuel	10.352	10.630	0.278
Blanket	2.370	2.434	0.064
Charcoal	1.029	1.197	0.168

It is assumed that flow through the charcoal is sufficiently fast that only the interparticle void is involved and that diffusion into the particle pores and adsorption there can be neglected.

If during irradiation the central void in the fuel is the major volume in the fuel region, then from Ref. (3) we can estimate the radius of the void to be 0.0914 cm (0.036 in.). Therefore, $V_F = 0.592\ cm^3$. If we assume that the fuel densifies to 100% TD, then the value of V_F would be $1.567\ cm^3$. The ratios of V_F/V_B calculated for various cases are:

	V_F/V_B	
	Fuel Central Void	Fuel Densification
Blanket	9.25	24.5
Blanket plus Trap	2.55	6.75

The results show that for the blanket–densified-fuel case, venting would be observed at power changes of 10% and greater. For the blanket plus trap case, venting would not be observed through the 30% power change regardless of the choice of V_F. For the blanket–central-void case, venting would be observed for power changes $\geq$ 20%.

Considerable experience exists which indicates that the failures of reactor fuel are more frequent during power-cycling or power-changing conditions than at other times or under other conditions.[4] Thus, in order to minimize the risk of capsule failure, the power-cycling tests in capsule GB-10 have been rescheduled from September 1974 to approximately the end of 1975.

3.2 INTEGRAL FUEL-ROD AND BLANKET-ROD BEHAVIOR

3.2.1. Fast-flux Irradiation Experiment F-1 (X094)

Irradiation of the encapsulated seven-fuel-rod F-1 (X094B) experiment has now achieved a maximum burnup exposure of 77,000 MWd/Te (8.3 at-%). Irradiation will continue to a maximum burnup of 125,000 MWd/Te, which is the new burnup goal for the experiment. The initially planned third interim examination has been eliminated because of the risk to the entire experiment that is inherent in carrying out the interim examination without the availability of spare capsules.

The revisions to the irradiation program were made to increase the yield of data from the experiment as follows:

1. One rod will be irradiated 25% beyond the maximum burnup of the GCFR reference design (100,000 MWd/Te) at the maximum reference cladding temperature (700°C).
2. One rod will be irradiated to the full maximum burnup of the GCFR reference design (100,000 MWd/Te) at the maximum reference cladding temperature.
3. Five rods will be irradiated to the average burnup of the GCFR reference design (75,000 MWd/Te) at the maximum reference cladding temperature.

Approval-in-principle for the above revisions has been received from the Division of Reactor Research and Development (DRRD). The F-1 experiment is now expected to reach the revised goal exposure by about the third quarter of FY-76.

Postirradiation examination of the rods removed from the F-1 experiment during the first and second interim examinations continued at ANL.

The results of biaxial gas-pressure-stressed creep rupture tests on 20% cold-worked stainless-steel fuel-rod cladding from rod G-3 of the F-1 (X094) experiment and on unirradiated controls are given in Table 3.4.

Table 3.4

CREEP RUPTURE TESTS ON ROD G-3 CLADDING

Test Specimen Identification	Exposure		Irrad. Temp. (°C)	Test Temp. (°C)	Test Stress (psi)	Time to Failure (hr)	Diameter Increase[a] (%)
	n/cm^2	Burnup (MWd/Te)					
Unirradiated control 1	-------	--	N.A.	550	83,700	68	5
Unirradiated control 2	-------	--	N.A.	700	32,100	24	9
Unirradiated control 3	-------	--	N.A.	700	25,900	107	7
G-3 upper blanket	0.7×10^{22}	--	480	550	83,700	1/4	2
G-3 upper plenum	0.3×10^{22}	--	460	550	83,700	28	1
G-3 bottom plenum	0.7×10^{22}	--	370	700	25,900	65	1
G-3 fueled region	2×10^{22}	27,000	700	700	25,900	37	1/2

[a]The approximate increases in diameter were obtained by taking micrometer readings at 1/2-in. intervals and extrapolating those values to the approximate point of rupture. This is not an accurate method of obtaining the strain at failure and thus these values should not be interpreted as indicating the actual ductility of the specimens, but rather as values to be used for comparison of the relative ductilities.

The results in Table 3.4 indicate a much larger reduction in rupture life as a result of irradiation at the lower test temperature (550°C) and higher stress (83,700 psi) than at the higher test temperature (700°C) and lower stress (25,900 psi). The results of the G-3 tests are compared with data from the LMFBR Materials Handbook in Fig. 3.5, and they appear to be in reasonable agreement. The creep rupture tests on cladding from rods G-1 and G-6 are currently under way.

The nondestructive testing at ANL of the G-2 fuel rod, which was irradiated to an exposure of 54,000 MWd/Te at a cladding temperature of 750°C and at a linear heat-generation rating of 15 kW/ft has been completed. In addition to the profilometry and gamma scanning, the rod was photographed at approximately 1X and eddy-current testing was performed. Visual examination of the G-2 rod showed no unusual results. Rod G-2 does have a change in appearance at the top of the fuel column similar to that previously observed in rod G-1. The shiny appearance changes to a satin or matte finish at the top of the fuel column; this condition extends approximately 3 in. above the top of the fuel column and then gradually returns to the shiny appearance.

Results of eddy-current scanning of G-2 to determine the condition of the cladding were similar to the results previously obtained for rods G-1, G-6, and G-7. The amplitude of the defect indications was somewhat greater than that on the previous rods. However, the previous results showed no correlation between the cladding attack observed metallographically and the results of the eddy-current testing. Efforts to improve the eddy-current scanning procedures have been held up because of delays in obtaining improved standards. New standards have recently been procured and reevaluation of the eddy-current testing will proceed as fast as the hot cell priorities at ANL will allow.

Results of the G-2 fuel-rod diameter measurements by profilometry (see Fig. 3.6) show a maximum postirradiation diameter of 0.3009 in. The results from above and below the core region indicate the original diameter of the cladding was 0.3004 in. Therefore, the maximum diameter change ($\Delta D/D_0$) was only about 0.15%. There are very small peaks in the diameter near the top and bottom of the fuel column. These are possibly

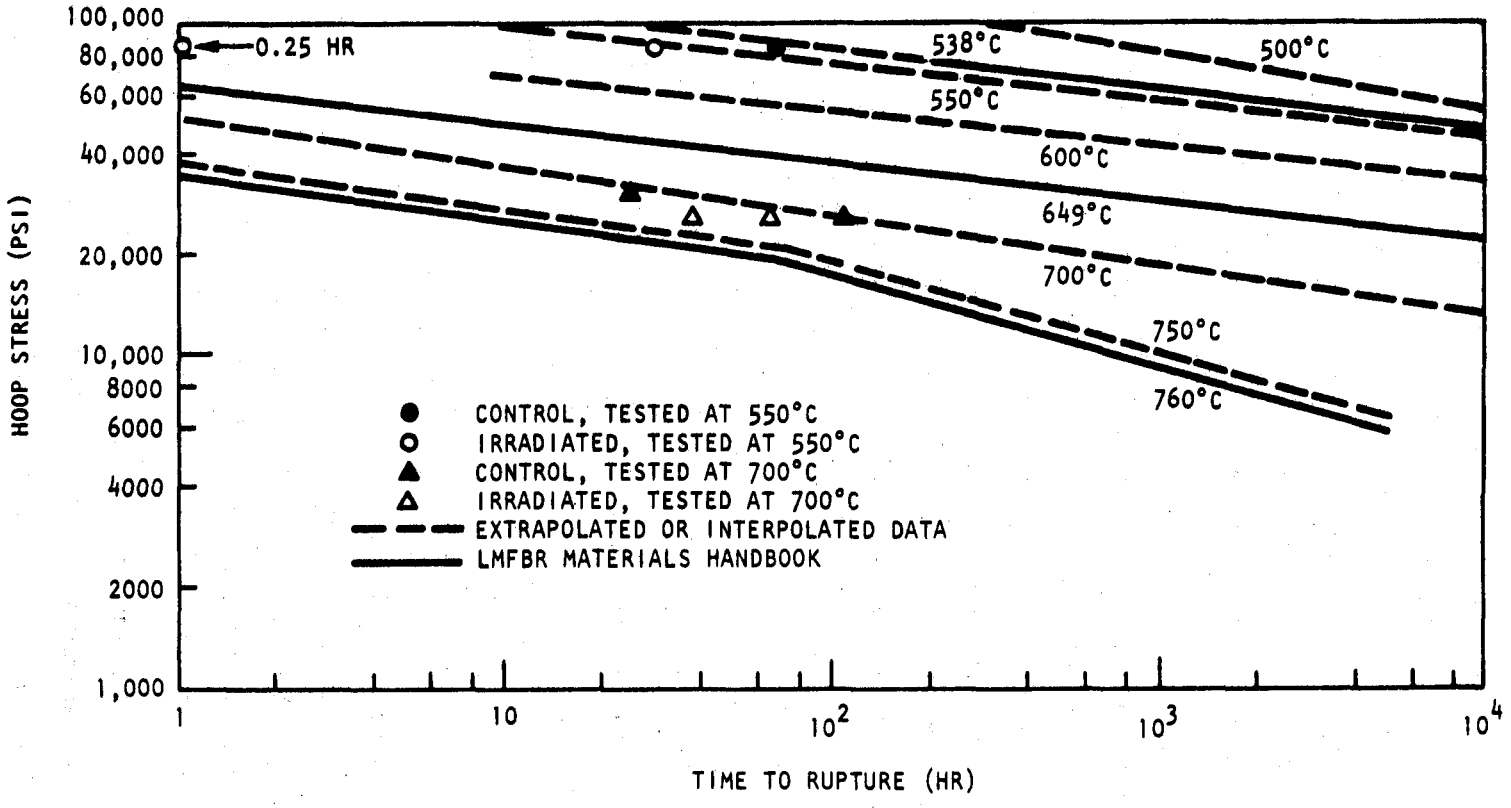

Fig. 3.5 Biaxial stress-rupture of 20% cold-worked Type 316 stainless steel

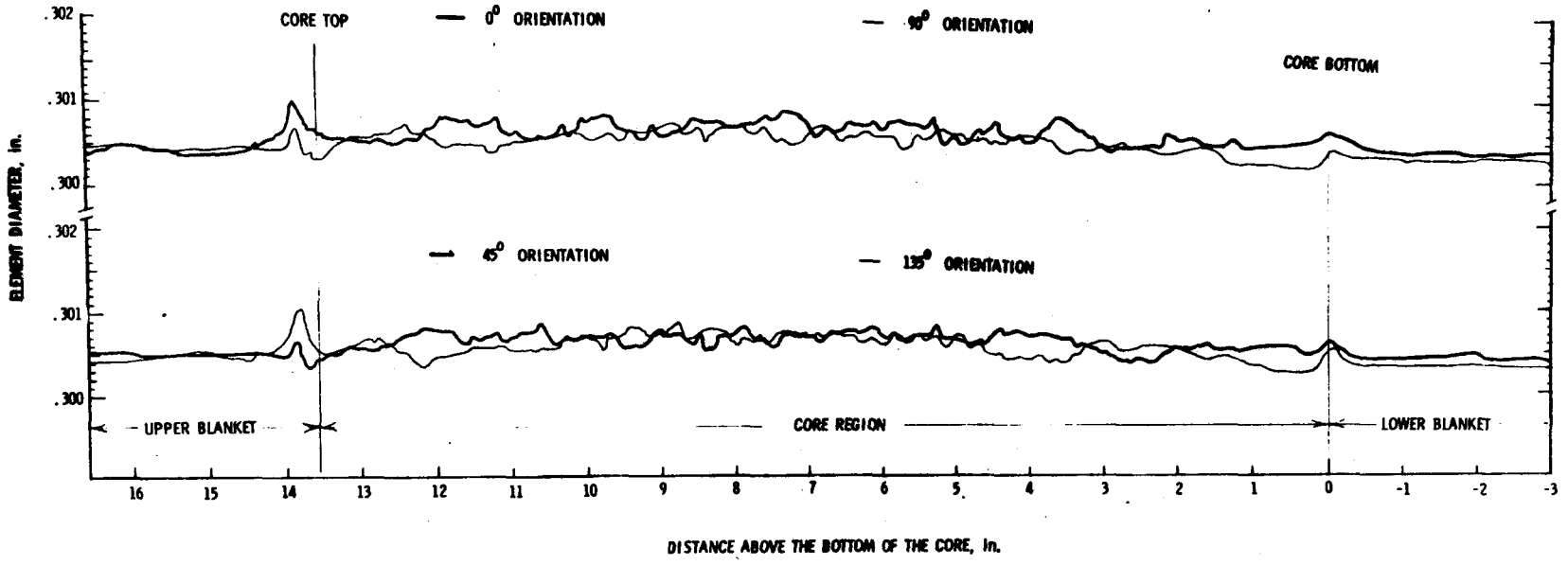

Fig. 3.6 Postirradiation diameter measurements (profilometry) for rod G-2

indications of reaction between cesium and the depleted UO_2 blanket pellets.

The gamma scans of the G-2 fuel rod (see Fig. 3.7) show cesium peaks at the top and bottom of the fuel and blanket interfaces. The highest relative activity for cesium is at the bottom of the fuel column, as it was in other rods of this series that were previously examined. The area under the peak, or amount of cesium present, may be greater at the upper end of the fuel column, particularly for rods G-6 and G-7. Peaks near the bottom of the fuel column, on the fuel side, were observed for ruthenium and rhodium. These are probably the result of metal fission-product ingots at the bottom of the central void, but they may also be an indication of fuel melting.

The depth of cladding attack versus temperature in sections examined from rods G-1 and G-6 is plotted on Fig. 3.8. The numbers in parentheses indicate the burnup in atom-% for the sections examined. Data from other experimenters are shown for comparison.

3.2.2. Fast-flux Irradiation Experiment F-3

Twelve fuel-rod capsules, the thermocouple filler strips for the subassembly, and the "as-built" addendum to the data package for the F-3 (X206) experiment have been shipped to and received at EBR-II. However, as they were not shipped in time for inclusion of the F-3 experiment in EBR-II Run 74, the experiment is now scheduled for insertion in EBR-II Run 75, which will start in early December 1974. As previously reported[2] these capsules have been designed for irradiation in an EBR-II core position (row 4) and will share a type J19A subassembly with an ANL Group-08 high-temperature chemistry experiment.

Of the twelve fuel-rod capsules now at EBR-II, ten will be inserted in the initial loading of the experiment. The other two fuel-rod capsules are spares. The EBR-II project requested dummy filler strips in order to perform a mockup subassembly flow test. The dummy filler strips were shipped to the EBR-II project at ANL-E, and it is reported that flow testing has been completed on the mockup subassembly.

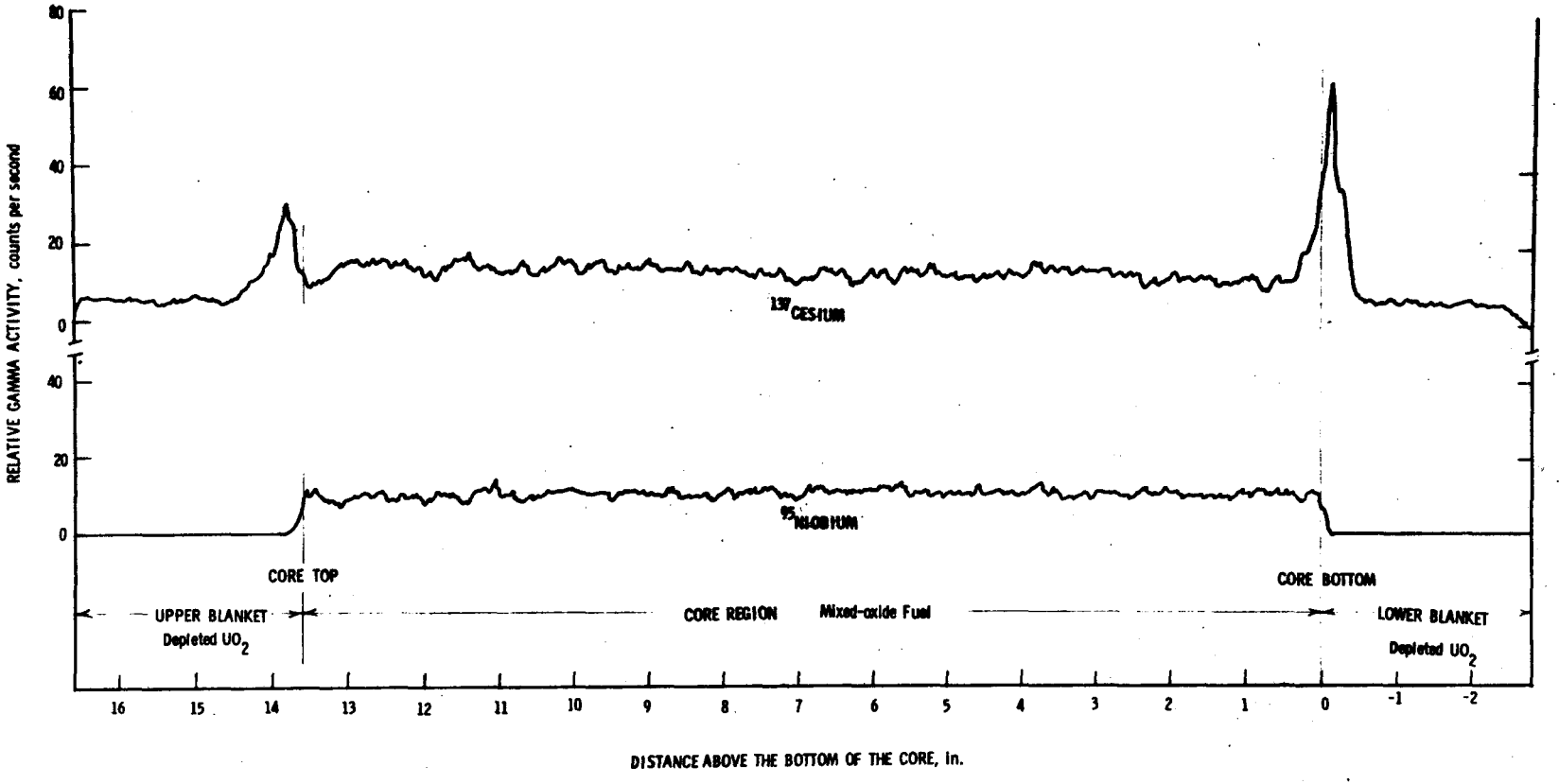

Fig. 3.7 Axial gamma scans of rod G-2

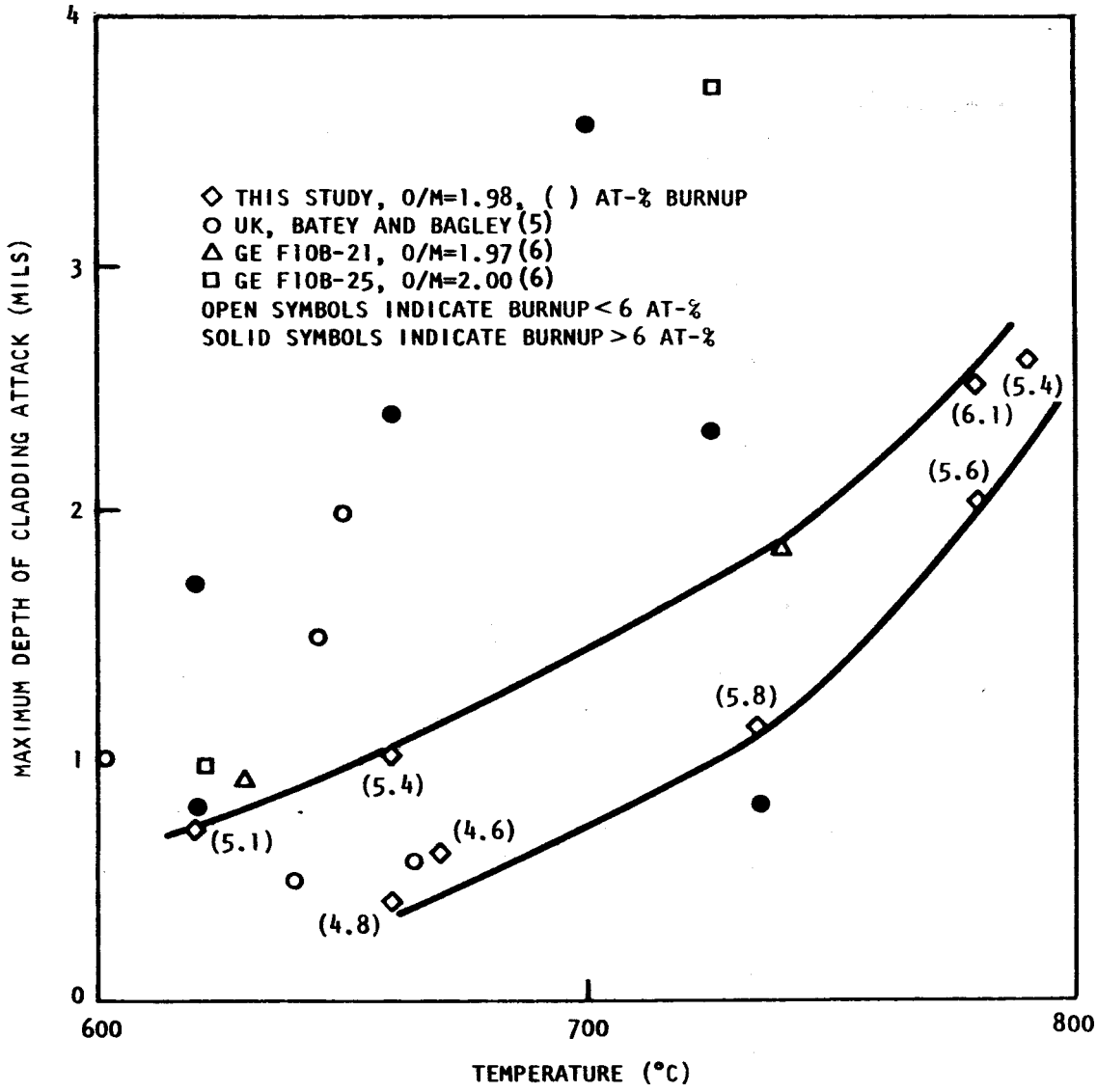

Fig. 3.8 Depth of cladding attack vs temperature in fuel rods G-1 and G-6 from the F-1 (X094) experiment

During assembly of the F-3 fuel rods, several nonconformances were noted and deviation requests were approved by GA:

1. The fuel column length of rod G-23 is 0.032 in. (0.8 mm) longer than the specified length; this was accepted as is.
2. The design of the fuel-rod top cap caused problems with the weld that joined the top cap and rod top plug; the cap was reworked to provide a vent hole and a plug for the vent.
3. The bond sodium level in the F-3 capsules was not within the specified tolerance range; this was accepted as is.
4. A dent was found in the G-19 capsule tube 1 in. below the capsule top end plug weld; this was accepted as is.
5. Capsules G-15, 16, 17, 18, 19, and 21 were oversize a maximum of 0.0025 in. (0.064 mm) about 9 in. (230 mm) above the capsule bottom; these were accepted as is.

Documentation supporting the decisions to accept the deviations as is or a design change is contained in the ANL-E addendum to the GA F-3 data package.

The x-ray radiographs taken of the assembled capsules at ANL-E after improvement in the sodium bond showed some relocation of the fuel-rod internal parts. Rod G-14 has a 0.35 in. (9 mm) gap between the top spacer tube and the bottom of the rod top plug. Rods G-15 and G-17 contain a small amount of unidentified material in the rod bottom void. In rod G-19, the rod bottom end-fitting is partially unscrewed from the capsule bottom fitting by 0.16 in. (4 mm). The subcapsule containing the shield material in rod G-29 is upside down and the rod is partially unscrewed, leaving a 0.04 in. (1 mm) gap. Rod G-21 has a 0.08 in. (2 mm) gap between the upper blanket and upper dosimeter holder and is partially unscrewed from the capsule by 0.12 in. (3 mm). Rod G-22 has a 0.06 in. (1.5 mm) gap between the lower spacer tube and the rod bottom end-fitting. Rod G-23 has a 0.18 in. (4.5 mm) gap between the top spacer tube and the bottom of the rod top plug and is partially unscrewed by about 0.03 in. (0.75 mm). The trap in rod G-27 has a speckled (unidentified material)

appearance with unidentified material in the rod bottom void and is partially unscrewed by 0.04 in. (1 mm).

3.3. CLADDING MATERIALS BEHAVIOR

3.3.1. GCFR Cladding Irradiation Tests

Inclusion of GCFR ribbed and smooth cladding specimens in a materials test experiment designed and fabricated by HEDL was reported in the preceding GCFR quarterly progress report.[1]

In addition to the cladding samples ribbed by etching that were incorporated in a HEDL experiment,[1] there is a possibility that some cladding ribbed by electrochemical grinding can be included in a material capsule that will be assembled by HEDL early in 1975. Additional cladding material is being ribbed by electrochemical grinding by the Swiss Federal Institute for Reactor Research (EIR). It is expected that the EIR ribbed cladding for approximately thirty test specimens will be shipped to GA from EIR in mid-November 1974.

Five samples previously ribbed by electrochemical grinding have already been shipped to HEDL. The specimens had ribs 0.004 in. (0.1 mm) high instead of the initially specified 0.006 in. (0.15 mm) height. GA, HEDL, and RRD concurred that the rib height was not an important parameter in the test and the samples will be incorporated into a materials test capsule by HEDL.

Irradiation of the initial series of forty GCFR cladding samples incorporated into a HEDL materials test capsule was started in EBR-II Run 74 on October 9, 1974.

3.3.2. Support of ANL Studies of Geometry Effects and Impurity Effects in Helium on GCFR Cladding

In FY-75, a study was initiated at ANL to determine the effects of rib geometry and the effects of impurities in a quasi-static helium on the behavior of GCFR fuel-rod cladding. Although the work at ANL is in a planning stage, ∿90 in. of cladding ribbed by etching and ∿130 in. of smooth cladding were supplied by GA to ANL for initial test purposes.

Also, to avoid end-fitting stiffening effects, a new, improved end-fitting design for fuel-rod cladding creep burst test specimens has been

proposed by GA, and some samples of the design have been sent to ANL for evaluation. The end-fitting design used by HEDL for cladding creep burst tests has also been submitted to ANL for evaluation. An instrumented welding test using the HEDL design (and a copper chill) showed that the heat-affected zone does not extend axially beyond 1/8 in. from the weld region.

3.3.3. Helium Loop Program at PNL

During this quarterly period, the objectives of this task were defined as follows:

1. To compare the effects of impurities in recirculating helium with the effects in quasi-static helium (at ANL) on the mechanical behavior of GCFR cladding.
2. To determine the corrosion and erosion behavior of ribbed tubing in recirculating helium containing impurities typical of the GCFR helium environment and to measure changes, if any, of the rib shape.
3. To determine the effects on ribbed cladding of the simulated GCFR steam inleakage accident (subject to evaluation of loop capability).
4. To provide samples with surface films typical of those generated in a GCFR helium environment for thermal conductivity measurements.

The scope of work to achieve the above objectives has been formulated and arrangements have been made to permit PNL to order the necessary impurity-level monitoring devices and equipment required for unattended operation of the loop. The report on the evaluation of techniques for monitoring pin-hole leaks and ruptures in pressurized cladding specimens has been received from PNL and it indicates that pin holes as small as 60 nm can be detected.

A visit was made to PNL (in association with a visit to HEDL) to discuss details of the program. The helium loop is suitable for fulfilling all of the objectives of the program except erosion testing. Mass

flow rates corresponding to GCFR conditions cannot be achieved in the helium loop, thereby limiting its usefulness for erosion testing. Evaluation of the loop capability for simulation of steam inleakage accidents is continuing. In the stress rupture tests, cladding test samples, both smooth and ribbed type, will be placed in the horizontal test section at 700°C and in the vertical test section at or near 600°C. The ribbed and smooth cladding will be provided by GA and PNL will fabricate the test specimens. Weight-change samples are being included in the test program to evaluate corrosion behavior. Thermal-conductivity specimens are also being included. In addition, tensile test specimens of various advanced alloys will be inserted in the test sections.

REFERENCES

1. "Gas-Cooled Fast Breeder Reactor Quarterly Progress Report for the Period May 1, 1974 through July 31, 1974," USAEC, Report GA-A13148, General Atomic Company, September 26, 1974.

2. "Gas-Cooled Fast Breeder Reactor Quarterly Progress Report for the Period November 1, 1973 through January 31, 1974," USAEC, Report GA-A12894, General Atomic Company, April 12, 1974.

3. Lindgren, J. R., et al., "Planned Thermal Irradiation of Manifold-Vented (U, Pu)O_2-fueled Rod in ORR Capsule GB-10," USAEC, Report Gulf-GA-A12596, Gulf General Atomic, April 1973.

4. Steinar, A. A. S., "Mechanical Interaction Between Fuel and Cladding," Nucl. Eng. Design, Vol. 21, 1972, pp. 237-253.

5. Batey, W., and K. G. Bagley, J. Br. Nucl. Energy Soc., Vol. 49, 1974.

6. Ellis, J. A., and R. F. Hilbert, "Fast-flux-irradiation Data on the Stoichiometry Dependence of Fuel/Cladding Chemical Interaction in Mixed-oxide Fuel Rods," Trans. Am. Nucl. Soc., Vol. 19, 1974, p. 134.

IV. NUCLEAR ANALYSIS AND REACTOR PHYSICS (189a No. 13127)

The scope of activities planned under this task encompasses the validation and verification of the nuclear design methods that will be applied to the GCFR core design. This will be done primarily by direct evaluation of the methods with a critical experiment program specifically directed toward GCFR development. Program planning and coordination activities, critical assembly design and analysis, and the necessary methods development will be carried out during the course of this program.

During the previous quarter, cross-section sets applicable to the core and blanket regions for the GCFR Phase I critical assembly were generated. Preliminary eigenvalue calculations were made with standard diffusion codes without provision for streaming corrections. Values of static parameters for the critical assembly were computed by first-order perturbation. Code development continued with evaluation of the MICROX spectrum code for fast-reactor design.

4.1. PREANALYSIS FOR THE PHASE I CRITICAL ASSEMBLY

The preanalysis for the parameters of the Phase I core has been essentially completed. Predictions of eigenvalue, kinetics parameters, spectral indices, and reactivity worths have been made utilizing a standard benchmark configuration. Comparisons with ANL analyses[1] have been made in many instances for identical calculational models. Using methods developed for adapting the Benoist formulation[2] to a two-dimensional anisotropic diffusion model, streaming corrections have been developed for the case where the radial diffusion coefficient D_r is equated to the perpendicular (to the plates of the ZPR unit cell) diffusion coefficient $D_\perp$, and for the case where the radial diffusion coefficient reflects an average of the x and y cell directions. (In all cases, the axial diffusion coefficient D_z is equated to the parallel diffusion coefficient $D_{||}$).

Selected parameters calculated for the Phase I assembly are listed in Tables 4.1 through 4.4 and are compared with ANL values.

Table 4.1

GCFR PHASE I CRITICAL ASSEMBLY KINETICS PARAMETERS

Parameter	ANL Methods			GA Methods		
	Without Streaming	With Streaming[a]	Percent Change	Without Streaming	With Streaming[a]	Percent Change
Beta-effective	3.2698×10^{-3}	3.2856×10^{-3}	0.5	3.0501×10^{-3}	3.1017×10^{-3}	1.7
Eigenvalue	1.0139	0.9949	-1.9	1.0285	1.0144	-1.4
Inhours/% $\Delta\rho$	981.79	979.92	-1.9	1041.11	1026.11	-1.4
Prompt neutron lifetime, sec	4.2749×10^{-7}	4.1924×10^{-7}	-1.9	4.7853×10^{-7}	4.7795×10^{-7}	-0.1

[a]Using $D_r = D_{\perp}$, $D_z = D_{||}$.

Table 4.2

GCFR PHASE I CRITICAL ASSEMBLY SPECTRAL INDICES AT CORE CENTER

Reaction Ratio Relative to ^{239}Pu Fission	ANL Methods			GA Methods		
	Without Streaming	With Streaming[a]	Percent Change	Without Streaming	With Streaming[a]	Percent Change
^{235}U fission	1.0032	0.9989	-0.43	1.0417	1.0379	-0.36
^{238}U capture	0.1349	0.1338	-0.82	0.1410	0.1401	-0.64
^{238}U fission	0.02967	0.03016	1.65	0.02898	0.02943	1.55
^{239}Pu capture	0.2065	0.2038	-1.31	0.2317	0.2292	-1.08
^{240}Pu capture	0.1805	0.1788	-0.94	0.1958	0.1942	-0.82
^{240}Pu fission	0.2429	0.2456	1.11	0.2293	0.2316	1.00
^{241}Pu capture	------	------	-----	0.2144	0.2127	-0.80
^{241}Pu fission	1.2742	1.2698	-0.35	1.3017	1.2979	-0.29
^{232}Th capture	0.2147	0.2123	-1.12	------	------	-----
^{232}Th fission	0.006415	0.006523	1.68	------	------	-----
^{233}U fission	1.4777	1.4724	-0.36	------	------	-----

[a]Using $D_r = D_\perp$, $D_z = D_{||}$.

Table 4.3

GCFR PHASE I CRITICAL ASSEMBLY REACTIVITY COEFFICIENTS FOR FUEL ISOTOPES

(10^{-5} Δk/k-kg)

Material	ANL Methods			GA Methods			
	Without Streaming	With Streaming[a]	Percent Change	Without Streaming	With Streaming[a]	Percent Change	With Streaming[b]
^{235}U	123.89	122.36	-1.2	124.4	125.1	0.6	124.56
^{238}U	-8.48	-7.95	-6.3	-9.541	-9.240	-3.2	-9.046
^{239}Pu	165.22	163.38	-1.1	161.1	162.0	0.6	161.4
^{240}Pu	24.86	27.23	9.5	22.71	23.57	3.8	23.79
^{241}Pu	------	------	----	223.0	223.3	0.1	222.0
^{242}Pu	------	------	----	17.71	18.56	4.8	18.69
^{232}Th	-17.93	-17.11	-4.6	------	------	----	------
^{233}U	213.68	210.50	-1.5	------	------	----	------

[a] Using $D_r = D_\perp$, $D_z = D_{||}$.

[b] Using $D_r = \frac{1}{2}(D_\perp + D_{||})$, $D_z = D_{||}$.

Table 4.4

GCFR PHASE I CRITICAL ASSEMBLY REACTIVITY COEFFICIENTS FOR STRUCTURE AND OTHER MATERIALS

(10^{-5} $\Delta k/k$-kg)

Material	ANL Methods			GA Methods			
	Without Streaming	With Streaming[a]	Percent Change	Without Streaming	With Streaming[a]	Percent Change	With Streaming[b]
H	------	------	-----	-1455	-1289	-11.4	-1190
He	-118.18	-114.91	-2.8	-98.69	-98.67	0	-98.25
Be	------	------	-----	-28.08	-26.40	-6.0	--------
10_B	-2182.6	-2082.7	-4.6	-2469	-2409	-2.4	-2370
C	------	------	-----	-21.14	-20.38	-3.6	-19.80
O	------	------	-----	-12.09	-11.72	-3.1	-11.42
Na	------	------	-----	-6.795	-6.643	-2.2	-6.526
Cr	------	------	-----	-5.122	-5.084	-0.7	-5.038
Fe	------	------	-----	-4.660	-4.607	-1.1	-4.561
Ni	------	------	-----	-7.994	-7.831	-2.0	-7.730
Mo	------	------	-----	-16.65	-16.34	-1.9	-16.15
Stainless steel	-6.15	-6.06	-1.5	--------	--------	-----	--------
Steam	-241.2	-220.8	-8.5	-173.6	-154.6	-10.9	-143.3
CH_2	-315.4	-272.2	-13.7	-227.2	-202.7	-10.8	-187.6

[a] Using $D_r = D_\perp$, $D_z = D_{||}$.

[b] Using $D_r = 1/2(D_\perp + D_{||})$, $D_z = D_{||}$.

An important aspect of the Phase I assembly is a limited-scope steam-entry experiment. The parameters of the experiment are listed in Table 4.5. In the first evaluation, the eigenvalue difference calculations with properly reaveraged cross sections for the polyethylene-filled core region gave a net worth of approximately -18 inhours (Ih) (assuming 1000 Ih/% $\Delta\rho$). The effect of not reaveraging the core cross sections with the moderated spectrum is small for this limited region. This is shown by the -17 Ih value in the second evaluation, which was given by the difference in eigenvalue by adding the appropriate C and H atom densities and cross sections to the core region in the base case for anisotropic diffusion. In each of these two cases, the central region reflects the effect of the perturbed real flux. By comparison, in the last evaluation, a first-order perturbation using unperturbed real and adjoint fluxes gave approximately -147 Ih.

Studies at General Atomic have shown the sensitivity of the hydrogen worth to the method of preparation of the ^{238}U cross sections, and thus the steam-entry experiment is expected to be a sensitive test of design methods.

Radial worth profiles of major nuclides are shown in Figs. 4.1 through 4.5. No particular aberrations are evident and the general shapes of the radial profiles are comparable to those generated at ANL.[1]

Some general conclusions that can be drawn from examination of the preanalysis comparison are:

1. The ANL methods result in generally larger changes to the parameter when anisotropic diffusion is accounted for.
2. There are significant differences in the calculation of the real flux spectrum, and the GA calculation is significantly softer, as seen from the ^{10}B and ^{238}U worths.
3. Differences in eigenvalue are apparent.
4. Changes in fissile worths when streaming is considered are small and positive by GA methods, but larger and negative by ANL methods.
5. Radial worth profiles are quite comparable.

A topical report describing the preanalysis of the Phase I GCFR assembly is in preparation and will be issued prior to criticality of the assembly.

Table 4.5

GCFR PHASE I CRITICAL ASSEMBLY STEAM ENTRY EXPERIMENT

Parameters

Entry region . . . . . Central 5 x 5 core, 24 in. height

Simulation material . . . . . H_2C, polyethylene, 0.035 g/cm^3

Equivalent steam density in 300-MW(e) GCFR . . . . . 0.0475 g/cm^3 (same hydrogen density)

	Isotropic Diffusion, $D_r = D_z$	Anisotropic Diffusion, $D_r = D_\perp$, $D_z = D_{\|\|}$
Base case	k = 1.028514	1.014442
With reaveraged steam region X-S	k = 1.027993	1.014090
Reactivity change, $\Delta\rho$	-49.28×10^{-5}	-33.83×10^{-5}
Correction for U_3O_8 resonance shielding	-15.57×10^{-5}	$\sim-15.57\times10^{-5}$
Net worth for insertion of H_2C	-33.7×10^{-5}	-18.26×10^{-5}
Net worth for H_2C, no reaveraging	-------	-17.3×10^{-5}
$\Delta\rho$ for H_2C by FOP[a]	-------	-146.8×10^{-5}

[a]First-order perturbation theory.

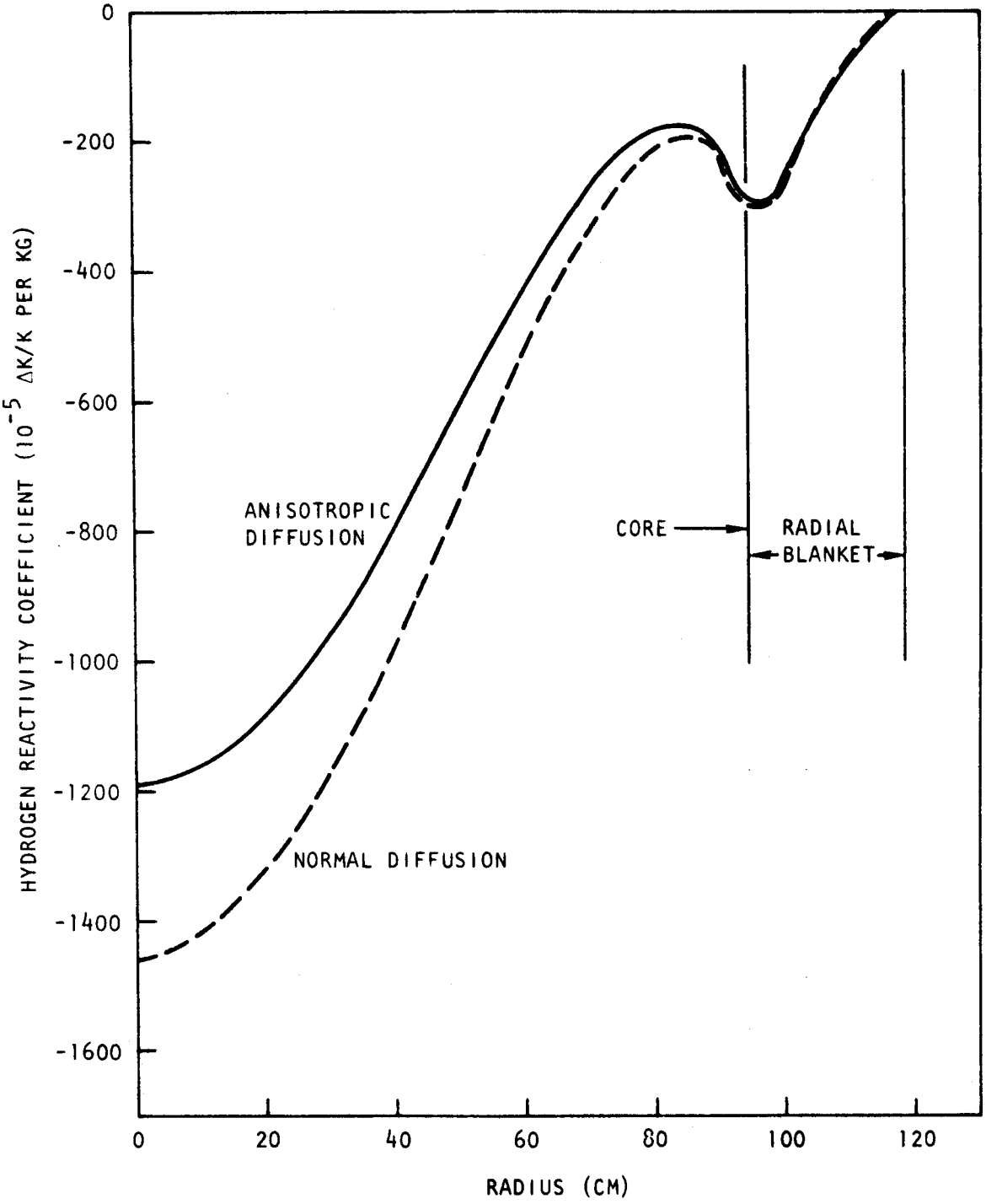

Fig. 4.1 Radial profiles of hydrogen worth in planned Phase I GCFR critical assembly

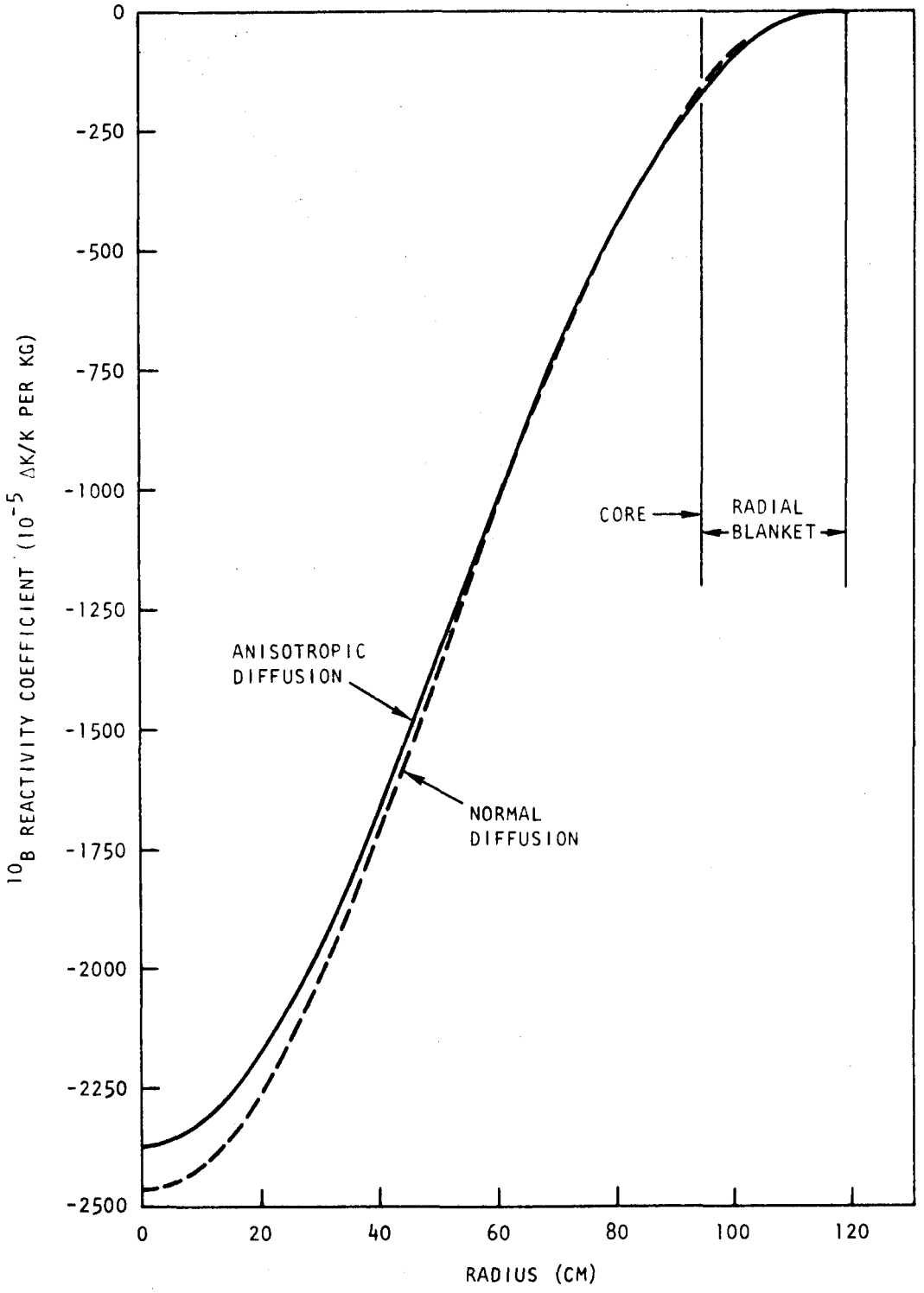

Fig. 4.2 Radial profiles of ^{10}B worth in planned Phase I GCFR critical assembly

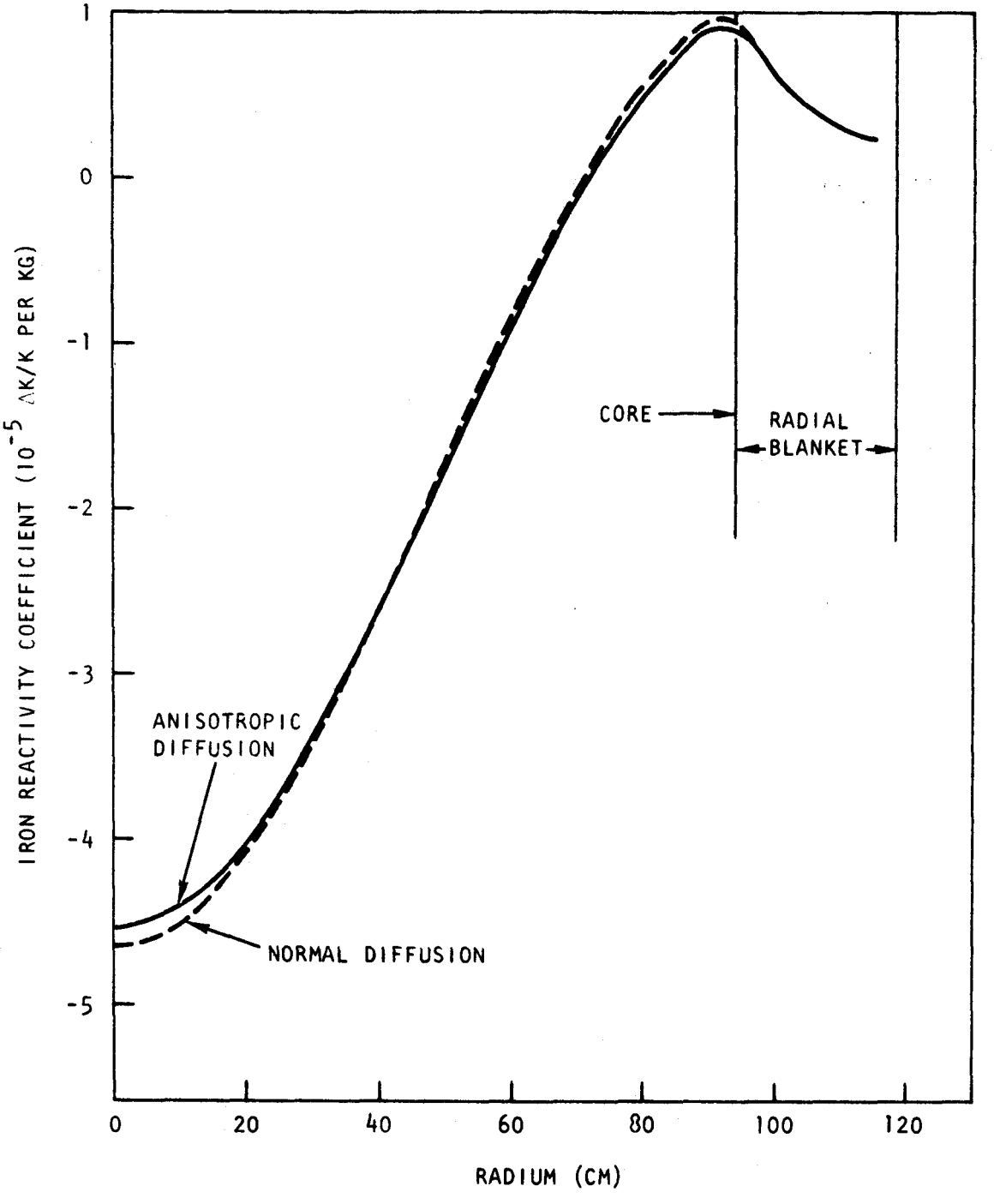

Fig. 4.3 Radial profiles of iron worth in planned Phase I GCFR critical assembly

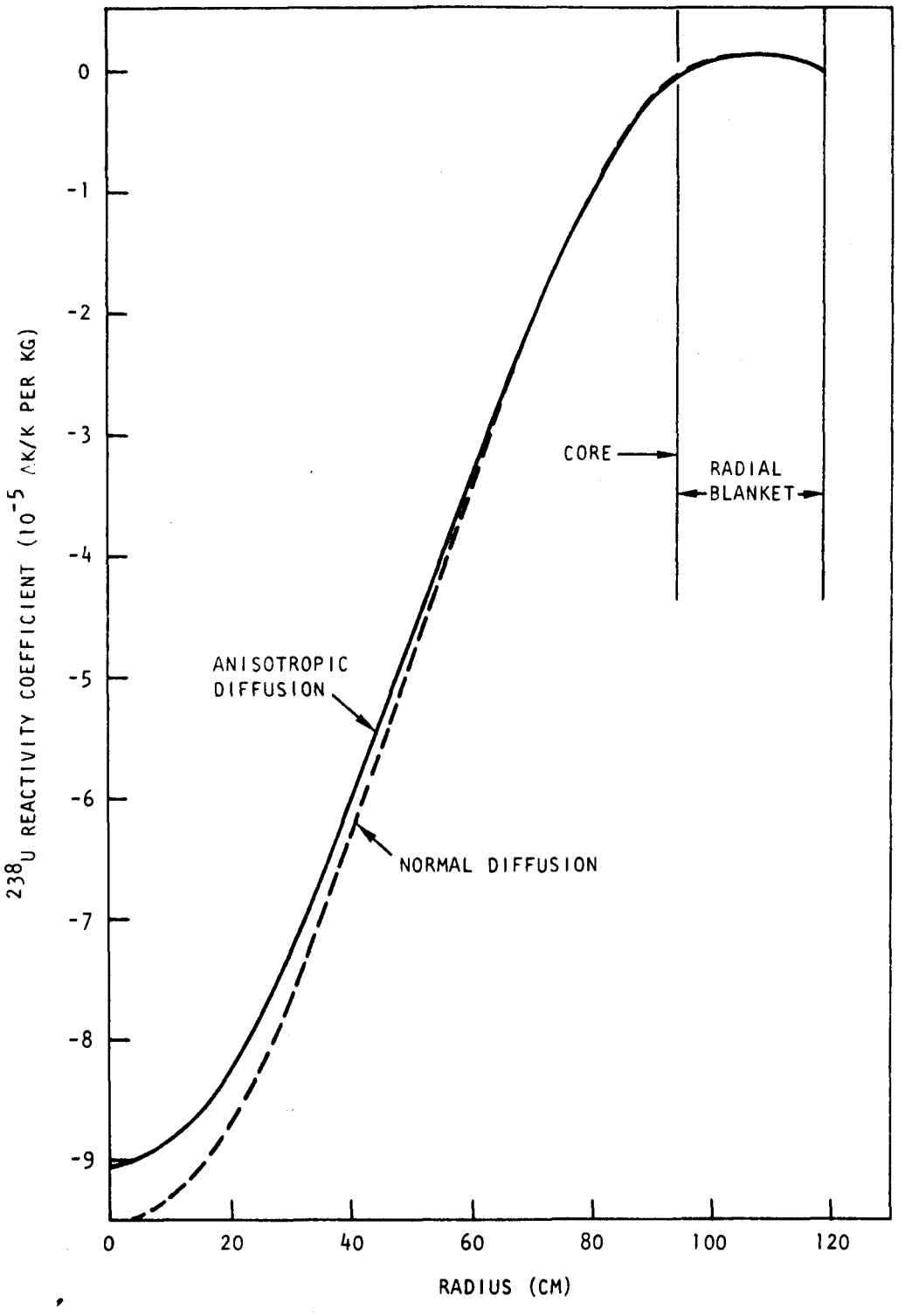

Fig. 4.4 Radial profiles of ^{238}U worth in planned Phase I GCFR critical assembly

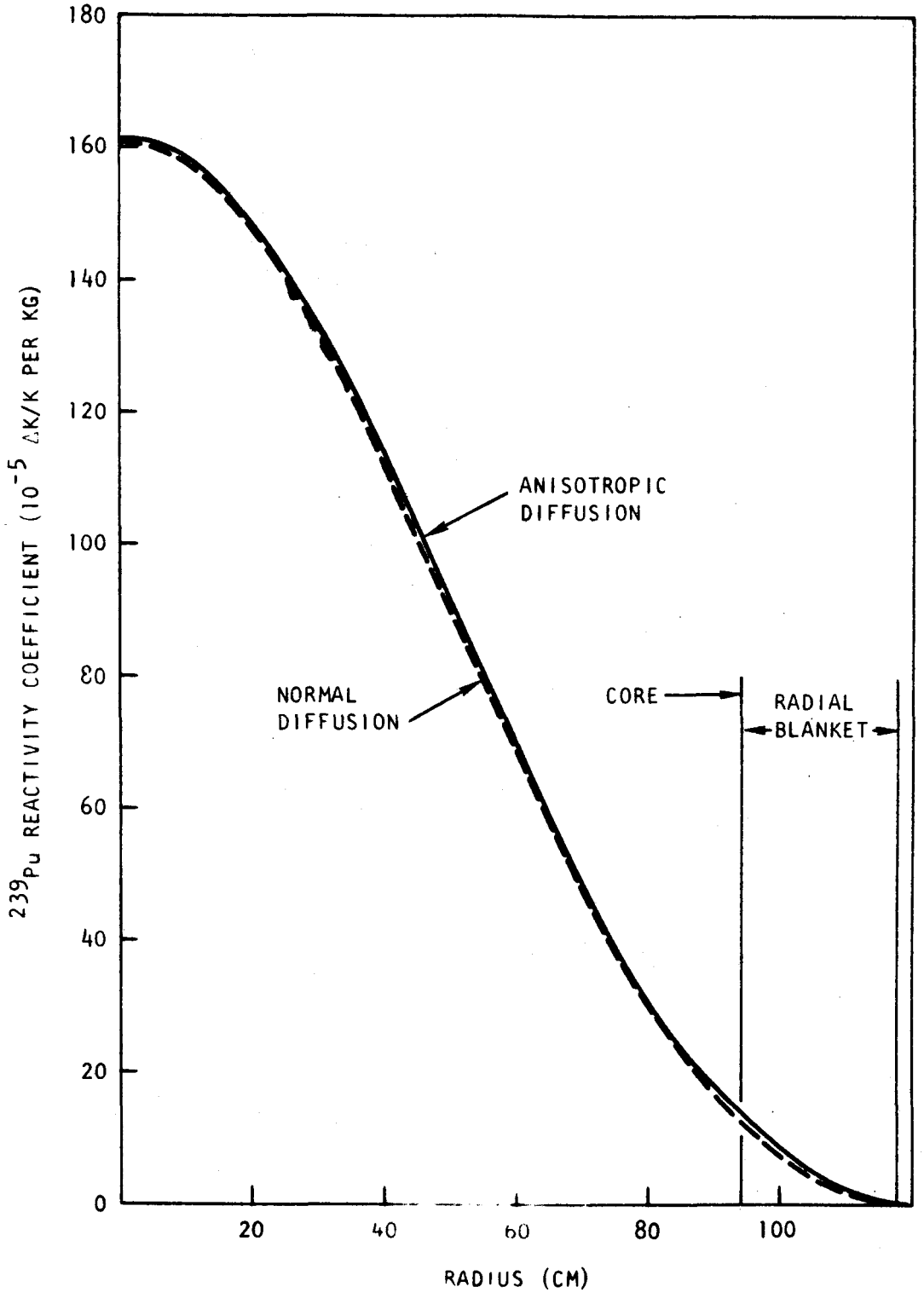

Fig. 4.5 Radial profiles of ^{239}Pu worth in planned Phase I GCFR critical assembly

4.2. METHODS DEVELOPMENT

Directional diffusion coefficients, i.e., diffusion coefficients that depend on direction, have been calculated for the Phase I critical assembly and for the 300-MW(e) GCFR plant. Directional diffusion coefficients are necessary because calculations and experiments with systems that involve large voids indicate that a value of $D = 1/3\Sigma_{tr}$ does not give correct results in that it underestimates the total leakage and overestimates k_{eff}. The augmented leakage due to the large void fraction is referred to as neutron streaming. Many attempts have been made in the past to make corrections for neutron streaming. Of those, the work of Benoist is the most general.[2] In the following, the method of Benoist is used for the calculation of directional coefficients which were subsequently utilized in the two-dimensional diffusion code ADGAUGE.

Benoist takes neutron streaming into account by writing the neutron leakage for a particular volume and energy group as:

$$L = \int_V \text{div } J(\vec{r})\, dV \quad . \tag{4.1}$$

The leakage may also be written as

$$L = \sum_k D_k B_k^2 \int_V \phi(\vec{r})\, dV \quad , \tag{4.2}$$

where k is direction, either x, y, z, or r,z. If proper expressions for $J(\vec{r})$ and $\phi(\vec{r})$ are introduced into Eq. (4.1) and the resulting equation is separated into k components, one obtains

$$D_k = \frac{\sum_i \sum_j V_i \phi_i \lambda_j P^*_{ij,k}}{\sum_i V_i \phi_i} \quad , \tag{4.3}$$

where the summations go over all the media of the volume, V, and

V_i = volume of medium i in the cell,

ϕ_i = flux of medium i in the cell,

λ_i = transport mean free path for medium i,

$P^*_{ij,k}$ = directional collision probabilities.

Equation (4.3) gives the directional diffusion coefficients, provided one calculates the directional collision probabilities, $P^*_{ij,k}$. These probabilities were defined by Benoist in such a way that combining Eqs. (4.1) and (4.2), the diffusion coefficients are given by Eq. (4.3). The physical meaning of the $P^*_{ij,k}$ will become clear if one looks at the average probability P^*_{ij}, where P^*_{ij} is the probability that a neutron starting in medium i will have a collision in medium j. Thus, the quantity $P^*_{ij,k}$ may be considered the "component" of P^*_{ij} along the direction k.

The directional diffusion coefficients have been calculated for the GCFR and the ZPR Phase I unit cells.

The GCFR unit cell consists of two media: fuel, which is a cylinder of radius a, and a void of radius b surrounding the fuel. The diffusion coefficient is given by

$$D_k = \frac{\lambda_i}{3}\left\{1 + \frac{b^2 - a^2}{b^2}\left[1 + \frac{b - a}{\lambda_i}(Q_k + Q'_k) + \frac{b^2 - a^2}{a^2}\,\frac{(1 - \eta_i w_k)^2}{1 - \eta_i T_k}\right]\right\}, \quad (4.4)$$

where λ_i is the transport mean free path in the fuel and $\eta_i = a/\lambda_i$. The definition of the functions Q_k, Q'_k, w_k, T_k is given by Benoist. A computer program has been written for the calculation of D_k for any number of energy groups.

For the 300-MW(e) GCFR, the parameters that were used for the cell are

$$a = 0.358 \text{ cm}, \qquad b = 0.537 \text{ cm}.$$

The results for the ten-group directional diffusion coefficients are given in Table 4.6.

The ZPR cell consists of plates and is described by plane geometry. For Phase I, a cell in the core, the axial blanket, or the radial blanket consists of 16, 13, or 12 regions, respectively. If x is the axis perpendicular to the plates, the y and z directions are parallel to the plates and it is in these directions that neutron streaming takes place.

The diffusion coefficient is given by Eq. (4.3), with k being x or z (or y). The probabilities $P^*_{ij,k}$ have been calculated with a computer

Table 4.6

DIFFUSION COEFFICIENTS AND DIRECTIONAL MODIFIERS CALCULATED FOR THE GCFR CELL

(Average core composition)

Group	D_{Hom}[a]	D_r/D_{Hom}	D_z/D_{Hom}
1	5.0724	1.0102	1.0206
2	4.3359	1.0120	1.0243
3	3.3435	1.0157	1.032
4	2.2428	1.0238	1.0488
5	1.9640	1.0273	1.0562
6	1.5290	1.0357	1.0736
7	1.4555	1.0376	1.0776
8	1.0306	1.0547	1.1130
9	1.1177	1.0473	1.0976
10	1.0287	1.0548	1.1133

[a] $D_{Hom} = 1/3\Sigma_{tr,Hom}$, $\Sigma_{tr,Hom}$ is the transport cross section for the homogenized cell.

program written by P. Kier[3] of ANL and modified at GA. The results of the calculation are given in Table 4.7, where $D_{\perp}$ is the diffusion coefficient for a direction perpendicular to the plates and $D_{||}$ is the diffusion coefficient for the direction parallel to the plates. The ANL results are also listed for comparison.

REFERENCES

1. Bohn, E. M., Argonne National Laboratory, Private Communication, November 7, 1974.

2. Benoist, P., "Streaming Effects and Collision Probabilities in Lattices," Nucl. Sci. Eng., Vol. 34, 1968, p. 285.

3. Kier, P. H., Argonne National Laboratory, Private Communication, August 1974.

Table 4.7

DIRECTIONAL DIFFUSION COEFFICIENTS FOR ZPR PHASE I GCFR ASSEMBLY

	Core						Axial Blanket				Radial Blanket			
	D_{Hom}		$D_{\|\|}/D_{Hom}$		$D_{\perp}/D_{Hom}$		$D_{\perp}/D_{Hom}$		$D_{\|\|}/D_{Hom}$		$D_{\perp}/D_{Hom}$		$D_{\|\|}/D_{Hom}$	
Group	ANL	GA	ANL	GA	ANL	GA	ANL	GA	ANL	GA	ANL	GA	ANL	GA
1	4.6957	4.5744	1.0584	1.0620	1.0019	1.0020	1.0010	1.0012	1.0354	1.0438	1.0010	1.0010	1.0294	1.0302
2	4.0378	3.9301	1.0743	1.0744	1.0029	1.0028	1.0016	1.0017	1.0459	1.0550	1.0014	1.0014	1.0378	1.0379
3	3.3596	3.1497	1.1043	1.1003	1.0045	1.0045	1.0033	1.0033	1.0744	1.0809	1.0027	1.0027	1.0585	1.0579
4	2.3231	2.1615	1.1592	1.1524	1.0095	1.0097	1.0080	1.0081	1.1210	1.1309	1.0066	1.0065	1.1022	1.0970
5	2.0744	1.8268	1.1738	1.1563	1.0125	1.0120	1.0094	1.0085	1.1270	1.1238	1.0077	1.0069	1.1048	1.0859
6	1.6531	1.3567	1.1842	1.1792	1.0167	1.0179	1.0097	1.0108	1.1142	1.1241	1.0087	1.0096	1.0931	1.0811
7	1.7533	1.4399	1.1787	1.1739	1.0150	1.0164	1.0110	1.0121	1.1270	1.1409	1.0094	1.0101	1.1036	1.0951
8	1.0258	1.1280	1.1801	1.2132	1.0237	1.0258	1.0145	1.0199	1.1035	1.1447	1.0170	1.0186	1.0880	1.0940
9	1.1483	1.0606	1.1965	1.2348	1.0252	1.0306	1.0114	1.0193	1.1032	1.1742	1.0123	1.0163	1.0848	1.1159
10	0.9727	0.7549	1.2299	1.2782	1.0365	1.0486	1.0130	1.0254	1.0993	1.1874	1.0150	1.0215	1.0839	1.1161
11	0.4872	------	2.4394	------	1.5772	------	1.0099	------	1.0828	------	1.0118	------	1.0588	------

V. PRESSURE EQUALIZATION SYSTEM FOR FUEL (189a No. 13715)

The technology to support the design and construction and the reliable, safe, and maintainable operation of pressure equalization systems for GCFRs is being developed. The technology developed for the fuel purge system of the Peach Bottom HTGR is being extended for application to GCFRs. Design models and computer codes for design and performance evaluation are being developed and verified by test programs. Quantitative design input information is being gathered with respect to (1) transient flow to maintain the pressure balance across the cladding of the fuel rods, (2) fission-product-transport mechanisms and their relative importance during steady and transient operations, (3) the extent and composition of radioactivity vented to the storage traps and reactor coolant, and (4) the monitoring of the radioactivity flowing through the system to indicate the location of leaking fuel elements and to monitor leak-rate changes. First-of-a-kind components are being developed based on a reference GCFR demonstration plant design to determine feasibility, practicality, fabrication processes, quality control, inspection procedures, and cost.

5.1. FUEL-ELEMENT AND VENT-CONNECTION-SEAL TEST PROGRAM

In the GCFR reference design, the fuel, control, and blanket elements and their vent connections are sealed to the grid plate by clamping the conical surface of the elements to the matching surfaces in the grid plate with a force sufficient to effect a seal and to support the elements, which are cantilevered from the grid plate. These element seals must function at the coolant-pressure difference between the reactor core inlet and exit plenums. The effectiveness of the seals over the life of the core is uncertain, not only because each element may be rotated or relocated several times over its useful life, but also because the seals must be effective in a high-purity, high-temperature helium environment while

subject to mechanical, vibrational, and thermal effects. Most of the uncertainties are expected to be resolved in a two-part test program: (1) a materials screening test program for the prevention of static adhesion of mated fuel-element and grid-plate parts and (2) leakage tests of fuel-element and vent-connection seals to the grid plate. Current progress in these activities is given below.

5.1.1. Static Adhesion Tests

The element-seal test program includes a simulation test of small-scale samples of conical seal parts clamped together and tested in a hot helium environment. The test will simulate the conditions of a full-scale fuel element clamped to a grid plate.

The first 3,000-hr static adhesion test was started on August 26, 1974, in helium flowing at 50 cm^3/hr at 300°C and with impurities of 9,000 μatm of H_2 and 90 μatm of H_2O. The 316 stainless steel parts were photographed by scanning electron microscopy (SEM) at 37 times power to characterize the surface prior to testing. Four SEM pictures were taken of each of the 36 conical surfaces. Three typical photographs of the samples with an 8-, 16-, and 32-μin. surface are shown in Fig. 5.1. Each couple was leak-checked on a helium mass-spectrometer leak detector to establish a sealing index before testing was initiated. These examination tests will be repeated at the conclusion of testing, which is expected to be in late January 1975.

The procurement of alternative materials, Inconel 718 and Type 304 stainless steel, for static adhesion testing has been initiated. Inconel 718 is considered to be an alternative fuel element material and would be tested with both the reference Type 316 stainless steel and the alternative grid-plate material, Type 304 stainless steel. The current tests are being conducted with both the simulated grid-plate and the element test parts made of Type 316 stainless steel.

5.1.2. Seal Leakage Testing

Fuel element and vent connection seals are being tested for leakage using full-size test pieces at reactor operating temperature in an impurity-controlled helium environment. The test pieces are clamped together at

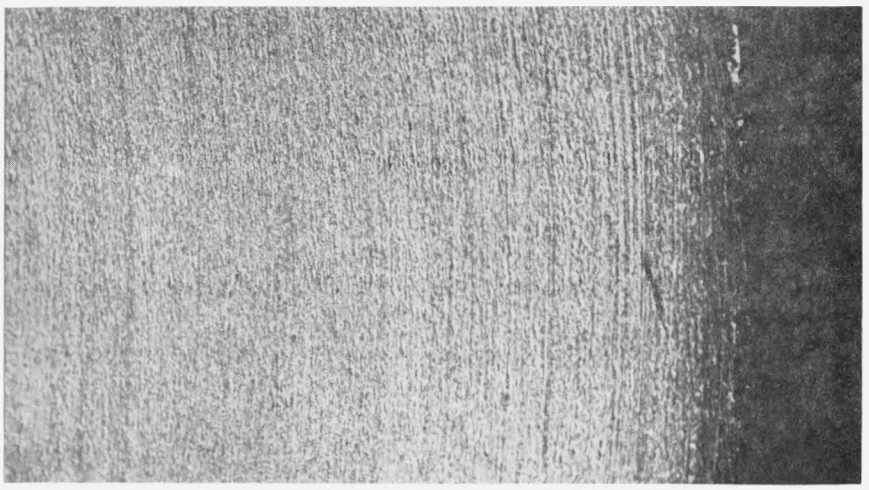

32- in. surface
(35X)

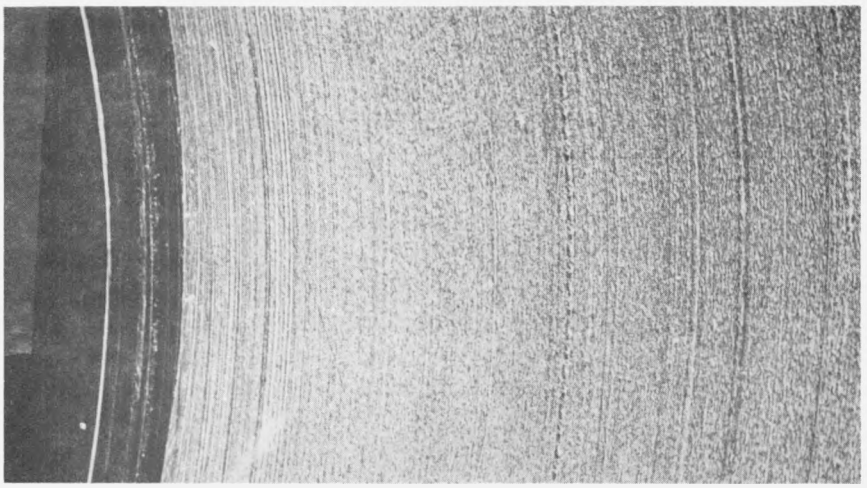

16- in. surface
(35X)

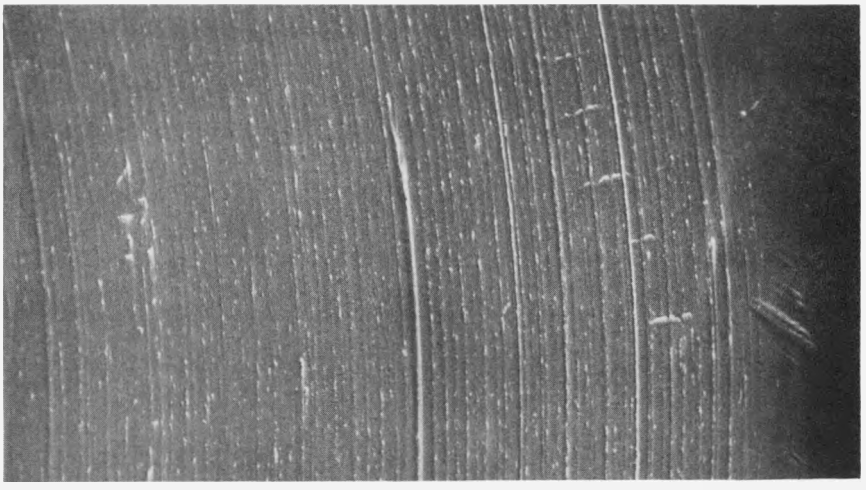

8- in. surface
(35X)

Fig. 5.1 Scanning electron micrographs of conical surface static adhesion parts

their matching conical surfaces to form metal-to-metal seals. The parameters being tested for their effects on the leakage rate are the cone-angle tolerance, surface finish, and clamping force.

The first leakage tests were started during this quarterly reporting period. The first test series being conducted is of conical seal parts that have the following specifications:

Surface finish: 8 μin. AA
Grid-plate cone angle: 30° 4' ± 1/2'
Element cone angle: 29° 56' ± 1/2'

During leak-checking at room temperature with a clamping load of 2,500 lb and a pressure differential across the seal of 40 psi, the element seal leakage rate was observed to be less than 10 ft^3/hr. The tests at temperature (300°C) were then initiated according to test procedures. The first test indicated a leakage rate of 200 ft^3/hr or higher at a clamping load estimated to be about 2,000 lb and at a pressure differential of 10 psi. The leakage through the seal is very sensitive to the load in this range of clamping load.

The system was then cooled to room temperature to investigate the reasons for the large change in leakage. At room temperature, with the test parts remaining inside the autoclave, the leakage was still in the range of 200 ft^3/hr or higher. The parts were then taken out of the autoclave and rotated 180°. At this position the leakage was again low and less than 10 ft^3/hr. A series of leakage measurements at various clamping loads and pressure differentials were taken at this position at room temperature. The data were corrected for the effect of temperature, which is a viscosity correction for volumetric flow rate. The preliminary data are plotted in Fig. 5.2. The specified allowable design leakage rate for the element seal is 200 ft^3/hr. The corrected clamping load is the load cell reading corrected for the gas pressure differential load, which tends to reduce the surface-bearing stress between the clamped conical seal parts. It is noted that the leak rate is more sensitive to clamping load than it is to pressure differential. Further correlations will be made when more test data are obtained.

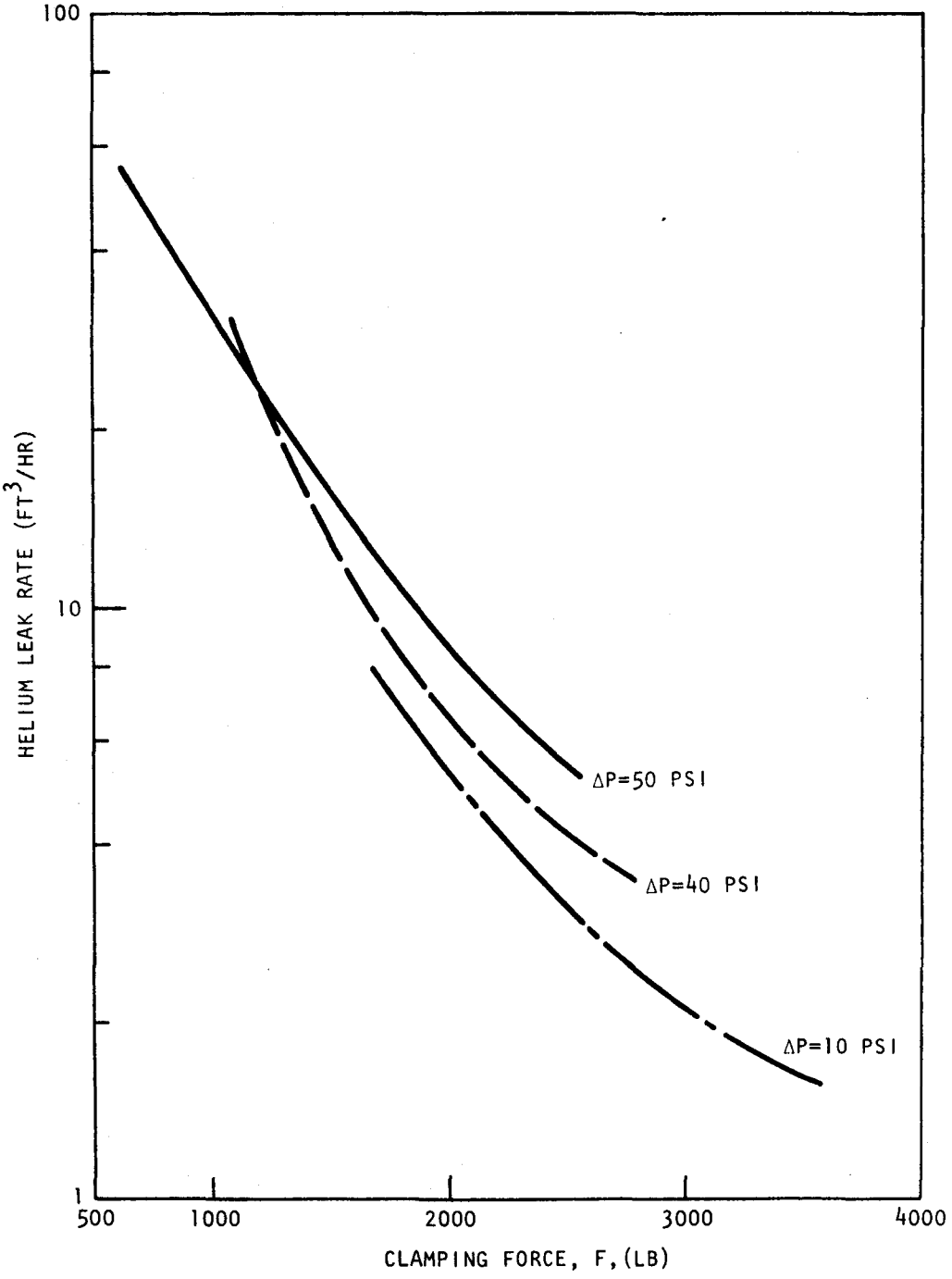

Fig. 5.2 Preliminary test data from GCFR element seal leakage test

The parts were then again rotated 180° and the higher readings again prevailed. Also, the leakage seemed to be much higher on the side where the vent connection leakage had been low ($\sim$1.3 ft^3/hr). It was decided to reinspect the parts to determine if they were oval or "egg-shaped" or if misalignment of the clamping rod was causing some offset between the parts. An ovality of 0.0007 in. was found in the element cone. The clamping load center was within tolerance. The conical surfaces are being remachined.

The set of test parts from another vendor were inspected and found to be out of tolerance on the cone angle. These parts will be stress-relieved before final machining to bring them into tolerance, since stress relaxation may have caused the ovality found after testing the first set of parts at elevated temperature.

5.2. COMPUTER CODE DEVELOPMENT AND ANALYSES

Two codes are currently being developed for analyses of the PES: (1) a transient flow network code and (2) a radiation detection and gamma-spectrum-monitoring instrumentation design and performance code called COUNT.

Prior to FY-74, a steady-state flow network code, FLAC, was adapted and applied to the PES with good results. Development of this code has resumed and is directed toward transient flow network design and analyses. Development of the COUNT code is a continuation of its development as part of the subtask to design and install an on-line Ge(Li) gamma spectrometer on capsule GB-10. Activity on each of the code developments is reported below.

5.2.1. Transient Flow Network Code

The PES is designed to prevent or minimize contamination of the reactor coolant system by gaseous and volatile fission products that may be vented from the fuel. The PES is also designed with a large number of monitor lines and cross-connections through which the vented fission products are swept to the storage traps in the helium purification system (HPS). The resulting flow network shown schematically in Fig. 5.3 has

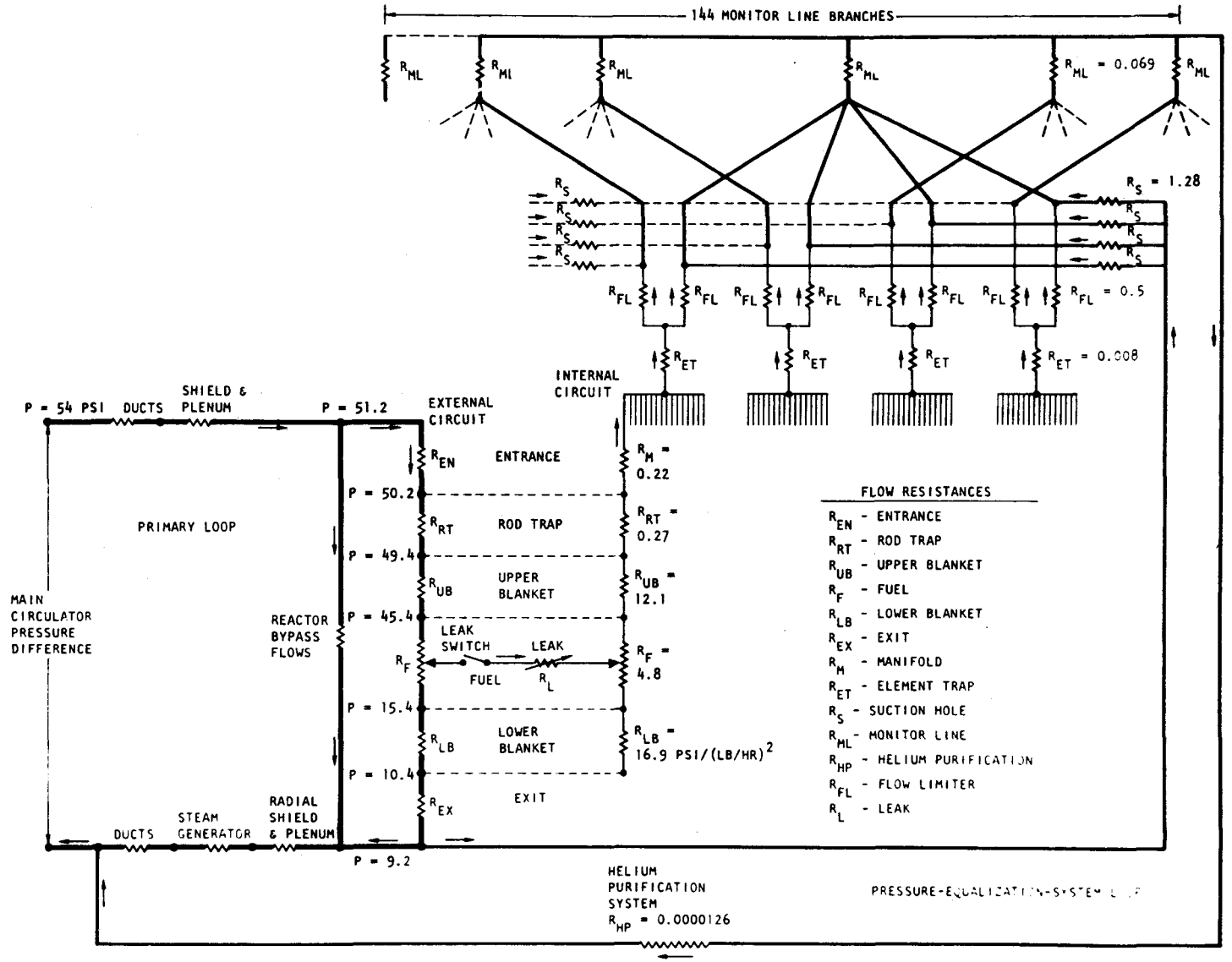

Fig. 5.3 Pressure equalization system flow network and its relationship to the primary coolant circuits

been analyzed under a number of steady operating conditions that will normally occur in the plant operation.[1] Also, some analysis of individual components under transient conditions has been performed to determine general characteristics, such as depressurization time constants. However, transient analyses of the flow network are necessary to design the PES for transient operations, including normal plant load variations that will result in fuel-element breathing, normal transfer to shutdown, depressurization for refueling, and during refueling operations. Analyses of the PES during coolant depressurization up to and beyond the design-basis accident (DBA) depressurization rates are also necessary to verify the design and establish design margins and define development activities. A computer code is needed as a design and performance analysis tool that can be applied to the GCFR type of flow network. That is, it is a flow network with a very high flow-rate coolant stream at very high absolute pressure and small differential pressure, coupled to small PES network streams, a relatively large PES volume (HPS unit in the PES), and many low-resistance cross-connections. Any existing flow network codes will probably require modification to be applicable to GCFR flow networks. It is expected that existing analytical methods and machine computer techniques will be applicable.

A comprehensive literature survey concerning transient one-dimensional flow phenomena has been completed. This survey indicates that several operational transient isothermal pipe network codes have been developed and are available from the gas pipeline industry; however, the exact limitations of transient lumped subvolume codes currently available should be ascertained.

The primary objectives of this effort were to survey and evaluate the current state of the art of solution methodologies and the availability of existing computer codes pertaining to transient compressible-flow networks with friction and heat-transfer effects included. All of the methodologies considered were surveyed with respect to flow problems applicable to the GCFR PES requirements. In particular, a transient network code was thought to be a logical extension of existing steady-state network codes. Moreover, the literature survey was performed cognizant

of future requirements for analysis of transient flow in GCFR PES networks. A summary of existing operational network codes and an evaluation of current unsteady-flow solution methodologies and related support material is presented below.

5.2.1.1. Transient Flow Codes Currently Available at GA.

RATSAM: This is an unsteady-flow (quasi-steady for given incremental time step) lumped subvolume-node code that was developed to evaluate transient thermodynamic behavior of the primary coolant system of a large HTGR during depressurization accidents. In addition, the dynamic behavior of the circulators and heat transfer between the coolant, the core, and the steam generators is determined. The flow between nodes is assumed to be subsonic and turbulent. This type of program is quite typical of current codes utilized to solve transient flow problems.

North American Aviation - Multiple Venting Program[2] (documentation and program listing only): This multiple venting program is a lumped-node compressible-flow program that evaluates the quasi-steady conservation equations formulated for computing the internal thermodynamic conditions of a system of reservoirs connected by orifices and/or pipes, which are labeled conductors. The presented methodology takes into account frictional line losses, heat transfer to the system, and consideration of mixtures of gases other than air. An iterative solution may be required during each time step, depending on the pipe entrance and exit pressure ratios and whether the pipe exit Mach number is known. This approach is typical of flow conditions governed by Fanno or Rayleigh lines. Heat transfer is evaluated using the Reynold's analogy.

ODUF TRW Systems Group[3]: ODUF is a one-dimensional, unsteady-flow code developed for studying transient flow of a perfect gas in a duct with constant area (allowances can be accommodated for fractional area variations), including friction and heat-transfer effects. The conservation equations are solved using the method of characteristics. Presently, the code is restricted to the open-end conditions, such as inflow and outflow, and a movable boundary, such as a piston.

5.2.1.2. Transient Flow Network Codes. In recent years, the natural-gas pipeline industry has provided the primary motivation for development of transient gas-flow network codes. The codes resulted from a need to generalize steady-flow network codes in order to simulate more accurately the dynamic response of pipeline networks to transient pressure and/or flow-rate temporal demands. Flow in the network was assumed to be subsonic and isothermal and to be contained in constant-area ducts; the equation of state of the flowing gas was assumed to be that of a perfect gas modified by a compressibility factor. The conservation-of-momentum equation did not include an inertial term, although it did include provision for a pipe-reach elevation change.

Four basic documented programs evolved in the period 1965 to 1971. Two used the explicit finite differencing technique in the solution of the differential equations: PIPETRAN,[4] developed by Electronic Associates, Inc., under contract to the American Gas Association; and SATAN, developed at the London Research Station of the Gas Council.[5] These explicit techniques were limited by the usual stability difficulties unless temporal and spatial step sizes were restricted. Each incremental time step, Δt, was limited to a pipe reach, $\Delta \chi$, divided by the isothermal speed of sound of the fluid, c_t, and hence slowly varying transients (hours-days) in long pipes (miles) were studied or, for example, helium at 1000°F and pipe reaches of the order of 10 ft, in which the incremental time steps must be less than 2 milliseconds. Two reported implicit programs—the G.E. Simulator, developed by General Electric Co., and CAP, developed at the Engineering Research Station of the Gas Council[6]—had the disadvantage of large storage requirements for large pipe networks since during each time step, a system of simultaneous equations had to be solved.

The intent here is to report only existing documented codes; several other investigators have reported studies using the method of characteristics, differencing techniques, and/or combinations of methodologies. These studies are summarized in following sections under specific solution methodologies. In addition, it should be noted that these codes, though valid for unsteady flow in networks, do not include spatial accelerations and thus are limited to flows with small velocity changes along a given reach, which is generally the case for gas transmission lines.

5.2.1.3. Computer Literature Search.

1. Nuclear Safety Information Center (NSIC): A NSIC computer search yielded no information concerning unsteady-gas network codes. The search provided several references applicable to two-phase transient fluid flow and heat-transfer codes.

2. Computer Software Management and Information Center (COSMIC): The COSMIC search (initiated through NSIC) yielded no information for unsteady pipe network systems. The Boeing Company program MFS-443 will determine steady-state flow of a compressible gas in a piping system.

3. Defense Documentation Center (DDC): No generalized unsteady compressible network codes were located. Documented unsteady-flow codes are directed to specific rocket-related hardware.

4. National Aeronautics and Space Administration (NASA): One search yielded eight items, but none was applicable to unsteady networks. A second search was keyed to alternate search words and yielded eighty references concerning unsteady compressible flow. The second search listed considerable work concerning compressible, unsteady flow in ducts. References 7 and 8 concerning unsteady flow codes and unsteady flow in branched ducts should be obtained and reviewed.

5.2.1.4. Transient-flow Solution Methodologies. Numerical analysis of the hyperbolic differential equations governing unsteady flow is based on finite-differencing techniques (explicit and implicit), method of characteristics, combinations of the first two techniques applied to a given system, and, finally, what will be identified as signal theory techniques. Explicit finite-differencing techniques have been successfully utilized in one-dimensional network problems. However, more recently, Forester[9] has presented several algorithms using unevenly spaced grids for two-dimensional pipe-flow configurations, such as bends or tees, that may be utilized with one-dimensional spatial unsteady systems to provide additional local flow field information.

In addition to the implicit differencing codes, Wylie, et al.,[10] demonstrated that implicit finite differencing schemes could be used for analysis of unsteady-flow pipe networks. The solution, though not limited by stability constraints for large time steps, did require the usual increase in computer storage capacity. This type of analysis was later extended and combined with the method of characteristics for more efficient solution of pipe networks. Recently, a University of Michigan group has returned to the classical technique generally applied to the solution of hyperbolic partial differential equations, i.e., the method of characteristics. The basic advantage of the implicit technique for solving hyperbolic equations is that for fast transients, short time steps may be used, resulting in an increase in information concerning pressure pulses.

The method of characteristics (MOC) has been utilized for solving unsteady-flow problems and is extensively reported in the literature. Generally, the method has been applied to single pipes; however, Stoner has successfully applied Streetor's hydraulic waterhammer MOC work to isothermal gas network problems.[11] Stoner excluded spatial inertial terms, yet included elevation gradients in the momentum equation. Since spatial inertial terms were removed, the hydrocarbon gaseous flow velocities were limited to 30 FPS. More recently, Yow has incorporated an inertia multiplier with the MOC technique that then allows for inclusion of spatial accelerations, yielding an increase in solution efficiency for slow-speed transients.[12] Current unsteady network MOC solutions are restricted to one-dimensional isothermal flow of a perfect gas with included steady-state friction formulations. An inherent disadvantage of MOC network solutions is the difficulty in developing simple pipe exit boundary conditions. Branch nodes and pipeline components are assumed to be points of zero inertia.

The method of characteristics has also been successfully applied to one-dimensional compressible, nonhomentropic flow of a perfect gas with included heat transfer and steady-state friction in constant-area ducts (or dA/dx must be small). Complexity in solution technique is incurred because two compatible ordinary differential equations (ODE) along characteristic slopes and an additional ODE along the particle pathline

characteristic must be solved for each time step. The work of E. Wright[13] and that of R. Benson[14] demonstrate typical MOC techniques for nonhomentropic flow in single ducts. V. K. Jonsson, et al.,[15] have combined the MOC technique with finite differencing methods, thus yielding solution variables at fixed locations along the duct, a decided advantage when compared with many previous MOC studies. The characteristic lines were located in the physical plane by linear interpolation between grid points and then used to convey information to the lattice point of the time-space domain for the next incremental time step. The MOC technique can be quite effectively applied to single-duct problems; however, the method is presently of only limited utility for complex network systems.

F. T. Brown[16] has applied a quasi method of characteristics with included frequency-dependent wall shear and heat transfer for pipelines. This work stresses the need for considering time dependency when applying steady-state friction and heat-transfer formulations to transient problems. However, the incurred solution complexity, though germane, is not warranted for present codes when compared to the other simplifications presently used in existing unsteady-flow codes. Several other works have been presented in the literature concerning the dynamic behavior of transmission lines, but, generally, they are restricted to single constant-area long-pipeline reaches.

H. H. Rachford and T. Dupont[17][18] have successfully used variational methods to study gas pipeline systems. Their technique is valid for isothermal flow of a perfect gas in networks with frictional, elevation, and inertial terms included in the momentum equations. Approximately 100 processor seconds per simulated hour on a CDC-6600 computer was required for a 1,000-pipe network problem. This method is essentially a second-generation technique for pipeline network problems and will be of considerable utility in the future.

5.2.1.5. Conclusions and Recommendations.

1. A comprehensive literature survey concerning one-dimensional transient flow phenomena has been completed and pertinent references have been cataloged.

2. Several operational transient isothermal pipe network codes have been developed and are available from the gas pipeline industry.

3. Exact limitations of currently available transient lumped subvolume codes at GA should be ascertained to prevent acquisition of inferior methodologies.

4. The computer code FAT, which is a transient version of FLAC,[19] and the RATSAM code will be further examined and one code will be selected for trial application to simplified PES transient flow network analysis.

5. The MIDAS code,[20] utilizing a digital simulation of analog computing, will be applied on a trial basis for comparison with either the FAT or RATSAM codes, whichever is selected.

5.2.2. COUNT Code

The COUNT code is being developed for design and performance analysis of the GCFR type of radiation-monitoring instrumentation that will be used to indicate the occurrence of a leak in a fuel element, to uniquely locate the leaking element in the core array, to estimate the leak rate, and to monitor the changes in leak rate with time. This is a unique design feature of the GCFR and thus no applicable codes are available. The signals generated by the detection instrumentation result from a mixture of fission-product gases being swept through the monitor station by helium flowing through the PES monitor lines. The gas mixture and the relative amounts of the isotopes change according to leak conditions. Also, the isotopes emit their radiation according to their decay schemes, which in some cases are quite complex. Machine computer processing is necessary to manipulate the large quantities of data that are involved in the computations.

In FY-74, options for planar and coaxial Ge(Li) detectors were added to the COUNT code, which was then used to help design a monitor for capsule GB-10 which contained a pressure-equalized and vented GCFR fuel rod. Data taken with this monitor (an on-line gamma-ray spectrometer) are now available; data will continue to be taken during FY-75. These data will

be used as a basis for further development and verification of the COUNT code.

Calibration data for three of five source-chamber-collimator-detector arrangements were received from ORNL late in the reporting period. The principal difference in each arrangement is the size of the collimator hole. The hole size may have secondary effects, i.e., beyond the geometric relationship of the source chamber and detector in that regions of exposure are changed with each collimator. Analysis of the calibration data and revisions to the code are in progress.

A typical comparison of calibration data to the empirical correlations taken from the literature and used in COUNT is shown in Fig. 5.4. The calibration data have been converted to analytical expressions by fitting polynomial equations to curves drawn through the calibration points. Two expressions are determined for each collimator arrangement, one expression for photons with energies of $E \leq 160$ keV and another for energies of $E > 160$ keV. These equations are of the form

$$\ln \varepsilon = A + B \ln E + C(\ln E)^2 \quad ,$$

where ε = efficiency of the counting system (counts/photon/cm),

E = gamma photon energy (keV),

A, B, C = coefficients required to fit the experimental calibration curves.

The values of A, B, and C for each collimator arrangement are given in Table 5.1. These coefficients were determined by least-squares fitting via the computer at ORNL. To replace the empirical analytical expressions taken from the literature in COUNT by the resulting polynomial equations for ε, the following correlation was identified:

$$\frac{2 r_c V_s}{\ell_s 4} (r_c/d)^2 \, \eta = \varepsilon \frac{V_c}{\ell_s} (d/d_c)^2 \quad ,$$

where V_s = volume of the source chamber exposed by the collimator (cm^3),

r_c = radius of the collimator (cm),

d = separation distance between source and detector centerlines (cm),

η = photopeak detection efficiency (counts/gamma),

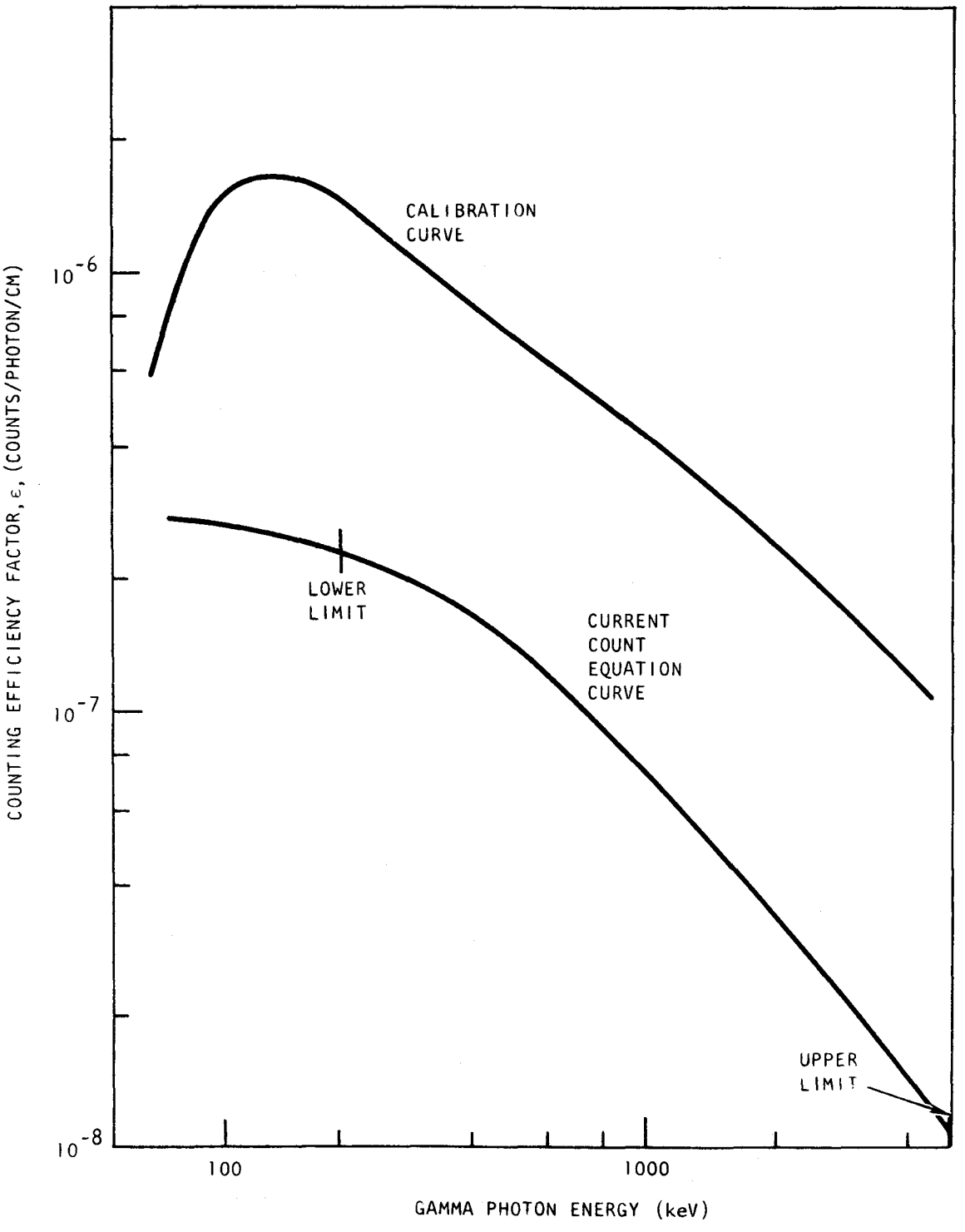

Fig. 5.4 Calibration curve for collimator 1 compared to the equivalent theoretical equation in COUNT

Table 5.1

COEFFICIENTS TO Ge(Li) CALIBRATION CURVES

Collimator		Energy Range (keV)	Coefficients to Polynomial Equation		
No.	Hole Radius (mm)		A	B	C
1	15.875	≤160	-56.591	+20.158	-2.0809
		>160	-3.55406	-0.747287	+0.0166054
2	6.35	≤160	-87.640	+32.099	-3.3121
		>160	7.50204	-0.2646192	-0.4440247
3	2.38125	≤160	-90.481	+31.722	-3.2598
		>160	-10.19356	-0.5188292	-0.01927577

ε = calibration efficiency (counts/gamma/cm of source length),

ℓ_s = source chamber length (cm),

d_c = calibration separation distance between source and detector (cm).

The left side of the equation currently programmed into COUNT will be replaced by the right side of the equation for the Ge(Li) option. However, this approach is then specific to the monitor installed on capsule GB-10. Thus, either similar specific calibration data will be needed for each different monitor to be analyzed or a more general approach must be found. The latter solution is obviously more satisfactory but effecting it will be deferred until other development items in the code have been demonstrated.

Rearranging the above equation, we have

$$\varepsilon \text{ (counts/photon emitted/cm of source length)} = \left(\frac{r_c^3}{2d_c^2}\right)\eta \quad .$$

The left (calibration curve) and right (COUNT equation) sides of this equation are plotted versus photon energy in Fig. 5.4. The discrepancy of the COUNT curve relevant to the calibration curve may be attributable to the much larger active volumes of the Ge(Li) coaxial

semiconductor used relative to those available in 1969 when the correlations found in the literature were formulated. In addition, an error in a factor used to normalize relative efficiency to absolute efficiency may be present. Comparison of the calculated and measured count rates for the xenon and krypton isotopes of interest in capsule GB-10 will be made using the revised formulation.

5.3. FISSION-PRODUCT MANIFOLD FABRICATION DEVELOPMENT

5.3.1. Fuel Rod to Manifold Joints

In the previous quarterly report,[21] three screwed fuel-rod to manifold joints that had been selected for further evaluation were described. During this reporting period, the results of tests made at Kraftwerk Union (KWU) and at GA on joints were analyzed further.

Based on the experience at KWU and the relatively good results from tests by GA on the KWU flat-bottom seal, the KWU design was chosen as the prime candidate for further testing. The spark-plug, taper, and copper-gasket seals (with the sealing surfaces within the perimeter of the threads of the joint) were selected as backups for further study because of their ruggedness and relative ease of replaceability.

Relative to the total cost of the fuel-element assemblies, the differences in the costs of the seals evaluated was not considered to be significant.

With regard to other candidate mechanical joints, the lockring is too bulky for joining the rods to the manifold, but it may well be adaptable for use in joining the manifold to the element charcoal trap.

Further testing of the joints (vibration and thermal cycling) are expected to be conducted at KWU.

5.3.2. Evaluation of Alternative Fabrication Processes

The evaluation of alternative fabrication processes for the manifold during this reporting period consisted of the following:

1. Completion of fabrication, by electrodischarge machining (EDM), of a one-third segment of a manifold structure and initiation of a quality control evaluation of the segment.

2. Evaluation of forming fission-product passages by EDM and by conventional drilling.

3. Evaluation of electron-beam welding and tungsten-inert-gas (TIG) welding for sealing the ends of the passages.

4. Contacts with vendors for quotes on (a) forming of manifold structures and (b) forming the passages, other holes, and threads.

5. Preliminary evaluation of small segments of a variation of the manifold design with welded connections from the manifold to the fuel rods and a welded cover plate over the passages.

A one-third segment of the manifold structure fabricated by first machining the hexagonal-shaped blank and then forming the webs by EDM from solution annealed 316 SS rolled plate is being evaluated (see Fig. 5.5). Measurements of the as-fabricated segment showed the dimensions to be within or acceptably close to the tolerances specified. Hardness measurements of the machined surfaces yielded consistent values of $R_b 80$, indicating that the machining had not changed the condition of the material to an extent measurable by the hardness test.

A low-temperature (350°C for 4 hr) stress relief has been performed on the one-third manifold segment to allow the determination of whether or not residual stresses thus relieved would cause dimensional changes to occur. Dimensional measurements after the stress relief have not yet been completed.

As previously reported,[22] the use of EDM has been demonstrated as a process for fabricating manifold gas passages by GA. A hole 6.125 in. long and nominally 0.040 in. in diameter was drilled into a single web in 7 hr (15 mils/min) with less than a 0.005 in. runout. Measurements showed the hole diameter at the finishing end to be $\sim$0.005 in. larger than at the beginning end. This is also shown by careful examination of an x-ray radiograph of the hole in the web (see Fig. 5.6).

Conventional drilling by itself is not considered a viable method for deep hole drilling. However, guide tooling for the purpose of keeping a conventional drill straight and free from wobble may make it viable

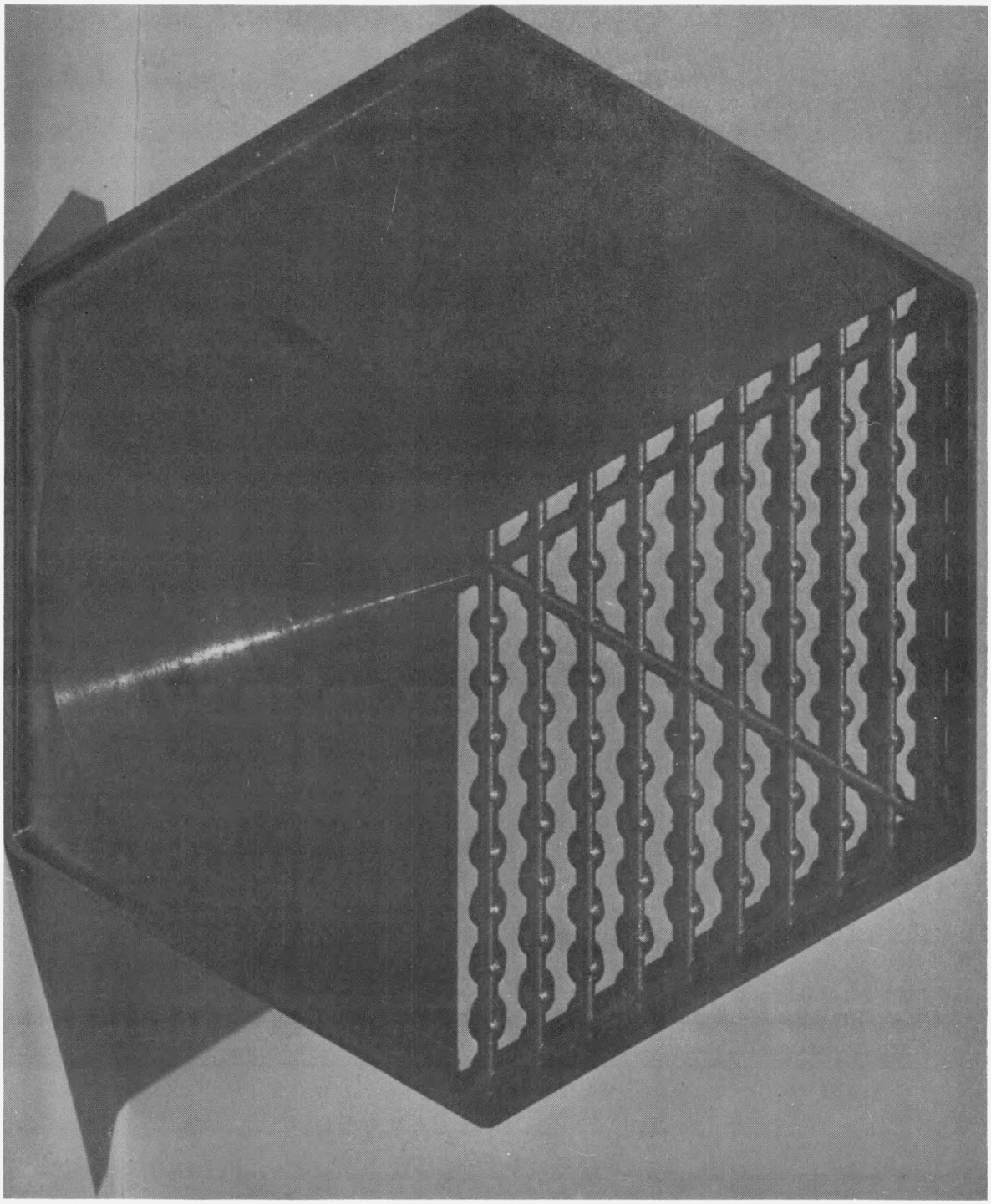

Fig. 5.5 One-third segment sample of the fuel-element manifold structure fabricated by the EDM process

and the tooling has been built. The suitability of "guided" conventional drilling has not yet been demonstrated.

Sealing the ends of the passages by TIG welding has been evaluated. A TIG weld (no filler was used) was made on the end of a hole in a single web. Measurements before and after welding showed that no dimensional changes of the web occurred. The weld was leak tight to helium mass-spectrometer leak-checking and sound and of adequate thickness (see Fig. 5.7). A sample with a fitted end cap for sealing the ends of passages by electron-beam welding has been prepared for trial purposes.

Some fifteen vendors have been contacted for requests for quotes on forming of the manifold structure and the passages, holes, and threaded connections. The information obtained from vendor responses to date are given in Table 5.2.

Samples were fabricated in preparation for electron-beam welding trials on rod to manifold joints and cover plate to manifold seals in the variation of the manifold designs shown in Fig. 5.8. The trial welds will be performed in a conventional vacuum chamber type of electron-beam welding equipment.

5.4. PLATEOUT AND PLUGGING

For the PES to function reliably, it must be designed to accommodate the transport of fission products. Such a design requires a detailed understanding of the transport mechanism of fission products and the conditions under which fission-product plateout could lead to plugging of the passages. This knowledge will, in turn, lead to the development of means to eliminate or minimize the deleterious effects of fission-product plateout.

This subtask is concerned with the acquisition and analysis of laboratory experimental data relating to fission-product transport in the PES.

Investigation of the potential for plateout and plugging in the PES separates naturally into two parts: (1) the effects of plateout and plugging in the fuel element, especially in the fuel rod and (2) those effects

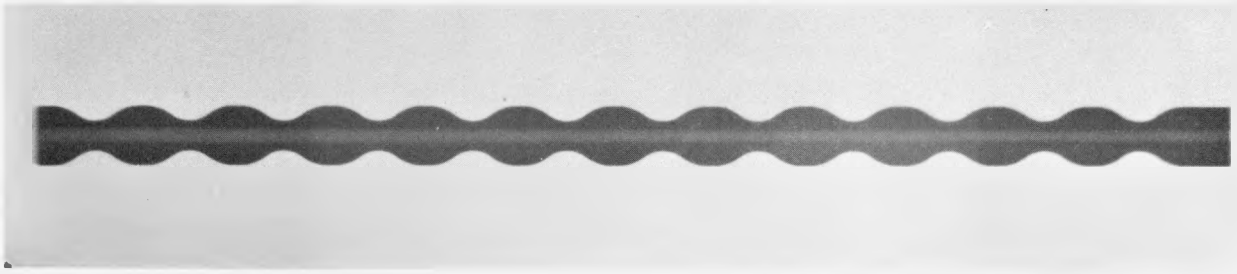

Fig. 5.6 Radiograph of fission-gas passage in a manifold strut fabricated by the EDM process

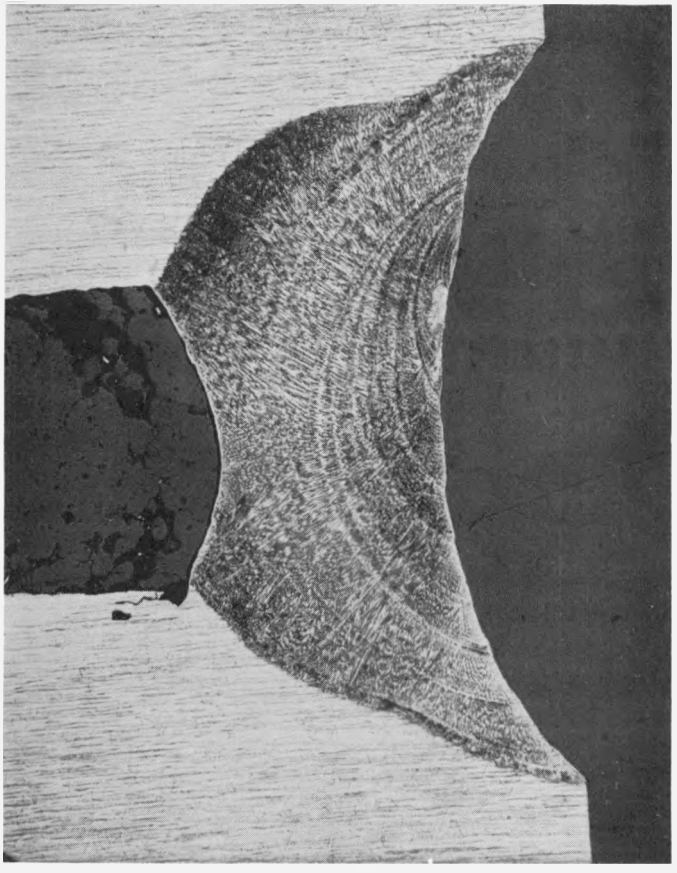

Fig. 5.7 Heliarc-welded closure of a fission-gas passage at the outer edge of a manifold structure

Table 5.2

VENDORS QUOTES FOR FORMING MANIFOLD PARTS

Vendor[a]	Item to be Formed	Fabrication Method	Part Cost per Single Item ($)	Part Cost In Quantity ($)	Tooling Cost ($)	Time for Delivery Weeks
Arwood	1/3 segment, shape only	Investment casting	300	94	4,800	10-12
Arwood	Full manifold, shape only	Investment casting	500	218	9,200	14-16
Adept	1/3 segment, all holes, threads only	Not specified	8,925	---	---	14
Adept	Full manifold, all holes, threads only	Not specified	3,425	---	---	14
Windsor	1/3 segment, all holes, threads only	Not specified	9,737	---	---	6-8
Windsor	Full manifold, all holes, threads only	Not specified	4,843	---	---	10

[a]Several additional vendors have indicated interest in forming of the shape and holes but quotes have not yet been received.

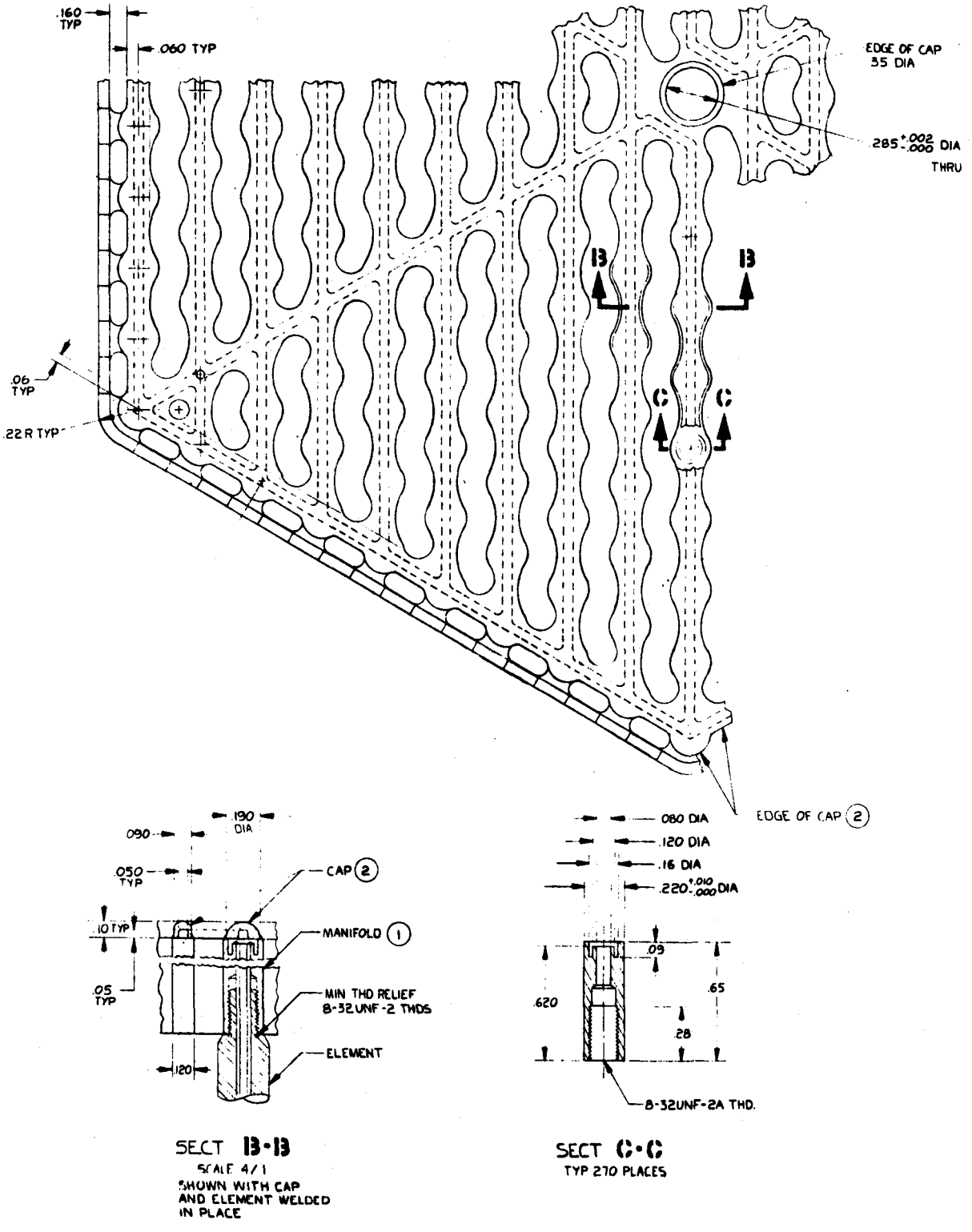

Fig. 5.8 Design of fuel-element vent manifold

in the grid-plate passages and the monitor lines. In the fuel, where the fission products are generated at high temperature, conditions exist that may result in fission products reacting chemically with each other, with fuel components, and/or with cladding components. In addition, large temperature gradients exist not only in the solid pellets but also in the gas phase in the axial direction in the cracks, pores, gaps, and interstices. Also, good radial heat removal through the cladding to the coolant is present. Thus, in the fuel element (rod) there are strong factors that influence the transport, plateout, and plugging of the gas-flow passages over the 3-yr life of an element.

In contrast, in the grid-plate passages and in the monitor lines, nearly isothermal conditions at relatively low temperature (< 325°C) are expected to exist. The transport of stable volatile fission products from the fuel elements and the decay of gaseous fission products in transit to condensable ratioactive and stable decay-chain products will occur. However, the life of these components is the same as the life of the plant (i.e., 30 yr for a demonstration plant and 40 yr for a commercial power plant). Thus, the potential and conditions that influence plateout and plugging in these components must also be known and require investigation.

In the earliest design of the PES for the GCFR it was necessary, as a conservative approach in the absence of experimental data, to assume that all of the gaseous and volatile (and condensable) fission products were released from the fuel and transported through the PES without experiencing any chemical interactions enroute. Under such assumptions, there exists a considerable potential to plateout, constrict, and possibly plug passages, especially in the grid plate and monitor lines where operation over a very long life time is required. At the same time, no plugging that resulted in isolation of the fuel region from the fuel rod plenums had been observed in large numbers of LMFBR fuel-rod irradiations. Thus, GCFR research and development planning of the PES emphasized investigation of the grid-plate passages and monitor lines.

As the result of data obtained more recently from irradiation capsules GB-9 and GB-10 containing pressure-equalized and vented GCFR type

fuel rods, much data and reliable models have become available for evaluating the release and transport of gaseous fission products. Some data are also available for the volatile fission products, especially iodine and cesium. These data complement and confirm data obtained from post-irradiation examination (PIE) of sealed rods, which simulate GCFR pressure-equalized and vented fuel rods, irradiated in the F-1 capsule assembly in EBR-II. The data show substantial peaking of iodine and cesium at the fuel-blanket interfaces. There is evidence of chemical reaction of the cesium with UO_2 blanket material. In addition, fuel transport has closed the central holes at the ends of the fuel pellet stacks in both annular- and solid-pellet starting geometries and, possibly in combination with cesium, has resulted in constriction of the flow passages as determined by measuring flow resistances during PIE at room temperature. One rod, G-7, was found to be plugged at the upper end (hotter during irradiation) in a room temperature PIE test. A hot flow test (100°C) will be conducted at ANL to determine if liquid cesium was present at operating conditions and if capillarity effects of cesium in small passages may be important. In addition, increasing flow resistance to sweep-gas flow through the fuel rod of capsule GB-10 has been reported from in situ measurements after burnup of 50,000 MWd/Te. But no flow constrictions in the normal venting and monitoring lines were noted during operation of capsule GB-9 to 55,000 MWd/Te or in capsule GB-10 to its current burnup of > 50,000 MWd/Te. Irradiation toward a goal of 75,000 MWd/Te is continuing, the burnup goal may be revised upward to 100,000 MWd/Te (maximum GCFR burnup) in the future.

Thus more recent data indicate that condensation and chemical interactions are occurring in the fuel rods which results in substantial reduction in the quantity of fission products to be transported through the PES. On the other hand, the result is probably a shift of the burden of accommodating the fission products from the grid-plate passages and monitor lines to the fuel element. Although this potential problem has been experimentally identified, it is not one of feasibility but one of fuel life, since satisfactory operation to greater than 50,000 MWd/Te has already been demonstrated in this respect without reaching a limiting

condition and current irradiation is continuing to higher burnups. It is not even regarded to be a critical problem since there are believed to be many design alternatives from which to choose to extend the fuel life if necessary to economically desirable burnups once the true nature of the processes involved have been identified. The design alternatives include such things as adjustment of the oxygen-to-metal (O/M) ratio and smear density in the mixed-oxide fuel to limit cesium transport, adjustment of the axial blanket pellet O/M ratio to reduce the chemical reactivity of condensed cesium in the first few blanket pellets near the fuel-blanket interface, changes in configuration of the blanket pellets adjacent to the fuel, such as central holes, axial serrations, or slots to control temperature distribution and condensation locations, and to accommodate the volume of material transported without significantly impeding gas flow.

Although the plateout and plugging aspects both in the fuel rods and fuel elements and in the grid-plate passages and monitor lines are important to a total PES design, laboratory tests simulating certain aspects of the constriction at the fuel-blanket interface in the fuel rods will probably be implemented first because (1) a potential problem has been experimentally identified; (2) a large amount of supporting information developed can contribute to the irradiation experiments in progress, in preparation, and during PIE; and (3) the equipment and test apparatus for laboratory tests are smaller, require less space, less design and engineering effort, and can be brought into operation more quickly than a plateout and plugging loop, which will be built for the grid plate and monitor line experiments.

This subtask was initiated in this reporting period. Initial and current efforts are the collection, condensation, and review of the literature in the field of fission-product migration as it pertains to the processes associated with the potential for fuel-rod plugging. This literature survey will be used to define a plan for experimentation to be carried out during the course of the subtask. References (23) through (31) comprise a bibliography of the most important and pertinent material selected from the literature reviewed to date. The literature search is expected to be completed in the next quarterly period and the conclusions reached will be reported then.

REFERENCES

1. "Gas-Cooled Fast Breeder Reactor Quarterly Progress Report for the Period May 1, 1972 through July 31, 1972," USAEC, Report Gulf-GA-A12252, Gulf General Atomic, August 31, 1972.

2. Sexton, H., "IBM-7094 Multiple Venting Program," North American-Rockwell, Space Division, January 5, 1967.

3. McCarron, T. J., and J. B. Peterson, "One-Dimensional Unsteady Flow Program," Program No. AF-26B, TRW, Systems Group 9852.21-55, July 9, 1965.

4. Distefano, G. P., "A Digital Computer Program for the Simulation of Gas Pipeline Network Dynamics, PIPETRAN, Version IV," American Gas Association, New York, March 1970.

5. Goacher, P. S., "Steady and Transient Analysis of Gas Flows in Networks," Research Meeting of the Institute of Gas Engineers, London, November 1969, Paper GC157.

6. Heath, M. J., and J. C. Blunt, "Dynamic Simulation Applied to the Design and Control of a Pipeline Network," J. Inst. Gas Engr., Vol. 9, No. 4, 1969, pp. 261-279.

7. Hoskin, N. E., "MCCOY and SIMLA, General-Purpose Programs for One-Dimensional Unsteady Compesssible Fluid Flow," Atomic Weapons Research Establishment, Aldermaston, England.

8. Deckker, B. E. L., and D. H. Male, "Fluid Dynamic Aspects of Unsteady Flow in Branched Ducts," Proc. Instn. Mech. Engrs., London, Vol 182, Part 3H, 1967-1968, pp. 167-174.

9. Forster, K., "Technically Oriented Algorithms for Unsteady Pipe Flow," Computer Methods in Appl. Mech. and Engr., Vol. 2, 1973, pp. 279-303.

10. Wylie, E. B., M. A. Stoner, and V. L. Streetor, "Network System Transient Calculations by Implicit Method," Soc. Petroleum Eng. J., December 1971, pp. 356-362.

11. Stoner, M. A., "Analysis and Control of Unsteady Flows in Natural Gas Piping Systems," ASME J. Basic Engr., September 1969, pp. 321-340.

12. Wylie, E. B., V. L. Streetor, and M. A. Stoner, "Unsteady-state Natural Gas Calculations in Complex Pipe Systems," Soc.Petroleum Eng. J., February 1974, pp. 35-43.

13. Wright, E. J., "Generalized Algorithm for the Simulation of Unsteady Fluid Flow in Mechanical Systems," Simulation, April 1971, pp. 156-167.

14. Benson, R. S., "An Approximate Solution for Non-steady Flows in Ducts with Friction," Int. J. Mech. Sci., Vol. 14, 1971, pp. 819-824.

15. Jonsson, V. K., L. Matthews, and D. B. Spalding, "Numerical Solution Procedure for Calculating the Unsteady, One-dimensional Flow of Compressible Fluid," ASME, Paper No. 73-FE-30.

16. Brown, F. T., "A Quasi Method of Characteristics with Application to Fluid Lines with Frequency Dependent Wall Shear and Heat Transfer," ASME J. Basic Engr., June 1969, pp. 217-227.

17. Rachford, H. H., and T. Dupont, "A Fast, Highly Accurate Means of Modeling Transient Flow in Gas Pipeline Systems by Variational Methods," Soc. Petroleum Eng. J., April 1974, pp. 165-178.

18. Rachford, H. H., and T. Dupont, "Some Applications of Transient Flow Simulation to Promote Understanding the Performance of Gas Pipeline Systems," Soc. Petroleum Eng. J., April 1974, pp. 179-186.

19. Malek, G. J., "Development of the Flow Analysis Code FLAC," USAEC, Report GA-9482, Gulf General Atomic, June 1969.

20. Bonine, K. C., et al., "MIDAS IV, A General Digital Simulation Program," General Dynamics Corporation, Convair Division, GDC-ERR-AN-1043, 20 April 1968, Revision B, 1 June 1969.

21. "Gas-Cooled Fast Breeder Reactor Quarterly Progress Report for the Peribd May 1, 1974 through July 31, 1974," USAEC, Report GA-A13148, General Atomic Company, September 26, 1974.

22. Gas-Cooled Fast Breeder Reactor Quarterly Progress Report for the Period February 1, 1974 through April 30, 1974," USAEC, Report GA-A13021, General Atomic Company, June 14, 1974.

23. Aitken, E. A., et al., "Transport and Reaction of Cs, Te, I, and Mo with Fast Reactor Fuels and Stainless Steel Cladding," USAEC, Report GEAP-12268, General Electric Company, 1972.

24. Aitken, E. A., et al., "Thermodynamic Data Program for Plutonia and Urania at High Temperature," Quarterly Reports No. 20, GEAP-12355, 1972; No. 21, GEAP-12368, 1972; No. 22, GEAP-12389, 1973; and No. 23, GEAP-12418, 1973, General Electric Company.

25. Crouthamel, C. E., et al., "Fuels and Materials Division Semiannual Report," USAEC, Report ANL-7877, Argonne National Laboratory, 1971.

26. Maiya, P. S., "Interaction of Volatile Fission Products with Austenitic Stainless-Steel Cladding Alloys," Trans. Am. Nucl. Soc., Vol. 14, 1971, p. 599.

27. Neimark, L. A., et al., "Reactor Development Program Progress Report," USAEC, Report ANL-7900, Argonne National Laboratory, 1971.

28. Johnson, C. E., and C. E. Crouthamel, "Cladding Interactions in Mixed Oxide Irradiated Fuels," J. Nucl. Mat., Vol. 34, 1970, p. 101.

29. Crouthamel, C. E., and C. E. Johnson, "Reactor Development Program Progress Report," USAEC, Report ANL-7737, Argonne National Laboratory, 1970.

30. Neimark, L. A., et al., "Performance of Mixed-oxide Fuel Elements to 11 at-% Burnup," Nucl. Tech., Vol. 16, 1972, p. 75.

31. "Behavior and Chemical State of Irradiated Ceramic Fuels," Proc. of the Vienna 1972 Meeting, International Atomic Energy Agency, Vienna, 1974.

VI. CORE ASSEMBLIES STRUCTURAL-THERMAL-FLOW TESTS (189a No. 13759)

A series of out-of-pile heat-transfer and fluid-flow tests are to be performed to demonstrate the ability of the GCFR fuel-, control-, and blanket-element designs to meet design goals and to verify predictions of analytical models that describe design operation and accident behavior. The test emphasis will be to obtain thermal-structural data for steady-state, transient, and margin conditions using electrically heated rod bundles in a dynamic helium loop.

The Program Plan for the GCFR Core Flow Test Loop[1] that was issued during this quarterly period contains the requirements for and the test program to be conducted in the Core Flow Test Loop (CFTL) that will be constructed and operated by Oak Ridge National Laboratory (ORNL).

To the extent possible in an out-of-pile loop, the test facilities and test assemblies are required to simulate the GCFR environment and design. The principal steady-state conditions are given in Table 6.1; the limiting transient requirements are defined for power (Fig. 6.1), for flow (Fig. 6.2), and for depressurization (Fig. 6.3). By specifying transient functions up to the limiting response time, the complete range of GCFR transients and the resultant structural-thermal-flow interactions will be simulated. The margin testing principally involves undercooling, where helium temperatures will approach 2,500°F; this temperature established the need for attemperation cooling at the outlet of the test bundles to maintain the pressure boundary below the design temperature.

A preliminary test plan has been prepared. The recommended program includes a total of 13 test bundles with 8 fuel assemblies, 3 control assemblies, and 2 full-size blanket assemblies. The design of each test assembly will duplicate the corresponding GCFR assembly to the extent possible in an electrically heated bundle. This recommended test program will permit the basic test objectives to be met but will not include

Table 6.1

STEADY-STATE OPERATING REQUIREMENTS FOR THE CORE FLOW TEST LOOP

Requirement	CFTL	GCFR Demonstration Plant
Coolant	Helium[a]	Helium[a]
System pressure, psia	1,500	1,300
Test section		
Fuel element, $\Delta P/P$	0.034	0.032
Inlet temperature, °F		
Nominal	610	610
Minimum	500	---
Maximum	650	---
Outlet temperature, °F		
Nominal	1,020	1,020
Minimum	500	---
Maximum	1,100	---
Before attemperation	2,500	---
Maximum flow per fuel rod, lb/hr	240	220
Maximum linear rating (10% overpower), kW/ft	16.5	13.8
Total rod length, in.	90.0	90.0
Heater rod length, in.	39.2	39.2

[a]With controlled and measured trace impurities.

simulation of end-of-life configurations and only exploratory probing of the detectability and effects of local flow blockage.

Additional, lower-priority, test bundles are described that could enlarge the test matrix and thereby reduce design uncertainties at the expense of additional funding requirements. The tests with these bundles are not recommended at this time, but their presentation in the program plan shows the broad capabilities of the loop and also describes the comprehensive test matrix from which the recommended tests were selected.

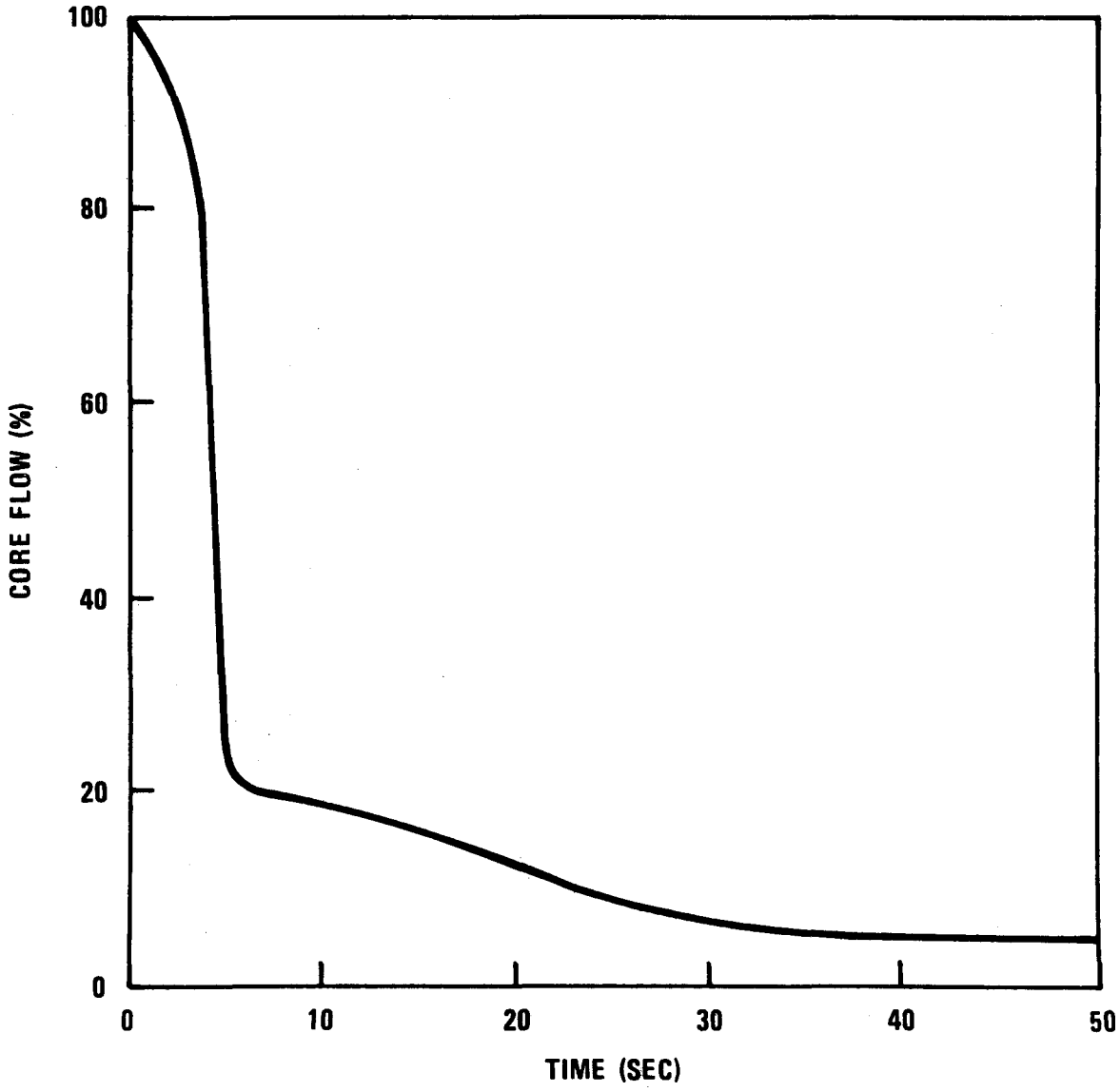

Fig. 6.1 Core flow following reactor trip

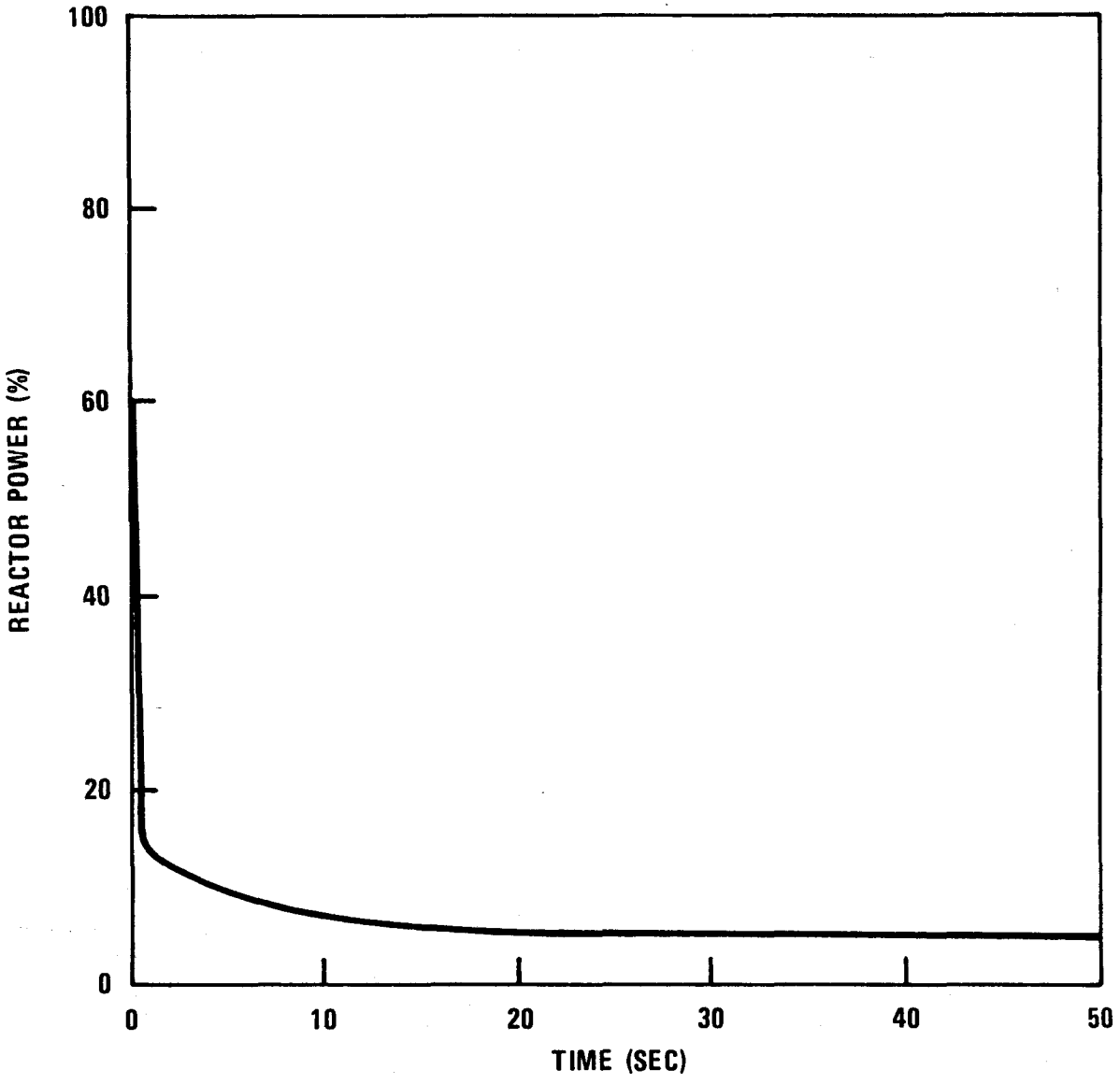

Fig. 6.2 Reactor power following reactor trip using primary and backup shutdown rods

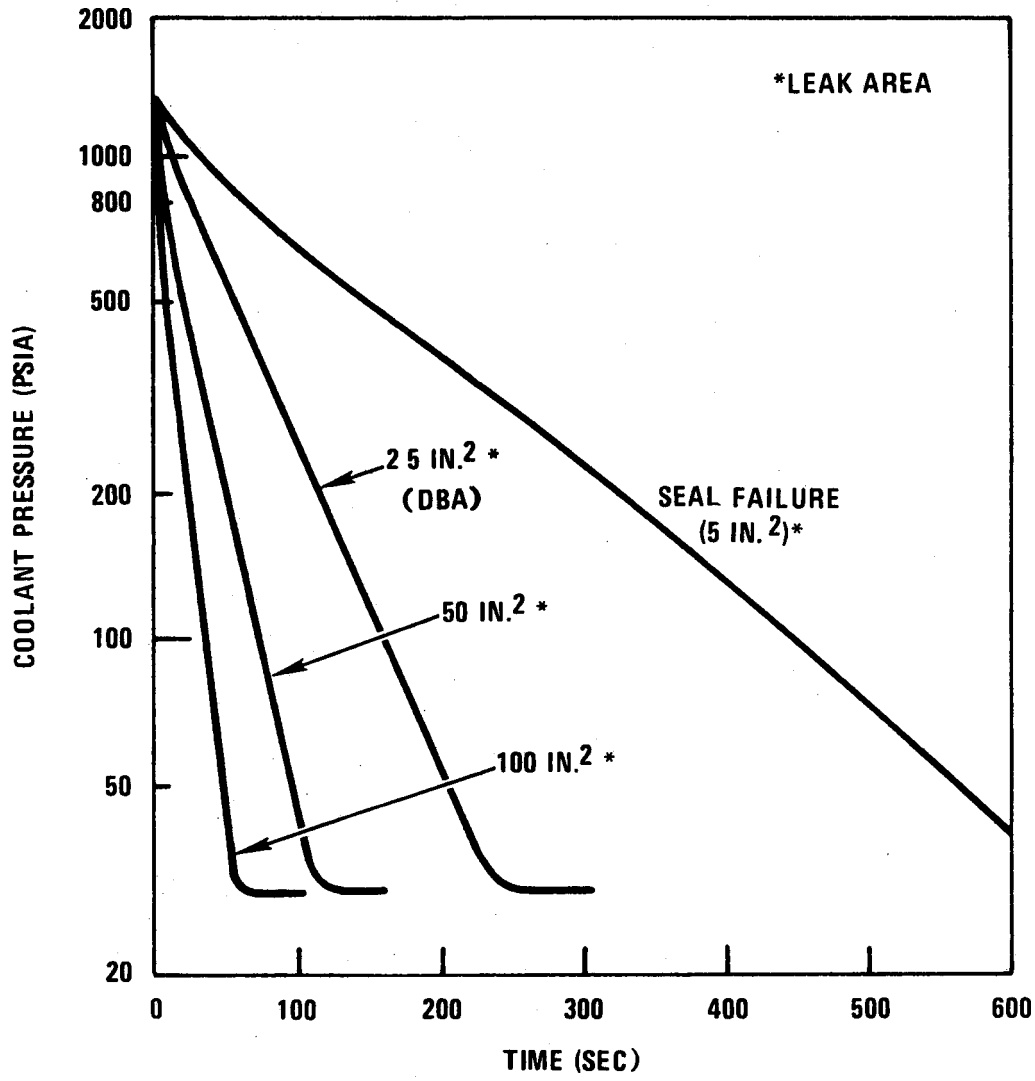

Fig. 6.3 Coolant pressure during depressurization

The planning of the analysis and prediction that is associated with testing has been initiated during the quarter. A list of analyses is being prepared covering the broad parameter prediction areas of loop operation, fuel- and control-bundle operation, and blanket-bundle operation. A work description will be prepared for each of the listed analyses, and one draft work description has been completed. This information will be added to the "Program Plan for GCFR Core Flow Test Loop" when that document is revised.

Work has been initiated on the following specific items:

1. The analysis code for studying GCFR depressurization, DEPTRN, is being reviewed, and a preliminary evaluation indicates that the DEPTRN algorithms may be adapted to model the CFTL under steady-state, transient, and depressurization. A simple path-volume model has been started to test the use of DEPTRN without detailing the specific behavior of each system component, test section, circulators, air-helium heat exchangers, and valves. Detailed computer modeling of each component will be required before an accurate predictive model of the CFTL can be realized.

2. The analysis code COBRA, as adopted for the GCFR, will be used to analyze and predict the performance of the CFTL fuel and control test bundles. Geometric input data for the 19-, 37-, and 61-rod fuel bundles have been computed for COBRA and input performance data are in preparation. A question requiring early resolution is the need to construct heater rods with sinusoidal axial power distribution rather than uniform power distribution.

3. A systematic algorithm is being developed to generate individual rod-power predictions from the core and blanket radial power values. A numerical listing and punch data cards of time versus power, flow, and pressure is being prepared for the main GCFR transients from output of the system codes GAFTRN and DEPTRN.*

*These codes were developed under a privately supported program.

REFERENCE

1. Hopkins, H. C., Jr., "Program Plan for GCFR Core Flow Test Loop," USAEC, Report GA-A13080, General Atomic Company, August 9, 1974 (Controlled Planning Document with Limited Distribution).

VII. IN-PILE LOOP FACILITY TEST PROGRAM (189a No. 13760)

An in-pile loop program is being investigated as a potential follow-on to the CFTL program (see Section VI). In-pile loop tests could serve to provide the information necessary to improve design margins of GCFR fuel assemblies and to verify the analytical methods developed. The tests would explore the consequences of overcooling, undercooling, and depressurization transients and could provide basic information useful to the understanding of core behavior under postulated severe undercooling accidents.

On this program, General Atomic has the responsibility for test planning and test-bundle design, whereas the loop design and fabrication is the responsibility of Aerojet Nuclear Company (ANC).

During the current fiscal year, a preliminary program plan is to be updated and revised, the test series including handling and examination requirements is to be defined and preliminary test bundle design is to be initiated. The test reactor being considered for this program is the Engineering Test Reactor at the National Reactor Testing Station.

During the previous reporting period, a scoping study for this in-pile loop program was prepared. The scoping study documents include an overall program description, a preliminary definition of the test series, a preliminary description of the test loop design, an evaluation of test reactors, and overall cost estimates.

During this reporting period, a meeting was held with RRD, AEC Idaho Operations Office, and ANC to review draft copies of the scoping study. Following that meeting, the documents were reviewed and updated and some of the documents have been submitted to RRD for review and comments.

Descriptions of test-bundle handling sequences and interim and post-test examinations have been initiated.

The test program presented in the scoping study has been reviewed and a somewhat smaller test program recommending seven test bundles instead of eleven test bundles is being evaluated.

VIII. REACTOR ENGINEERING (189a No. 13823)

This task will (1) evaluate and develop analytical methods and models applicable to the assessment of thermal, hydraulic, and structural performance of the GCFR core and core support, (2) evaluate, define, and conduct the development required for reactor control-rod, shutdown-rod, and core component locking mechanisms, and (3) evaluate methods and materials behavior models and information to assess the capability of the PCRV internal structures to serve as postaccident fuel containment.

8.1 CORE THERMAL-HYDRAULICS

The thermal-hydraulic performance of the core assembly and the core monitoring instrumentation requirements and methods are to be evaluated and the availability of accurate computer models for these analyses will be determined. The overall interfaces involved in defining and evaluating the performance of the core are shown in Fig. 8.1.

The study to date has focused on an analysis of the orifice system for distributing coolant flow through the core elements. The logic diagram describing this effort is shown in Fig. 8.2. The fuel and blanket elements are cooled by the downflow of high-pressure helium. The amount of flow in each assembly is regulated by a flow orifice at the outlet of each element. These orifices are fixed but are replaceable or adjustable at the end of each burnup cycle. The criterion for allocating coolant is that of achieving the highest mixed-mean coolant outlet temperature over the cycle consistent with the requirement of not exceeding the peak fuel and cladding operating temperatures. The current effort is focused on developing a computer model for determination of coolant distribution. In addition, the requirements for obtaining detailed power distributions have been identified. Perturbations on the simplest two-dimensional hexagonal and R-Z calculations of power distributions that have been identified

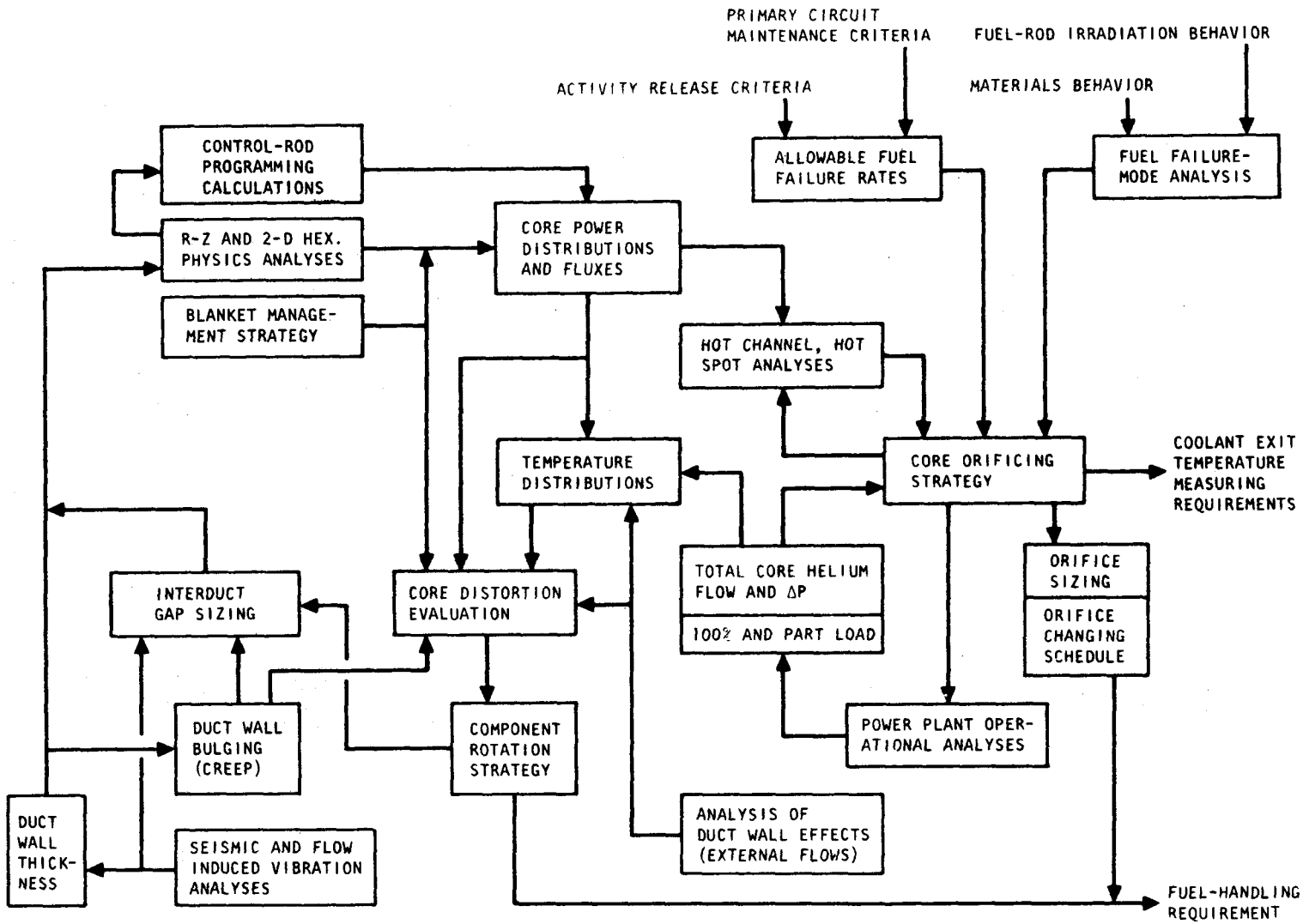

Fig. 8.1 Overall core and blanket performance interfaces

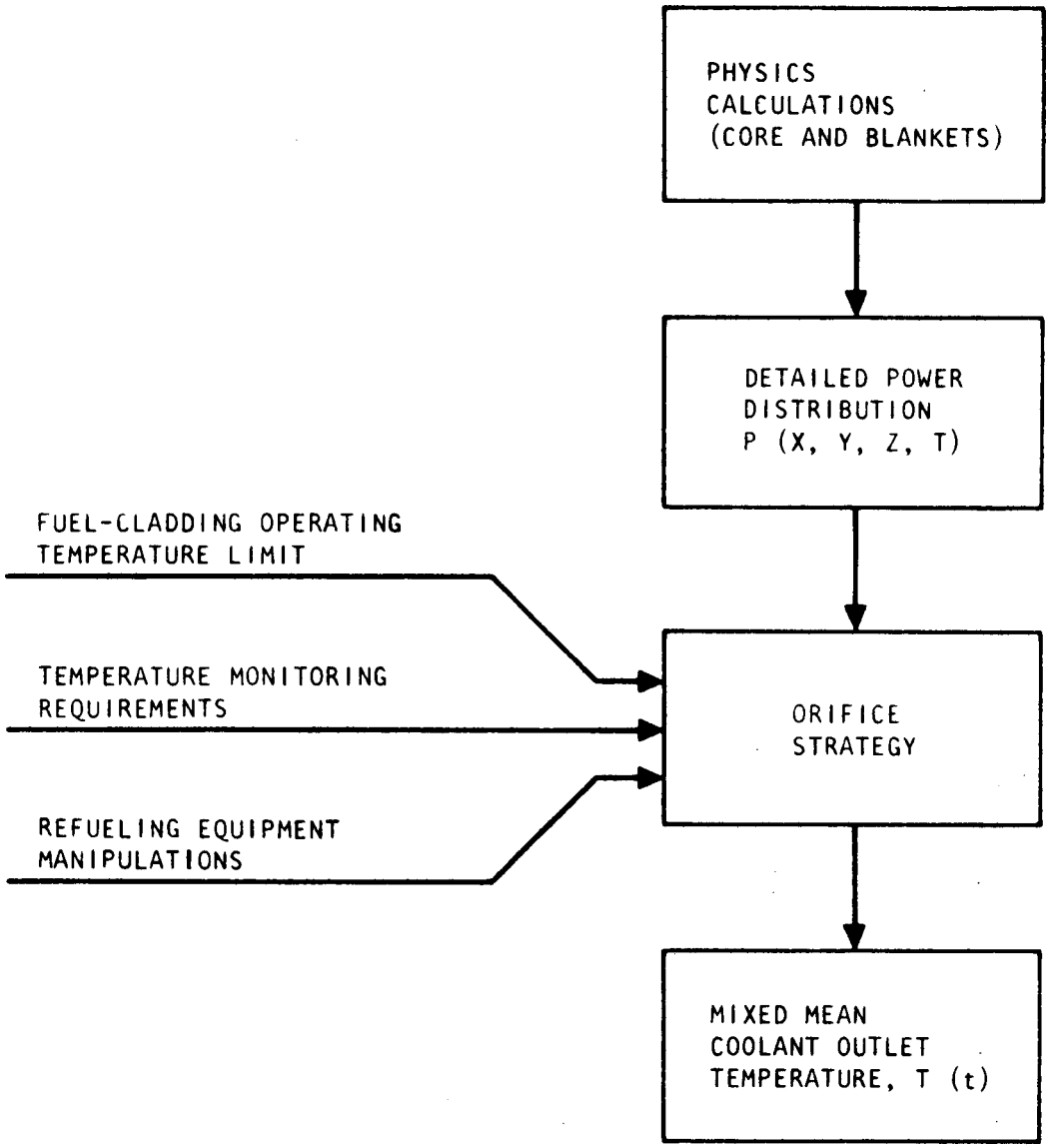

Fig. 8.2 Optimum coolant distribution analysis

as being potentially significant to the analysis of the coolant distribution include:

1. Spatial variations in the core conversion ratio,
2. Radial blanket fissile buildup,
3. Axial blanket fissile buildup,
4. Effects of control-rod withdrawal on adjacent elements,
5. Effects of control rods on the axial power profile,
6. Gamma heating in the core and blankets (both heavy metal and structural components),
7. Control-rod heating and coolant bypass,
8. Power gradients within elements,
9. Uncertainties in the calculated power distributions.

8.2. CONTROL, SHUTDOWN, AND ELEMENT-LOCKING MECHANISMS

The development of the components for locking the elements into the core assembly and the control-rod and shutdown-rod mechanisms will be carried out under this subtask; in addition, their performance and reliability will be demonstrated by testing under anticipated operating conditions. Currently, an evaluation study is being made of alternative systems for reactor shutdown.

Prior work resulted in a conceptual design for each of the three mechanisms and reviews of the designs have indicated the desirability of surveying and evaluating alternative shutdown systems that might be applicable to the GCFR. The present reference design will be compared with one or more concepts selected from the study and, in turn, their features will be evaluated against those of the GCFR control-rod drive, with diversity being the primary criterion.

During this quarterly period, additional concepts were generated and added to the material that will constitute a topical report on the evaluation study. Basically, of the three general classes of alternative shutdown systems, the one that pertains to insertion of the absorber into defined core positions was chosen as a field for this survey and evaluation.

8.3. CORE SUPPORT AND STRUCTURE

The purpose of this subtask is to determine the availability of adequate tools for evaluating the static and dynamic structural response of the core support structure.

8.3.1. Seismic Analysis of the Core Support and Structure

A review of the seismic analysis of the GCFR core and core support structure has been initiated to ascertain the current status of the pertinent techniques developed at GA for the HTGR and of those developed elsewhere for application to the seismic analysis of the GCFR. These tools will be modified as necessary for the analysis of the GCFR structures. The general plans are shown in the flow diagram in Fig. 8.3; however, it will not be possible to achieve satisfactory solutions for all these items in the current fiscal year. Further effort will be required in subsequent years.

Currently, the SAP-IV computer code[1] is being used for seismic analysis in the HTGR program because the previous method using the dynamic response of indeterminate space structures is now considered outdated. The previous seismic analysis of the 300-MW(e) GCFR also used the dynamic response of indeterminate space structures. Based on present experience and review, the SAP-IV code appears to be superior and will be employed in the future seismic analysis of the GCFR core structures. A review is being made of the seismic development and test program of the HTGR, and those studies will be utilized in the GCFR seismic analysis. A review of the docket materials of the different reactor manufacturers and of the pertinent seismic literature has also been initiated.

In a current seismic analysis of the GCFR structures, the dynamic response of indeterminate space structures was used with a 38-node point spring-mass model in which the grid plate was assumed to be rigid because of its estimated high frequency. Using the same mathematical model with the SAP-IV code, the results remain unchanged. Even though the rigid-plate model was the technique used in the early GCFR seismic analysis work, it apparently has some deficiencies that could lead to a nonconservative analysis.

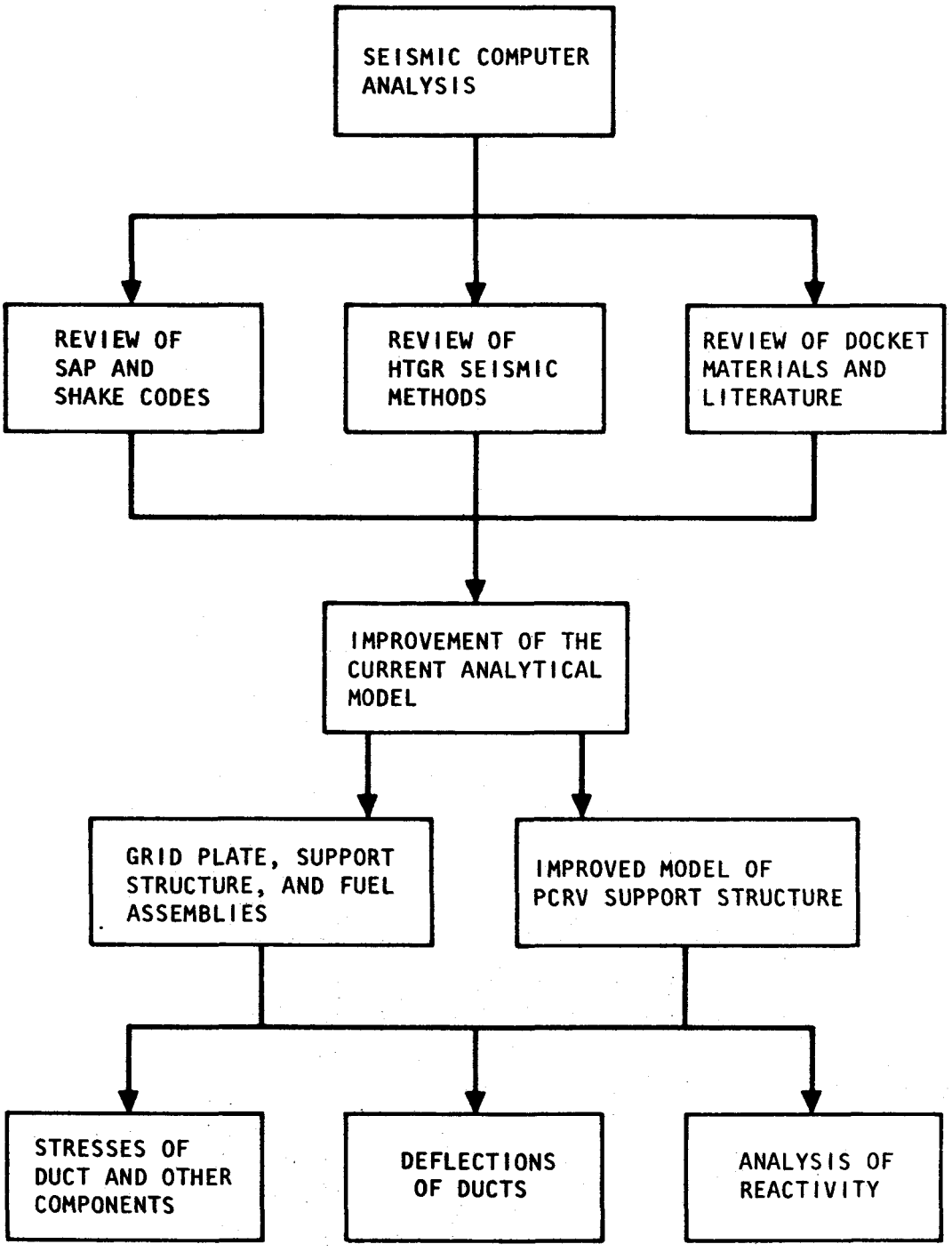

Fig. 8.3 Flow diagram for seismic analysis evaluations

The rigid-grid-plate assumption can only be justified if the lowest natural frequency of the grid plate is significantly higher than the lowest natural frequency of the fuel elements and the lower frequencies of the seismic model. In the past, the rigid-plate assumption based on the analysis of an oversimplified model appeared justifiable. However, the current work in seismic analysis indicates that the natural frequency of the grid plate is in the range of the fuel elements or may even be lower. As a result, the development of a realistic grid-plate–fuel-element model that takes into account the coupling effect between the grid plate and the fuel elements will be required. A review of the present seismic model has also revealed that the grid plate is defined as a rigid body and the fuel elements are lumped together as a single elastic beam. Consequently, omission of the coupling effect could lead to nonconservative results and the single-beam representation of the fuel elements will probably yield an overly conservative design. Further improvements in the seismic modeling technique will be obtained by the use of realistic boundary conditions between the core support cylinder and the PCRV and a better modeling representation of the PCRV support structure. Improvements in the soil model will also lead to an improved analysis.

Finally, the revelation of a lower frequency of the grid plate may influence the design philosophy regarding a fuel-element assembly test, in which the dynamic flexibility and coupling effect of the grid plate must also be taken into account.

8.3.2. Core-support Structural Analysis

An extensive literature review in the area of the perforated plate structural analysis has been initiated. The purpose of the review is (1) to understand the structural behavior of perforated plates more thoroughly and therefore to improve the structural analysis of the grid plate design and (2) to collect and analyze the published theoretical and experimental data of the effective elastic constants of perforated plates for use in the design analysis.

This study has emphasized the difference between thick- and thin-plate theories[2][3] and isotropic and anisotropic constitutive equations

as applied to the understanding of the structural behavior of perforated plates. In regard to this study, the dependence of the effective elastic constants of the mode of loading, e.g. bending and stretching, is also being investigated.

In addition, a review of the applicability of computer codes available at GA to the thermal stress analysis of reactor internal structures has also been undertaken. In particular, the axisymmetric thin shell method that was used in the thermal stress calculations for the 300-MW(e) GCFR grid support structure is being carefully studied.

8.4. POSTACCIDENT FUEL CONTAINMENT (PAFC)

The objectives of this subtask are (1) to develop an accurate description of the thermal and structural processes accompanying the events in a postulated core meltdown arising from a very low probability series of failures, (2) to define and coordinate experimental studies at ANL to verify thermal processes in molten fuel masses, and (3) to evaluate the feasibility of incorporating in the design of the PCRV the capability of postaccident fuel containment.

During this reporting period, work has been initiated on the uncertainty evaluation for the available analytical methods, material properties and decay-heat values, and models of the thermal processes accompanying core meltdown. To further evaluate the areas of defined uncertainties, an initial analytical study has been completed, and the results are encouraging with regard to the possibility of providing an in-vessel postaccident fuel containment capability.

8.4.1. Criteria for PAFC

The following criteria are proposed as the current basis for evaluating the capability of PAFC:

1. The maximum fuel temperature must be kept below the boiling point to limit fuel transport from the melt, and
2. The maximum cavity-liner temperature must be kept below its melting point to prevent breaching (melt through) of the cavity liner.

To meet the above criteria, it is currently believed necessary that the structural integrity of the core support and shielding structures not be impaired throughout the progression of the accident.

8.4.2. Areas of Uncertainties and Initial Evaluations

8.4.2.1. Analytical Methods. The mathematical problem of the PAFC study that involves melting and resolidification has been proved to be nonlinear.[4] Thus, the analytic solution of this problem relies on either closed-form approximation methods or on numerical means if a more general problem is concerned. A survey of existing computer codes capable of solving heat-conduction problems with change of phase has indicated that the NUTAP computer code,[5] which uses finite differences and an electric network analogy, is suitable at the present time. Other numerical methods, such as the finite-element method[6] and the method of Green's functions,[7] require further code development work.

8.4.2.2. Material Properties. There is considerable uncertainty in material properties of all the molten materials involved in the meltdown processes. For the molten fuel (mixture of UO_2, PuO_2, and ThO_2) and molten stainless steel, material properties including the thermal conductivity, viscosity, and the coefficient of volumetric expansion are especially uncertain. Measured values appearing in the literature[8,9] may vary by more than one order of magnitude. For the purpose of the initial analytical study, selected property values were taken from various sources. However, extensive experimental work is needed before dependable property values will be available.

8.4.2.3. Decay Heat. The magnitude and distribution of the decay-heat source are the most important parameters in PAFC studies. In the core meltdown process, the volatile fission products may be totally released from the molten fuel as vapor and an additional fraction of the fission products may be dissolved in the molten stainless steel. Thus, less heat is generated within the fuel and a lower temperature in the fuel can be expected. The distribution of decay-heat sources in oxide, metallic, and vapor phases has not been available for the GCFR fuel. The capability of performing this type of calculation is currently being

acquired. For the purpose of the initial analytical study, however, information from the FFTF[10] decay-heat curve was used to make approximations for the GCFR fuel.

8.4.2.4. Initial Conditions. It is assumed that in the progression of the core meltdown, the maximum-powered fuel elements will fail first and drop, followed by the remainder of the fuel elements. This debris will accumulate randomly on top of the preshield. As melting progresses, a liquid pool may start at the center part of the preshield, spread laterally, and eventually form a uniform liquid layer.

For long-time transients, the present problem is insensitive to initial conditions. However, the maximum fuel temperature occurs in the early time stage of the meltdown processes and therefore this temperature is strongly influenced by the initial conditions. Therefore, the ability to satisfy the criterion for PAFC stated in Section 8.4.1, that the molten fuel be prevented from boiling, is also very sensitive to the initial-condition assumptions.

To circumvent the complicated initial problem, a simplified model has been employed in which the fuel and structural material are treated as layers of solid material already on the lower axial preshield at the time immediately after shutdown. Although unrealistic in terms of the physical processes of a meltdown, the model is believed to be an accurate thermal representation of the problem, which will yield reasonable estimates of the maximum fuel temperature.

8.4.2.5. Natural Convection. Benard-type thermally induced natural convection will occur in the molten-fuel layer and the uppermost stainless-steel layer. Experimental work reported to date has been limited to the lower and medium range of the Rayleigh numbers. No experimental data are yet available in the higher Rayleigh number range, which covers the molten fuel and the molten stainless-steel conditions. Therefore, extrapolation of existing experimental data must be used in the evaluation of heat transfer across the molten mass. A better natural convection correlation is necessary in estimating more accurately the maximum fuel temperature as well as the partition of upward flowing and downward flowing decay heat.

8.4.2.6. Crust Forming and Cracking. A crust may be formed on top of the molten fuel surface if sufficient cooling is supplied from above. But this layer will break into chunks due to thermal stress resulting from the large temperature difference across it. These solid chunks are more dense than the liquid and will sink down and remelt into liquid. Thus, besides natural convection, the release and absorption of latent heat of the frozen fuel chunks adds another mechanism to enhance heat removal. However, these solid chunks may reduce the thermally induced current flow and thus reduce the natural convection heat transfer. A similar situation exists at the upper boundary of the molten stainless steel on top of the fuel layer. A crust may also be formed and cracked at the lower boundary of the fuel layer during the flotation of molten masses of stainless steel from the preshield.

8.4.2.7. Flotation of Masses. During the melting of the preshield, the less-dense molten stainless steel may penetrate through the molten fuel layer to form a liquid layer on top of the fuel. After the melting of the top steel layer of the main lower shield, graphite blocks are exposed to the dense molten fuel and may have the tendency to float atop the molten fuel layer. However, because of the sealing tendency of frozen fuel in gaps between graphite blocks, flotation of the graphite is likely to be prevented. Similarly, it has been assumed that the molten stainless steel and the molten silica layers beneath the graphite blocks will not be forced up through the side gaps of graphite blocks. The details of this process may best be determined by experiments; however, preliminary calculations have indicated that peak fuel temperature and peak liner temperature are not significantly affected when these molten layers are assumed to move above the graphite.

8.4.2.8. Chemical Reactions. During the transient process, several chemical reactions are likely to occur when the multiple layers of the lower shield assembly are heated up continuously by the fuel layer on top of them. When the uppermost graphite layer becomes exposed to the fuel layer, a chemical reaction progresses at the interface until a layer of UC_2 is formed above the graphite; then, the reaction rate will be slowed down since it can continue only by diffusion of carbon through the UC_2

layer. As shown by the experiments of Row,[11] there is no appreciable attack of molten UO_2 on a graphite crucible. When the lower shield assembly is continuously heated up, the lower steel layer will melt and also react with graphite to form iron carbide (Fe_3C). When the melting progression reaches the fused silica layer, another reaction takes place and silicon carbide (SiC) is formed. These chemical reactions not only increase the complexity of the present problem, but also result in unknown conditions that one must quantify in the transient analysis. These added unknowns are, primarily, the rates of the chemical reactions and the thermodynamic properties of the various chemical products. However, since all the chemical reactions involved are endothermic, it is consistent with a conservative initial analysis to ignore the effects of these chemical reactions until dependable experimental data are available.

8.4.3. Initial Analytical Study

The overall heat-transfer behavior of a molten core of the 300-MW(e) GCFR during a postulated core meltdown has been studied. A transient one-dimensional multiple-layered model was assumed for the solution. This history of the melting progression has been examined and the capability of the reactor cavity liner to serve as postaccident fuel containment was found to be adequate.

In the course of the melting process, two meltdown conditions were postulated: a full core meltdown involving all of the fuel and blanket material and a partial core meltdown in which only the core and lower axial blanket are assumed to be melted.

Natural convection in the molten fuel layer was calculated by the correlation of Kulacki and Goldstein,[12] whereas for the stainless steel layer, the correlation of Robinson[13] was applied.

The double solid layer model was chosen as the initial condition for the fuel and the uppermost stainless steel layer. The initial temperatures of these layers were taken as the average temperature of these materials in normal operation in the core.

Numerical results were obtained via the NUTAP computer code using the following input information:

Quantity of fuel = 13,160 kg (partial core meltdown)
= 50,278 kg (full core meltdown)

Quantity of steel = 4,489 kg (partial core meltdown)
= 15,596 kg (full core meltdown)

Area of cavity bottom = 254 ft^2

Helium { temperature = 600°F
convective heat-transfer coefficient = 50 Btu/(hr)(°F)(ft^2)

Water in the liner cooling coils { temperature = 180°F
convective heat-transfer coefficient = 140 Btu/(hr)(°F)(ft^2)

Typical results for the two meltdown conditions are summarized as follows:

Parameters	Partial Core Meltdown	Full Core Meltdown
Melting point of fuel, °F	5,050	5,600
Maximum fuel temperature, °F	4,977	5,812
Maximum cavity liner temperature, °F	342	365
Time to terminate melting, hr	28	40
Maximum heat flux at liner, Btu/hr-ft^2	16,800	18,800

Based on the initial analytical study, the following conclusions can be drawn:

1. The present transient analysis provides information about the history of phase changes and the variation of temperatures and heat fluxes. Thus, an overall picture of the course of events in the retention of a postulated core meltdown is obtained.

2. The criteria stated in Section 8.4.1 were found to be met with a large safety margin. Therefore, the capability of providing in-vessel postaccident fuel containment appears feasible based on these analyses.

3. The melt-through process stops at 30 to 40 hr after reactor shutdown.

4. The effect of storing heat in the massive reactor shielding materials provides ample time for raising the cooling capacity to the required emergency level.

5. As concluded from the results, the cavity liner and shield structures can be considered as a natural crucible for the molten mass for a number of hours without requiring any added design features. Long-term fuel containment would probably require a modification to the reference design to provide extra cooling capacity.

8.4.4. Impact of Uncertainties

Based on the initial analytical study, the impact of the uncertainties defined in Section 8.4.2 was investigated and the following observations are made:

1. The NUTAP computer code was found to take excessive running time. For the future two-dimensional analysis, a modification of the NUTAP code or the development of other numerical methods appears necessary.

2. A parametric study of the hard-to-measure material property values may demonstrate that the results are insensitive to those values and that the current estimates may be adequate for PAFC studies.

3. From the results of the study, the heat storage capacity of the massive reactor shielding was a promising finding. An optimum thickness of the lower axial shield may be specified that is most compatible with PAFC considerations.

4. Better knowledge of the decay-heat distribution, the thermally induced natural convection, and the effects of chemical reactions should increase the accuracy in future studies.

5. Experimental investigations of crust forming and cracking and the flotation of masses are necessary to assure the adequacy of the assumed configuration of the meltdown processes.

REFERENCES

1. Bathe, K. J., E. L. Wilson, F. E. Peterson, "SAP IV, A Structural Analysis Program for Static and Dynamic Response of Linear Systems," University of California, Berkeley, Report EERC 73-11, June 1973.

2. Slot, T., and W. J. O Donnell, "Effective Elastic Constants for Thick Perforated Plates with Square and Triangular Penetration Patterns," J. Eng. Industry, Transactions ASME, Volume 93, 1971, pp. 935-942.

3. Slot, T., "Orthotropic Analysis of a Thick Perforated Plate with Pressure on One Side," Second International Conference on Structural Mechanics in Reactor Technology, Berlin, Germany, September 1973.

4. Carslaw, H. S., and J. C. Jaeger, Conduction of Heat in Solids, Oxford University Press, Oxford, 1959, p. 284.

5. Leach, C. E., and E. L. Kelly, Jr., "TAP-Loop: A Stable Thermal Analyzer Code for Thermal Analysis of Closed Hydraulic Systems," USAEC, Report BNWL-1172, Battelle Northwest Laboratory, January 1970.

6. Cheng, R. T., and C. Y. Li, " On the Solution of Transient Free Surface Flow Problems in Porous Media by Finite Element Methods," J. Hydro., Vol. 20, 1973, pp. 49-63.

7. Kang, C. S., and Y. P. Chang, "Effects of Change of Phase on Temperature Distribution Due to a Moving Heat Source," J. Eng. Mat. Techn., (to be published), ASME Paper No. 74-Mat-X.

8. Kumar, R., L. Baker, Jr., and M. G. Chasanov, "Ex-Vessel Considerations in Postaccident Heat Removal," USAEC, Report ANL/RAS-74-29, Argonne National Laboratory, October 1974, p. 87.

9. "Reactor Fuels and Materials Development Programs for Fuels and Materials Branch of USAEC Division of Reactor Research, Quarter Progress Report, October-December 1969," USAEC, Report BNWL-1279, Battelle Pacific Northwest Laboratories, February 1970, p. 2.4.

10. Hesson, J. C., R. H. Sevy, and T. J. Marciniak, "Post-Accident Heat Removal in LMFBRs: In-vessel Considerations", USAEC, Report ANL-7859, Argonne National Laboratory, September 1971, p. 25.

11. Row, T. H., "Interaction of Molten UO_2 and Refractory Material," USAEC, Report ORNL-TM-1820, Oak Ridge National Laboratory, June 1967.

12. Kulacki, F. A., and R. J. Goldstein, "Thermal Convection in a Horizontal Fluid Layer with Uniform Volumetric Energy Sources," J. Fluid Mech., Vol. 55, 1972, pp. 271-287.

13. Robinson, J. L., "Finite Amplitude Convection Cells," J. Fluid Mech., Vol. 30, 1967, pp. 577-600.

IX. PRESSURE BOUNDARY INTEGRITY (189a No. 13824)

The long-range objective of this task is to verify the adequacy of the design of the PCRV pressure-boundary system. The work will include preparation of plans for initiating critical development tests for the thermal barrier and pressure barrier. The design basis for the liner of the PCRV will be critically reviewed with the objective of ensuring pressure boundary integrity over the plant life for the GCFR conditions. The basis for the radiation exposure criteria will also be evaluated.

Test planning, including supporting analysis, will be conducted for a PCRV model test. Key flow-restrictor tests will be designed and conducted.

9.1. DESIGN BASIS FOR THE INTEGRITY OF THE PCRV PRESSURE BOUNDARY

The objective of this subtask is an evaluation of the design basis for the integrity of the PCRV pressure boundary, including the liner and thermal barrier. The results of this evaluation will be issued as a topical report.

Prior work in this area has been on the design and analysis of a PCRV design for gas-cooled reactors in Europe and the United States, which has demonstrated the integrity of this type of pressure vessel. More recently, HTGR design and development has added to this background of technology. The GCFR design involves higher primary-coolant gas pressures than current HTGR designs and this has led to investigating and evaluating the effect of the higher pressure on the pressure-boundary integrity, which includes the prestressing system, the PCRV liner, and the thermal barrier that have been developed under private funding.

During this reporting period, an outline for the topical report was completed and the preparation of the report initiated. The sections

on the technology background, the prestressing system, the thermal barriers, the liners and anchors, and the liners cooling system are being written. For each of the sections of the report, the subject is generally being developed to include a description, performance objectives, a functional description, along with design requirements and design conditions and evaluations. In addition, the materials used, the method of fabrication, and quality assurance aspects will be discussed. Other subject matter to be presented will include methods of design analysis, operational modes, and failure considerations.

X. REACTOR SAFETY (189a No. 13825)

The purpose of this task is to study the reactor safety aspects of the GCFR by employing logical probabilistic methods to determine the probabilities associated with various Accident Initiation and Progression sequences and to help reduce risks by design modification, if appropriate. Additionally, this task maintains a liaison between GA and the RRD-funded GCFR safety task at Argonne National Laboratory

10.1. ACCIDENT INITIATION AND PROGRESSION ANALYSIS (AIPA)

Applying the AIPA analysis techniques developed in FY-74, work is being directed toward the probabilistic analysis of accident sequences leading to the high-consequence events that have been identified by the AEC-supported task at ANL on GCFR safety aspects of fuel and core.

Consistent with the accomplishment of a recommendation of accident classes for further study in FY-75, three broad classes of accidents have been identified for further study:

1. Loss of reactor coolant flow accidents,
2. Transient overpower accidents,
3. Reactor coolant system depressurization accidents.

All significant initiating events leading to high-consequence outcomes within each of these accident classes will be identified and their frequency of occurrence quantified by ongoing studies. The general consequence limiting mechanisms that are expected to be considered in terms of probability to function are the reactor shutdown systems and the residual heat-removal systems. For those paths leading to potentially high-consequence events, the functioning or failure to function of the postaccident heat-removal (PAHR) processes, the maintenance of PCRV integrity, and the operation of containment isolation and cleanup systems will be quantified in probabilistic terms.

Efforts during this quarterly period continued to be directed toward the evaluation of the first class of accidents—loss of reactor coolant flow accidents. As preliminary evaluations have indicated that the higher probability paths involve failures of shutdown cooling, initial efforts have been directed toward the analysis of the reliability of the shutdown cooling systems (main loop and core auxiliary cooling system).

Considerable effort during this period was spent in studying and analyzing the techniques employed by the recently released "Reactor Safety Study."[1] Employing the quantitative and qualitative methods of this study and of previous AIPA methodology development work, a probabilistic model of the GCFR shutdown cooling system was developed and computerized utilizing the GO code technique.[2] This model includes the interactions, on a probabilistic basis, of all significant systems, subsystems, components, and service systems that are necessary to perform shutdown cooling functions. The model has been quantified using, primarily, data from Ref. 1.

Anticipating that further consequence work will show that virtually all loss-of-coolant-flow accident sequences with scram have similar consequences, the effects of various accident initiators have been analyzed using the model and an initial set of the dominant (i.e., more probable) accident sequences involving loss of coolant flow with scram has been identified. As a result of this work, several system design configurations were identified as potentially significant contributors to the cumulative probability for loss-of-coolant-flow accidents. These relatively "weak-link" configurations are currently being analyzed in more detail and alternative designs are being considered.

Although initiating events in the the third class of accidents (depressurization accidents) change the criteria for shutdown cooling success, by and large they do not alter individual component reliabilities. Thus, further work is being directed toward adapting the probability model employed for the loss-of-coolant-flow accident to characterize the various depressurization events.

10.2. SAFETY RESEARCH AND DEVELOPMENT LIAISON

Close liaison is maintained with Argonne National Laboratory with respect to the RRD-funded ANL task on GCFR safety of fuel and core. Specific areas that were discussed include the generic approach to consequence analysis, analytical modeling, postaccident heat removal, and the potential effect of retained gases on fuel motion.

Outstanding commitments to supply the ANL task with design data were completed during the reporting period. Specifically, detailed tables of the reactivity worth of fuel and cladding in the 300-MW(e) GCFR were transmitted to ANL.

REFERENCES

1. "Reactor Safety Study - An Assessment of Accident Risks in U.S. Commercial Nuclear Power Plants," USAEC, Report WASH-1400, August 1974 (Draft).

2. Gateley, W. Y., et al., "GO - A Computer Program for the Reliability Analysis of Complex Systems," Kaman Sciences Corp., Report KN-67-704(R), April, 1968.

XI. REFUELING-SYSTEM DEVELOPMENT (189a No. 13831)

An evaluation of the reference design of the refueling system, the development of design concepts, and design verification of the equipment are to be carried out under this task. Initially, evaluation studies of the GCFR refueling system are to be performed, and through functional analysis and feasibility studies, a development plan for the system will be prepared. Analysis will be performed on system requirements for spent-fuel cooling and shielding requirements. Test plans for prototypical assemblies and subassemblies will be included and studies and identification of the required test facilities will be made. Prototypical test assemblies will be designed and analyzed, which will be followed by procurement and fabrication. Tests of these assemblies will be performed and the test results evaluated on a progressive basis. Final performance tests to verify achievement of performance goals will be performed and documented. Subtasks that are currently active include the preparation of the refueling system development program plan and the evaluation of cooling and shielding subsystem requirements.

11.1. REFUELING SYSTEM DEVELOPMENT PLAN

A comprehensive design verification and support program plan for the GCFR refueling system will be generated under this task. The refueling system development plan that serves as the initial basis for the work to be accomplished under this subtask is described in the previously issued overall GCFR development program plan.[1]

As an initial step in the preparation of a development plan for this system, a preliminary overall schedule was developed. The refueling system development plan, which is now being prepared, includes an evaluation of the functional and operational requirements for the system and its components. The evaluation considers such aspects as safety, number of

operations and quantity of equipment involved, feasibility, and reliability. This evaluation will be utilized, together with other analyses and studies, i.e., tradeoff studies, operations and equipment item reduction studies, etc., to prepare system design criteria and component design criteria after the system description is finalized.

The present reference design has been reviewed and all fuel-handling machines and supporting equipment have been identified. Additionally, background and historical data were gathered. The major item started in this quarterly period was a narrative step-by-step refueling sequence based on the reference design, starting with the reactor in a shutdown condition and ending with the refueling penetrations replugged and all refueling equipment items stowed. The intent of this effort is to verify the number of equipment items required for further studies of alternate refueling concepts to reduce the number of operations and potentially reduce the quantity of equipment.

11.2. COOLING AND SHIELDING SUBSYSTEM EVALUATION

To determine the full range of cooling and shielding requirements for the GCFR refueling system, analysis and feasibility studies and an evaluation of alternate methods to meet the requirements will be made.

The current system evaluation is proceeding under the assumption that uninterrupted forced cooling of spent-fuel elements is required from the moment they are removed from their grid positions until they are submerged in the storage-pool water. This necessitates element cooling systems integral with three major refueling machines: the fuel transfer machine, the fuel lifting machine, and the fuel transfer cask.

Work on this significant aspect of safe fuel handling was initiated during the quarter on the two in-vessel machines. The preliminary data obtained for effective element cooling during a refueling shutdown indicates a helium flow requirement of about 21 ft^3/sec per element. To facilitate this flow requirement, preliminary prototypical layout work was initiated for the grapple heads for the fuel transfer machine (bottom grappling) and the fuel lifting machine (top end grappling).

Three schemes are currently under consideration for cooling and on a basis of applicability common to both machines:

1. Ejector: Utilizes high-pressure helium from an external source, "driving" the ejector and pulling helium from the PCRV lower plenum through the element.

2. Direct Pressure: Utilizes high pressure helium as under (1) but is fed directly to the top or bottom of an element and forced through by the pressure differential.

3. Circulators: Utilizes helium within the plenum. Would very likely be designed as an integral part of the grapple assembly.

During the quarter, most of the effort on this subtask was applied to the circulator scheme. Preliminary sizing of the fuel handling machine circulators was aided by the use of "CENTRF" (a program for sizing centrifugal compressors). Data input was based upon preliminary calculations for flow requirements and pressure drops. Current results indicate that the physical size of a helium circulator package for this application is undesirably large and the associated motor reliability requirements may be difficult to meet.

In comparison, the two other cooling schemes offer distinct advantages in mechanical simplicity and evaluation is in progress.

REFERENCE

1. "Gas-Cooled Fast Breeder Reactor Demonstration Plant Development Plan," Vol. II, USAEC, Report GA-A10788, Gulf General Atomic, September 20, 1972.

XII. COMPONENT DEVELOPMENT ENGINEERING (189a No. 13840)

This task includes the preparation and issuance of the development program plans for the main components of the GCFR, an evaluation of existing HTGR standards against GCFR design criteria to determine additional standards requirements, and analysis of critical components.

12.1. DEVELOPMENT PROGRAM PLANS

In this subtask, the development program plans for the GCFR components will be prepared and issued. The plans will contain the evaluation of the main components, including the PCRV, the steam generator, and the main circulator.

Main-loop component designs have been successfully demonstrated by HTGR reactors in addition to gas-cooled reactors operating in Europe and the U.K. The GCFR designs feature higher coolant operating pressures, which necessitate higher pressure ratios, mass flow, and power and high-performance circulators and steam generators that require low-flow characteristics in addition to their normal operating performance.

These and other important considerations of the nuclear steam supply system require component development to extend the existing technology to make it applicable to the GCFR. The general scope of these development programs has been outlined in the overall GCFR development program plan.[1] In the latter part of FY-74, revisions to the development plans for the PCRV, steam generator, and main circulator and loop isolation valves were initiated. These revisions included extension of the scope and refinement of the previously proposed program plan.

12.1.1. Steam Generator Development

During this reporting period, a draft of the revised development plan for the steam generator has been prepared. A detailed schedule

shows the interaction of the various development tasks into the overall schedule for the steam generator design and fabrication.

The development tasks are detailed to include boiling stability, helium flow distribution, flow-induced vibration, and tube-wear-protection tests. The time span for each of these tasks was based on the HTGR development program.

12.1.2. Circulator Development

The revised circulator development plan incorporates a number of significant changes from the overall GCFR development plan. These changes are believed to contribute to a more predictable circulator design performance and higher operating reliability. A detailed schedule outlines the development program interfaces and milestones from initial predesign to completed installation in the demonstration power plant. Also, cost estimates were made of the individual tasks and of the facilities required. The qualification tests require construction of a new test facility because of the higher pressures and horsepowers of the GCFR main circulators.

A study was made of alternative methods for testing the demonstration plant circulators. As a result of this study, two alternative methods are being considered for full-scale testing of the GCFR main circulators: (1) a full-scale, full-load test facility integrated with a large electric power plant, which offers the advantages of full-power testing of the circulator prior to installation in the reactor, and (2) a part-power test facility similar to that to be used for the large HTGR circulator test program, which will utilize an electric-driven steam compressor for supplying high-pressure steam to the circulator turbine.

There are numerous performance demonstration advantages, but there are also cost disadvantages, to full-power, full-scale testing of a circulator system; however, it remains on the list of preferred systems and will tontinue to be a viable candidate.

12.1.3. PCRV Development

The revised development plan has been prepared for internal project

review. A detailed schedule of the various development tasks in the PCRV development program shows the interaction between the design and the development plan. The schedule follows the HTGR development schedule for the PCRV and the related pressure boundary components, including closures, closure seals, flow restrictors, and thermal barrier.

REFERENCE

1. "Gas-Cooled Fast Breeder Reactor Demonstration Plant Development Plan," Vol. II, USAEC, Report GA-A10788, Gulf General Atomic, September 20, 1972.

XIII. SHIELDING REQUIREMENTS (189a No. 13841)

The verification of the adequacy of the methods and data (physics and engineering) for the design of GCFR shields and an evaluation of the effectiveness of various shield configurations are to be conducted under this task. In addition, the analytical and experimental GCFR shielding activities will be coordinated with ORNL.

In the last quarterly report,[1] methods for generating neutron-coupled gamma-ray transport cross sections were reported. Comparison between measured and calculated neutron spectra in iron, the primary producer of gamma rays in the shield, were also reported.

During this quarter, a draft of the shielding development plan, which specifies the multiyear effort required to achieve the overall goals of the shielding program, was completed. In the physics analyses, preliminary one-dimensional calculations have been made to study the effect of multilayer shield configurations on the design of the radial shield. Preliminary results indicate that the present shield design can be optimized with a substantial reduction in shield thickness. Neutron-coupled gamma-ray transport, including gamma-ray heating calculations, have been completed for the radial shield. Finally, a synopsis of the DOT III calculations performed by ORNL are reported and tabulated for key points in the 300-MW(e) GCFR shield.

13.1. PHYSICS ANALYSIS

13.1.1. Radial Shield Studies

Preliminary one-dimensional transport calculations have been performed to investigate the possibility of reducing the radial thickness of the outer shield of the 300-MW(e) GCFR. Interest in such a reduction stems from a corresponding reduction in the cost of the shield as well as a reduction in the radius of the PCRV and subsequent reductions in construction costs.

The reduction in the radius of the outer shield was based on the magnitude of the fast neutron flux (E > 1.0 MeV), i.e., the radius was reduced to that point where the fast flux of the original shield calculation was about a factor of two to three less than the allowable upper limit of 2×10^9 neutrons/cm^2-sec. A comparison of the reduced and the initial configurations is shown in Fig. 13.1. In the reduced shield, a layer of graphite and a layer of stainless steel were eliminated from the outermost part of the outer shield and the PCRV liner was moved inward an equal distance. The reduced shield thickness is sufficient to attenuate the high-energy flux. However, to reduce the thermal flux to the allowable level of 10^9 neutrons/cm^2-sec, boron must be added to the remaining layer of graphite in the outer shield (see Fig. 13.1).

The radial flux profile obtained from a preliminary ten-group, P_3, calculation for the 300-MW(e) GCFR with a boronated graphite region (19.5 wt-% of natural boron) is shown in Fig. 13.2. Also shown in Fig. 13.2 are the calculated thermal and total fluxes for the same configuration without boron in the outer shield. A 1DFX calculation for the boronated shield configuration indicated a thermal flux of about 1.0×10^9 neutrons/cm^2-sec and a fast flux of about 1.2×10^8 neutrons/cm^2-sec at the liner. The results of this study suggest that further optimization of the radial shield with respect to shield material specification and configuration should be investigated.

13.1.2. Sensitivity Analysis for the GCFR Radial Shield

The purpose of the radial-shield sensitivity studies was to determine the optimum arrangement of the radial-shield material specification and configuration. In this initial one-dimensional study, the total thickness of the radial shield, thickness and composition of the (B_4C + C) homogenized layer, and the helium channel were kept constant. The thickness of the first layer of graphite was kept constant so that neutron backscattering into the blanket would not be altered. The thickness of graphite and stainless steel in the remaining layers as well as their configuration were varied. The sensitivity of the ratio of fast to thermal flux at the liner was then determined for the four shield configurations shown in Table 13.1. The most effective shield utilized steel to reduce

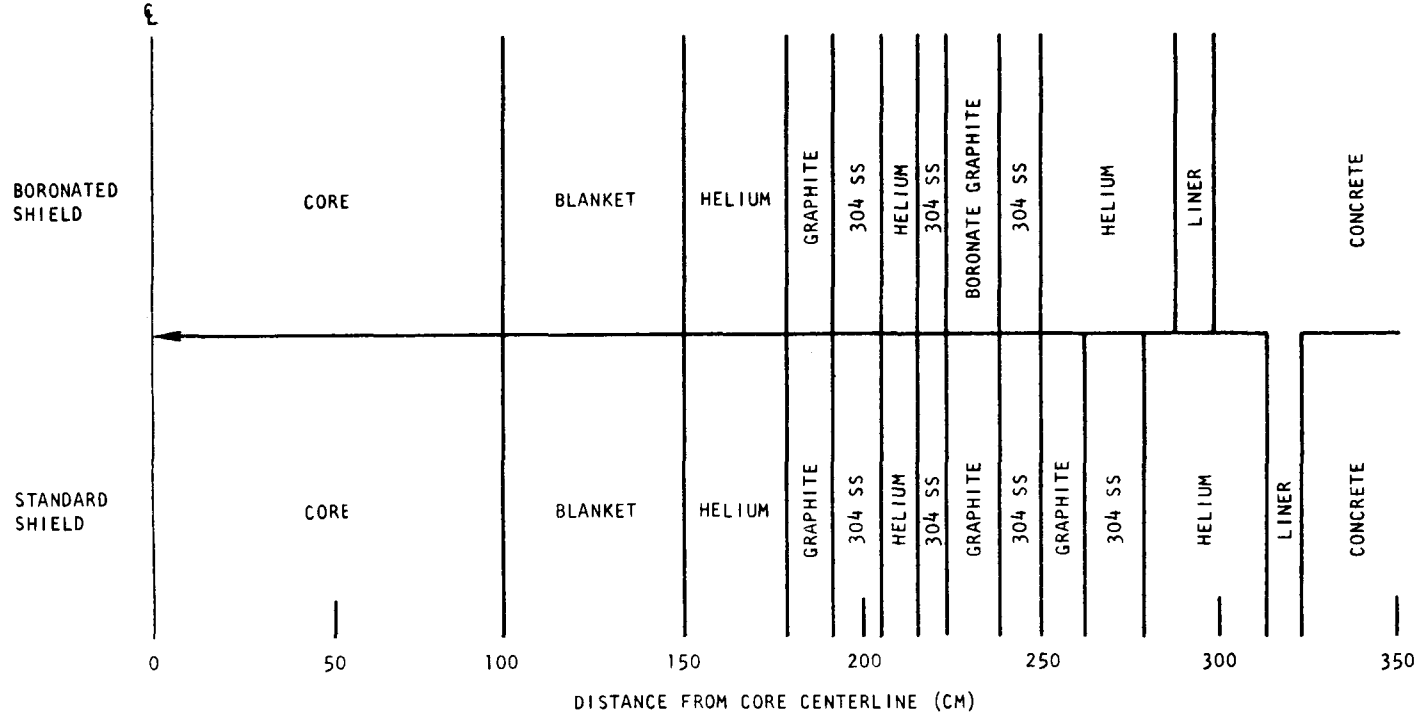

Fig. 13.1 Geometry for 1-D transport calculations of radial flux in a proposed boronated graphite shield for the 300-MW(e) GCFR and the geometry for the standard shield

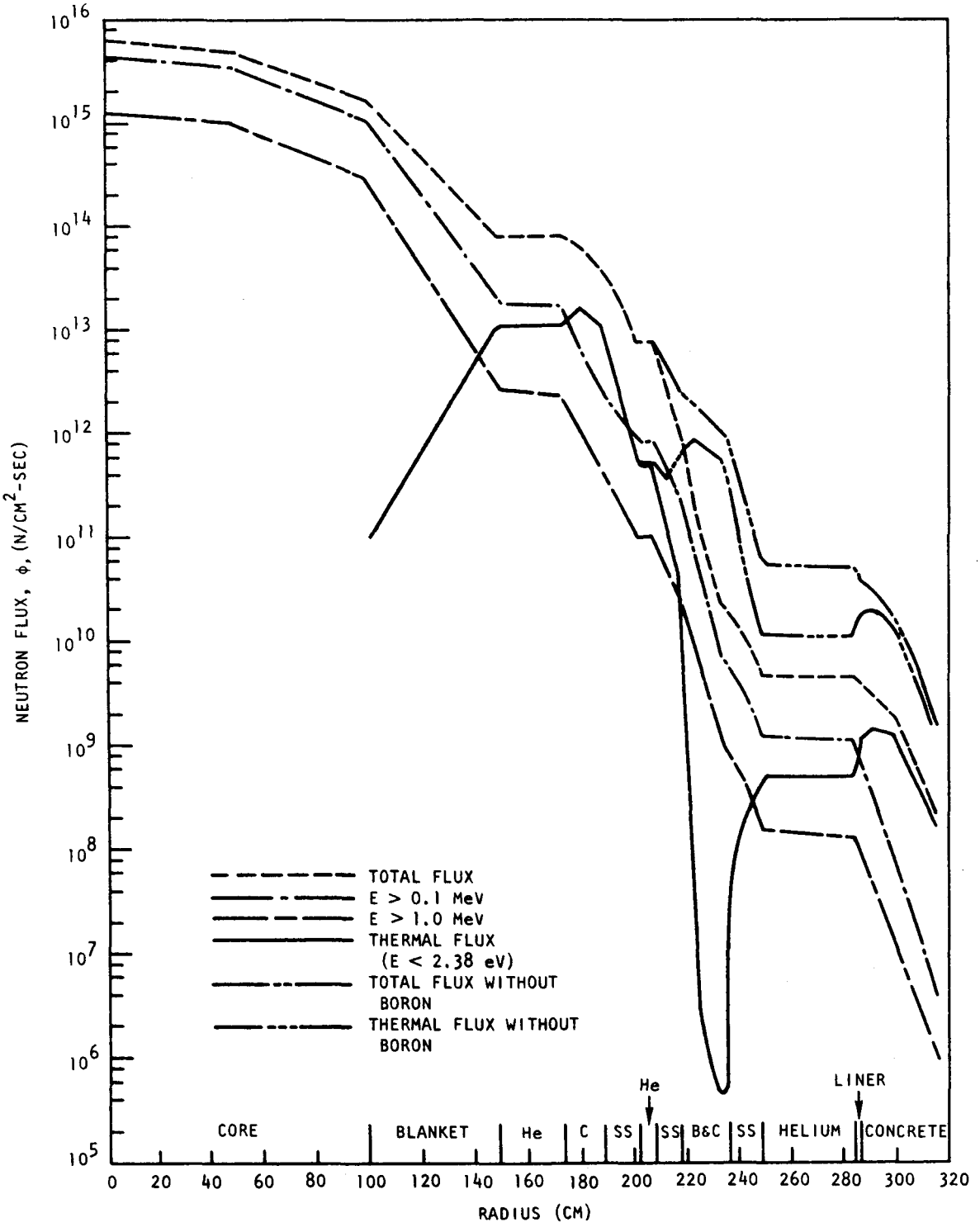

Fig. 13.2 Radial flux profile at the core midplane of the 300-MW(e) GCFR with a boronated graphite region (19.5 wt-% Boron) in the shield

Table 13.1

MATERIAL CONFIGURATION FOR SHIELD SENSITIVITY ANALYSIS

Shield 1									
Inner radius, cm	174	189.4	202.57	208.575	218.735	236.9	249.6	284.9	
Thickness, cm	15.4	13.175	6	10.16	18.165	12.7	35.3	1.9	
Material	C[a]	SS[b]	He	SS	C + B_4C	SS	He	Liner	
Shield 2									
Radii	174	189.4	202.57	208.575	218.735	226.435	244.6	249.6	284.9
Thickness	15.4	13.175	6	10.16	7.7	18.165	5	35.3	1.9
Material	C	SS	He	SS	C	C + B_4C	SS	He	Liner
Shield 3									
Radii	174	189.4	202.57	208.575	213.575	226.435	244.6	249.6	284.9
Thickness	15.4	13.175	6	5	12.86	18.165	5	35.3	1.9
Material	C	SS	He	SS	C	C + B_4C	SS	He	Liner
Shield 4									
Radii	174	189.4	202.57	208.575	226.435	244.6	249.6	284.9	
Thickness	15.4	13.175	6	17.86	18.165	5	35.3	1.9	
Material	C	SS	He	C	C + B_4C	SS	He	Liner	

[a] Graphite, density = 1.7 g/cm^3.

[b] Type 304 stainless steel.

the energy of fast neutrons by inelastic scattering and graphite to provide additional moderation to thermal energies, where the neutrons are captured in boron. Therefore, an optimum configuration is one in which the ratio of fast to thermal neutrons incident on the borated layer is a minimum. The ratio of the graphite thickness to the stainless steel plus graphite layer thickness (C/SS + C) was used as a parameter in the present study. This was done by the proper ordering of the material, as mentioned above, consistent with engineering constraints.

A measure of the effectiveness of the radial shield is the ratio of the flux at the liner ϕ_L to the incident flux ϕ_0, where ϕ_0 is the flux emerging from the radial blanket. The results of this study are tabulated in Table 13.2 for four representative shield configurations at four neutron energies. The following conclusions can be made:

1. In going from shield configuration 1 to shield configuration 4, the ratio of ϕ_L/ϕ_0 decreases by almost a factor of 3.
2. The total flux at the liner decreases as the ratio of C/(C + SS) increases.
3. The ratio of ϕ_L/ϕ_0 for fast neutrons increases as the ratio of C/(C + SS) increases.
4. An optimum ratio of C/(C + SS) is in the range of 0.50 to 0.65.

Table 13.2

RESULTS OF SHIELD SENSITIVITY ANALYSIS

Shield	C/(SS + C)	ϕ_L/ϕ_0 (thermal) E < 2.35 eV	ϕ_L/ϕ_0 E > 0.067 MeV	ϕ_L/ϕ_0 E > 1.35 MeV	ϕ_L/ϕ_0 Total
1	0.3	6.4×10^{-5}	4.22×10^{-5}	1.11×10^{-5}	4.85×10^{-5}
2	0.45	3.35×10^{-5}	2.265×10^{-5}	1.64×10^{-5}	2.62×10^{-5}
3	0.55	2.71×10^{-5}	2.16×10^{-5}	1.884×10^{-5}	2.12×10^{-5}
4	0.647	2.34×10^{-5}	1.735×10^{-5}	2.97×10^{-5}	1.84×10^{-5}

In summary, these preliminary one-dimensional radial shield sensitivity studies at the core midplane of the 300-MW(e) GCFR demonstrates

that it is possible to reduce the thickness of the outer shield and optimize the configuration of shield materials for the most effective use of B_4C. However, the final shield design will depend on the coupled effects of gamma-ray and nuclear heating and material damage by the thermal and fast neutrons, respectively. In addition, two-dimensional transport sensitivity calculations will be necessary to optimize the complete shield configuration relative to the above effects for the entire PCRV liner.

13.1.3. Gamma-ray Heating Calculations

Using the methodology discussed in the last quarterly report,[1] a series of coupled neutron-gamma-ray transport calculations were made for the radial shield of the 300-MW(e) GCFR. In addition to the gamma-ray heating calculations, a preliminary sensitivity analysis was made of the heating response of the liner and PCRV to the gamma-ray production in the various shield components.

13.1.3.1. Neutron-coupled Gamma-ray Transport Cross Sections. The neutron-coupled gamma-ray transport matrix consists of three contributions: (1) a neutron-transport cross-section matrix (n, n') generated by GGC-5,[2] (2) a gamma-ray-transport cross-section matrix (γ, γ'), generated by DINT,[3], and (3) gamma-ray-production cross-section matrix (n, γ) and (n, xγ) generated by LAPHANO.[4] These three components were combined via the RCOUPL code to generate the final neutron-coupled gamma-ray transport cross-section matrix.

In view of a lack of cross-section information on some of the GCFR shield nuclei, the following simplifications were made: iron was substituted for stainless steel, and the following concrete mixture (which closely approximates 4-B concrete*) was considered:

Element	Atom density (No. atoms/barn-cm)
H	8.00×10^{-3}
O	4.44×10^{-2}
Al	4.87×10^{-3}
Si	1.59×10^{-2}
Ca	3.63×10^{-3}
Fe	3.10×10^{-4}

*4-B is the concrete composition specified by HTGR PCRVs.

The procedure for generating the neutron-coupled gamma-ray cross sections were checked as follows: a transport calculation for a 56-cm slab of iron was carried out with the 1DFX code using the neutron-coupled gamma-ray cross section for iron. This calculation was compared to an ORNL measurement. The gamma-ray spectra for energies above 1.5 MeV indicated agreement between measurement and calculations better than 20%.

Because of core storage limitations on the GAC computer system, a complete S_{16} transport run for the GCFR shield in cylindrical geometry could not be carried out. Instead, the neutron flux emerging from the blanket for a cylindrical geometry was used as the initial flux in a slab configuration of the shield.

The energy deposition profile in the shield (slab geometry) starting with the neutron flux emerging from the blanket is shown in Fig. 13.3. This energy deposition profile is better understood when interpreted in the light of the thermal neutron flux and total gamma-ray flux shown in Figs. 13.4 and 13.5, respectively. To obtain the absolute magnitude for the energy deposition, the numbers calculated in ANISN (which were normalized to 1 neutron/cm^2-sec) must be multiplied by the appropriate total neutron flux at the blanket for the 300-MW(e) GCFR, i.e., 8.7×10^{13} neutrons/cm^2-sec. The right-hand ordinate of Fig. 13.3 is in absolute units. It is seen that for the reference shield design used in these studies, the energy deposition rate in concrete is more than an order of magnitude below the allowable criterion of 1 mW/cm .

13.1.3.2. Gamma-ray-heating Sensitivity Analysis. Studies were made of the sensitivity of gamma-ray energy deposition in the PCRV to the following factors:

1. Gamma rays absorbed in each of the constituents of concrete.
2. Gamma rays produced in the liner.
3. Gamma rays produced in the internal steel region shield and transported to the PCRV (see Fig. 13.3).

To analyze the contributions of the various 4-B concrete components to the total energy deposition in it, the following was done: The energy absorption coefficients for the multigroup gamma rays were determined

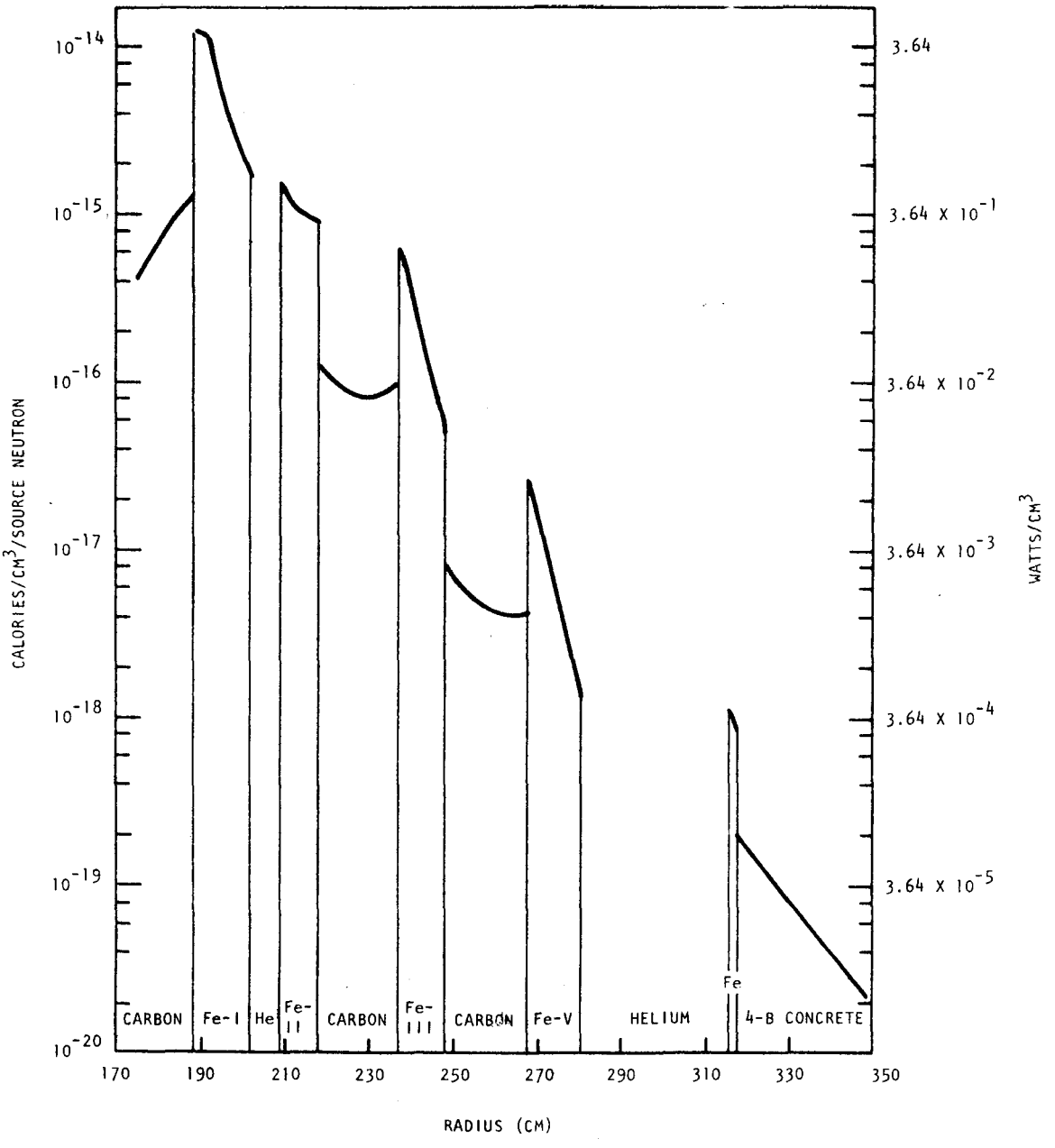

Fig. 13.3 Energy deposition profile in the GCFR shield (slab geometry) vs radial distance

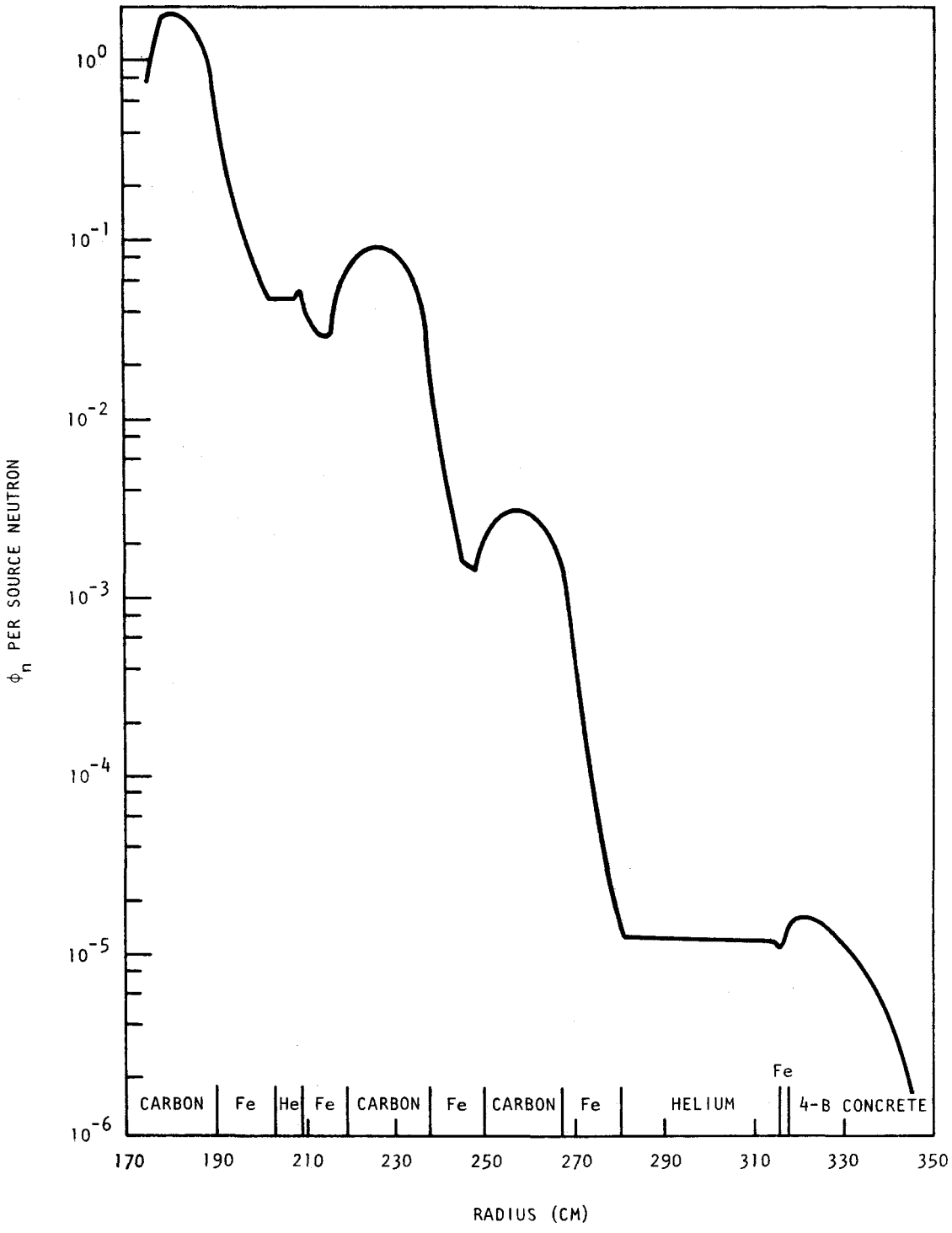

Fig. 13.4 Total neutron flux profile as a function of radial distance

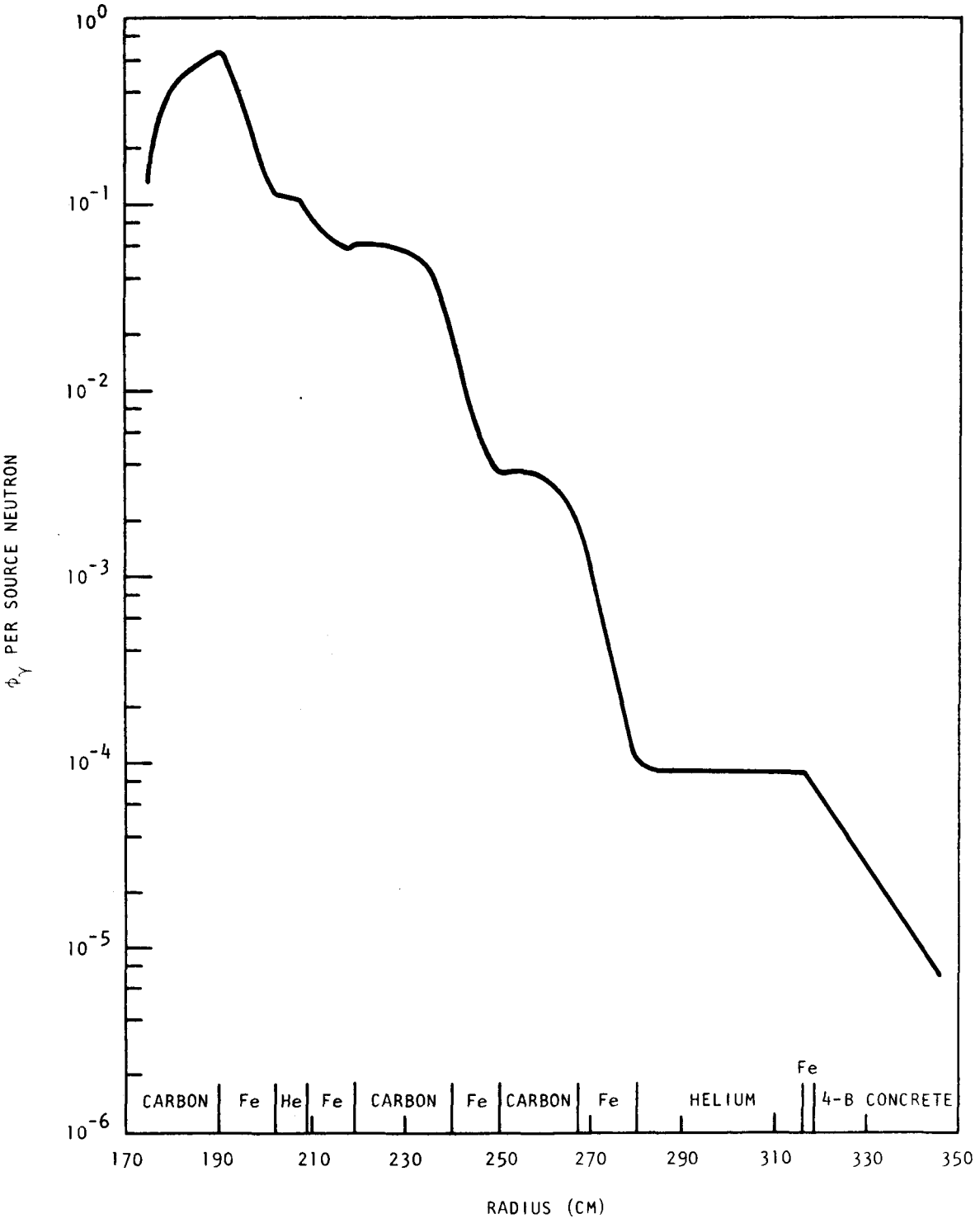

Fig. 13.5 Total gamma-ray flux profile as a function of radial distance

for each of the 4-B concrete components.[3] These were then multiplied by the corresponding atom density to give the gamma-ray energy absorption coefficient in calories/centimeter per incident neutron. The energy absorption effects in 4-B concrete on both an absolute and percentage scale are indicated in Figs. 13.6 and 13.7.

The following conclusions can be drawn from this gamma-ray-heating sensitivity study:

1. Gamma-ray absorption is largest for the high-energy gamma rays, and it drops by a factor of four for an order of magnitude decrease in gamma-ray energy.
2. Oxygen and silicon are the dominating nuclides for energy absorption in concrete.

To study the relative effect of gamma-ray transport from the liner and inner shields to the concrete heating, a series of calculations were made in which the gamma production from the various shield components could be switched on and off. The results of the transport calculations, shown in Fig. 13.8, indicate that

1. Gamma rays produced in the concrete contribute less than 15.5% to energy deposition in concrete.
2. Gamma rays produced in the liner contribute less than 15% to energy deposition in concrete.
3. Gamma rays produced in Fe III and Fe IV (see Fig. 13.3) are the primary contributors to energy deposition in concrete, i.e., ~60% of the total energy deposited in concrete by gamma rays.

13.1.4. Analysis of DOT III Calculations of the 300-MW(e) GCFR Performed by ORNL

In the analysis of the ORNL transport calculations using the DOT III (R-Z) code, the fluxes and fluences for 40 yr at a 0.8 load factor, or 32 EPY, and for 30 yr at a 0.8 load factor, or 24 EPY, were reviewed for three representative energy ranges; namely, $E > 1.0$ MeV, $E > 0.1$ MeV, and total flux. Seven key areas in the reactor shield are defined in Fig. 3.9

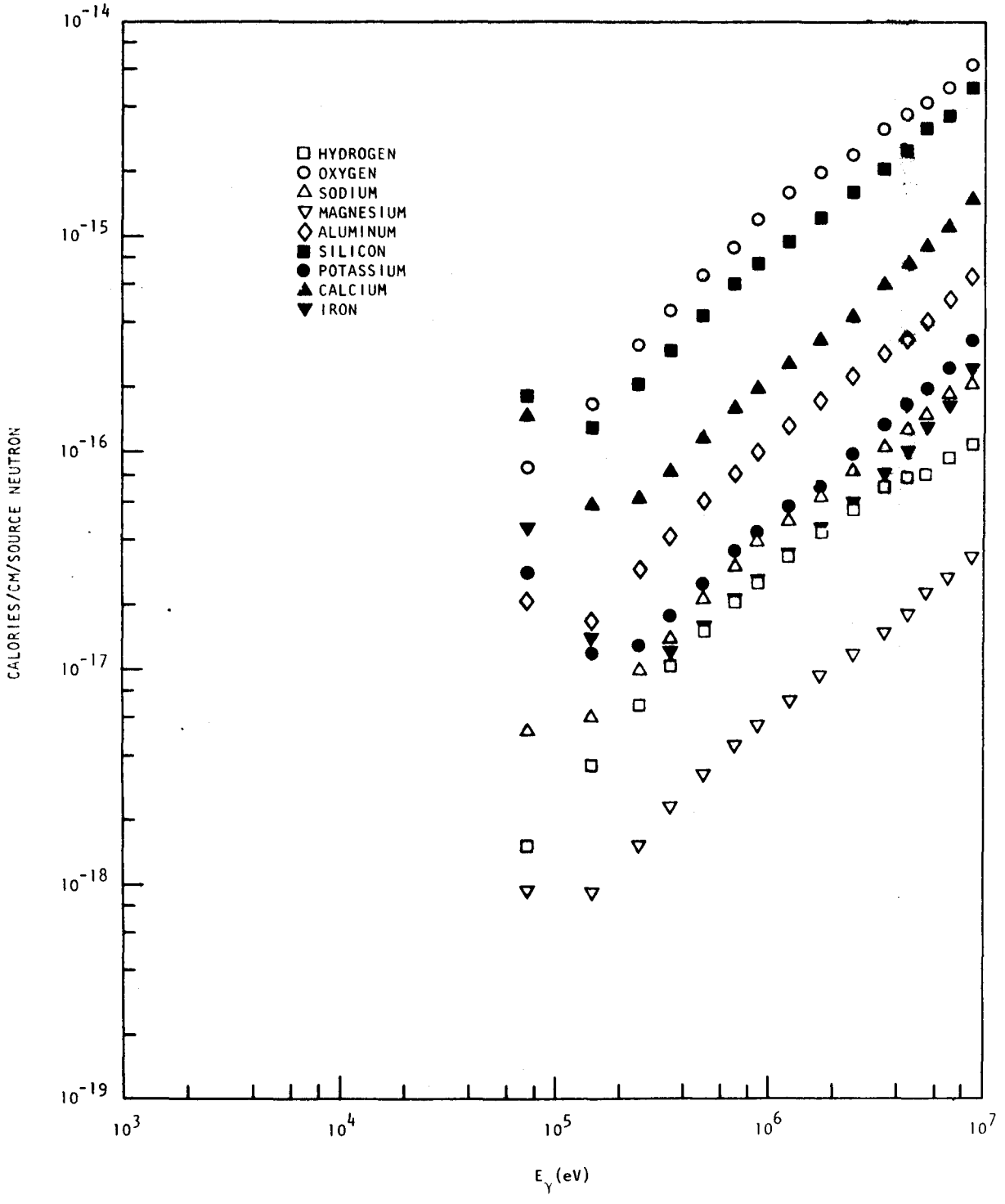

Fig. 13.6 Contribution of 4-B (PCRV concrete) concrete components to gamma-ray absorption as a function of gamma-ray energy

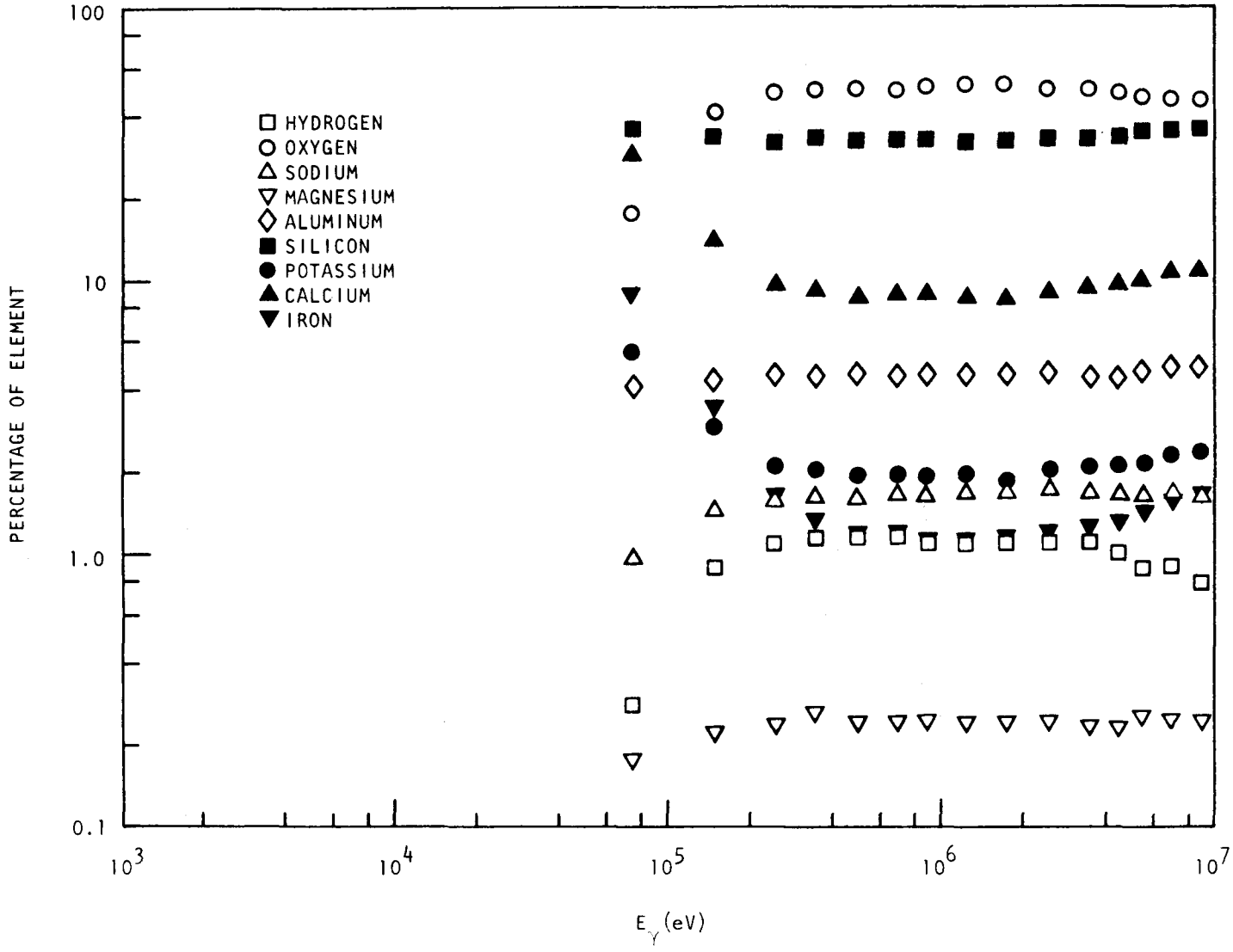

Fig. 13.7 Percentile contribution of 4-B concrete (PCRV concrete) components to gamma-ray absorption as a function of gamma-ray energy

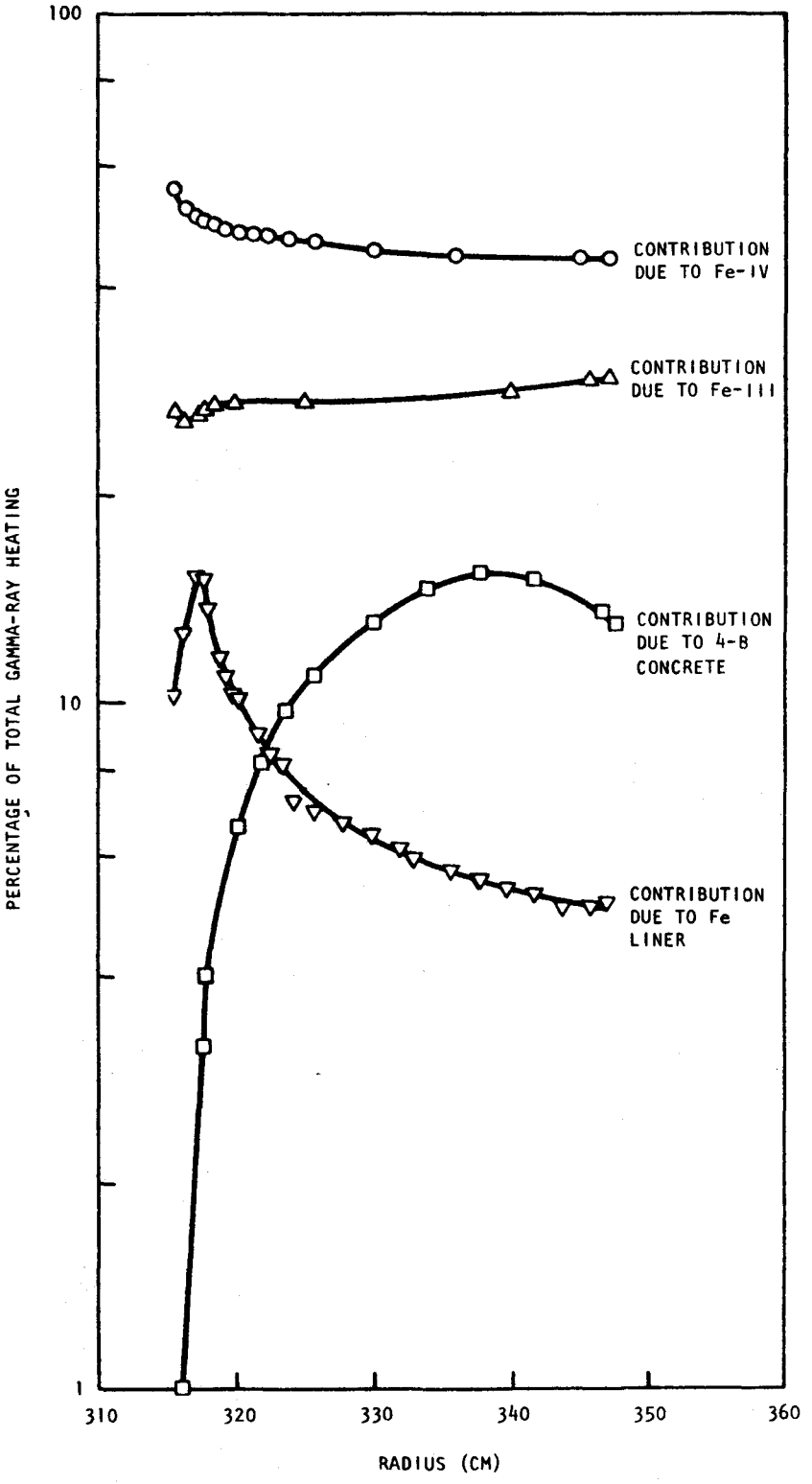

Fig. 13.8 Percentile contribution of GCFR shield components to gamma-ray heating in iron liner and PCRV concrete as a function of radial distance

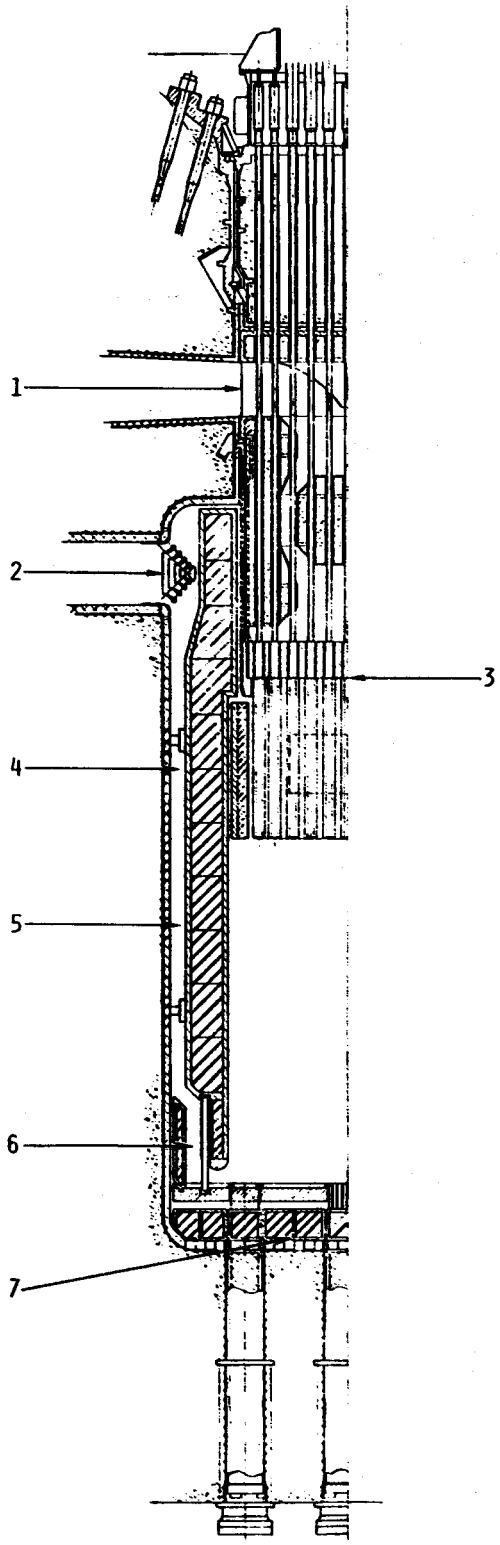

Fig. 13.9 Vertical section through reactor cavity

and the following guides were used for defining allowable levels:

1. The maximum fluence for stainless steel should not exceed 1.0×10^{23} nvt for E > 0.1 MeV.
2. At the PCRV liner, the fast fluence should not exceed 2×10^{18} nvt for E > 1.0 MeV.
3. At the liner, the thermal flux should not exceed 1.0×10^{9} neutrons/cm^2-sec for E < 2.38 eV.

The results of the calculations and analysis are summarized in Table 13.3. Note that at all points, the fast-flux criteria are met. However, at the lower portions of the PCRV cavity (at points 5, 6, and 7), the thermal flux appears to be high. (The thermal flux is estimated to be 10% to 50% of the total flux at the PCRV based on 1DFX calculations). The use of boron to suppress the thermal flux at the lower portions of the reactor shield appears to be desirable, as shown in the one-dimensional analysis discussed in Section 13.1.1.

13.2. SHIELD ENGINEERING

13.2.1. Structural Analysis

Thermal expansions in the axial direction of the outer radial shield, the inner radial shield, and the grid-plate support structure were calculated for evaluating the adequacy of clearances around these structures.

Similar calculations for thermal expansions in the radial direction of the grid plate and the reactor cavity closure plug were carried out to determine the relative displacement of the grid plate with respect to the cavity closure.

A study of the flow-induced vibration of the outer radial shield assembly is currently under way. Preliminary calculations have indicated that this phenomenon is not a problem for this structure.

The previously used seismic model with 38 node points was extended to incorporate the shield system with an additional 12 node points. Considering different shield support structures, the dynamic response of the shield assembly due to seismic excitation is now under study. The one-dimensional spring-mass seismic model presently used does not determine

Table 13.3

NEUTRON FLUXES AND FLUENCES IN THE 300-MW(e) GCFR SHIELD AND PCRV CAVITY

Point[a]	Description	E > 1.0 MeV		E > 0.1 MeV		Total Flux	
		nv	nvt[b]	nv	nvt[b]	nv	nvt[b]
1	Helium inlets at PCRV liner above reactor assembly	7×10^{-1}	7×10^{8} 5.2×10^{8}	1.4×10^{4}	1.4×10^{13} 1.0×10^{13}	7.2×10^{5}	7.2×10^{14} 5.4×10^{14}
2	Helium outlets at PCRV liner above reactor core and outside outer shield	$\lesssim 7\times10^{2}$	$\lesssim 7\times10^{11}$ 5.2×10^{11}	$\lesssim 7\times10^{4}$	7×10^{13} 5.2×10^{13}	$\lesssim 7\times10^{7}$	7×10^{16} 5.2×10^{16}
3	Below grid plate at centerline	3.5×10^{11}	3.5×10^{20} 2.6×10^{20}	1.1×10^{13}	1.1×10^{22} 8.2×10^{21}	4.5×10^{13}	4.5×10^{22} 3.4×10^{22}
4	PCRV liner at core centerplane	7.1×10^{4}	7.1×10^{13} 5.3×10^{13}	7.1×10^{6}	7.1×10^{15} 5.3×10^{15}	8.5×10^{8}	8.5×10^{17} 6.4×10^{17}
5	PCRV liner at about 190 cm below the reactor and inner shield	1.8×10^{6}	1.8×10^{15} 1.4×10^{15}	2.3×10^{8}	2.3×10^{17} 1.7×10^{17}	2.1×10^{10}	2.1×10^{19} 1.6×10^{19}
6	Between wraparound and outer shield near bottom of PCRV	5.7×10^{8}	5.7×10^{17} 4.3×10^{17}	7.1×10^{10}	7.1×10^{19} 5.3×10^{19}	1.4×10^{12}	1.4×10^{21} 1.0×10^{21}
7	Below lower shield near the bottom of the PCRV cavity	7×10^{4}	7×10^{13} 5.2×10^{13}	7.1×10^{6}	7.1×10^{15} 5.3×10^{15}	7.1×10^{9}	7.1×10^{18} 5.3×10^{18}

[a] See Fig. 13.9.

[b] The first value in each pair is for 32 EPY (40 yr at 0.8 LF) and the second is for 24 EPY (30 yr at 0.8 LF).

the impact forces between the shield elements. An improved analysis utilzing a three-dimensional seismic model could achieve more realistic results and diminish design uncertainties in this area.

REFERENCES

1. "Gas-Cooled Fast Breeder Reactor Quarterly Progress Report for the Period May 1, 1974 through July 31, 1974," USAEC, Report GA-A13148, General Atomic, September 26, 1974.

2. Mathews, D. R., et al., "GGC-5, A Computer Program for Calculating Neutron Spectra and Group Constants," Gulf General Atomic, Report GA-8871, September 27, 1971.

3. Adams, K. G., et al., "DINT: A Computer Program which Prepares Multigroup Coherent-Incoherent Cross Sections for Photon Transport Calculations," Sandia Laboratory, Report SC-RR-720684, December 1972.

4. Dudziak, D. J., et al., "LAPHANO: A P_0 Multigroup Photon-production Matrix and Source Code for ENDF," USAEC, Report LA-4750-MS, Los Alamos Scientific Laboratory, January 1972.

XIV. FUEL-ROD ENGINEERING (189a No. 13861)

The steady-state and transient performance of the fuel, blanket, and control rods is being evaluated under this task to determine performance characteristics, operating limits, and design criteria. The analytical tools (such as the LIFE-III code) are being adapted, updated and/or developed, and applied to the analysis of the rods and the evaluation of GCFR irradiation experiments. Continuous surveillance is maintained of the LMFBR fuels and materials development programs and technology to maximize use of developing technology and materials properties. Support is provided in the planning and designing of irradiation experiments.

14.1. FUEL-, BLANKET-, AND CONTROL-ROD ANALYSIS

The objectives of this analytical task are to adapt and assess the ability of analytical behavioral models and computer codes (such as LIFE-III) to analyze GCFR fuel, blanket, and control rods and to evaluate irradiation experiments. The definition of design criteria, operating margins, failure criteria, and mechanisms under steady-state, transient, and load-following conditions will follow from these analyses.

14.1.1. Fuel- and Blanket-rod Analysis

The LIFE-III code was made operational on the GA computer during the last quarter and a number of updates were made to the code. Several problem areas, such as improper fuel central-void closure, improper grain growth and restructuring of fuel, and mechanical coupling, which resulted in unduly long computer running times, were identified during the calibration runs made with standard problems furnished by ANL and while attempting an evaluation of rod G-1 from the F-1 series irradiated in EBR-II (see Section III).

The modified version of the LIFE code was received from ANL during this quarter and was made operational on the GA computer system. Additional updates, including one proposed by Westinghouse that was intended

to improve the stress and strain oscillation (convergence problem) and improper fuel central-hole closure, have been screened, incorporated into the code, and their effect on the code prediction evaluated. Basically, the solution consisted of modifying the procedure for conversion from deformed to new undeformed radii at the end of the thermal analysis. This simplified the thermal-mechanical coupling. This modification became necessary when PORMIG (the pore migration and fuel restructuring model) was recently introduced in the new version of LIFE. Comparison cases to the "prior to update" version of the code were run. It appears that the improper fuel central-void closure, as previously encountered, has been corrected and central void sizes more consistent with those observed from experimental observations are predicted. In addition, predictions on grain growth and fuel restructuring are now also in the range of what one would expect from experimental evidence. The problems of excessive GA computer running time, however, did not seem to have been improved as a result of these changes.

14.1.2. Analysis of Irradiation Tests

14.1.2.1. Analysis of Test Rods for Extended Irradiation. It was desirable to extend the irradiation of the fuel rods in the F-1 series being irradiated in EBR-II. This would result in burnups of 125,000 (25% in excess of the maximum burnup in GCFR), 100,000, and 75,000 MWd/Te for the three highest burnup rods at cladding outside temperatures from 700° to 750°C. Attainment of these goals will markedly increase the confidence level in the GCFR fuel-rod design.

An estimate of the total end-of-life cladding strains (at the peak power and peak cladding temperature location) resulting from the planned extended irradiation on the two limiting rods (G-4 and G-13, according to the combination of burnup, power level, plenum volume, and cladding temperature) was obtained using the LIFE code. The LIFE-II code was used for this analysis because an acceptable version of LIFE-III was not yet operable. The rod parameters used for the analysis, including rod G-1 for comparison because the postirradiation total cladding permanent strain measurement has been made on it, are listed in Table 14.1. The measured

Table 14.1

PARAMETERS USED FOR RODS G-1, G-4, AND G-13

Parameters	Rod G-1	Rod G-4	Rod G-13
Cladding OD, in.	0.300	0.300	0.300
Cladding ID, in.	0.2630	0.2630	0.2630
Fuel OD, in.	0.2595	0.2595	0.2595
Central void diameter, in.	0.058	0.058	0.058
Cladding material	20% CW 316 SS	20% CW 316 SS	20% CW 316 SS
Length of cladding, in.	36.2	34.4	32.6
Length of fuel column, in.	13.5	13.5	13.5
Fill-gas volume, moles at STP	0.00112	0.00092	0.0009
Cladding OD temperature, °C	800	700	750
Peak power, kW/ft	15.3	14.8	15.6
Fast flux, n/cm^2-sec	1.16×10^{15}	1.18×10^{15}	1.16×10^{15}
Irradiation time, hr	7,000	18,000	10,250
Burnup, at-%	6.1	13.2	8.2
Burnup, MWd/Te	55,000	125,000	75,000

postirradiation maximum cladding strain for rod G-1 (see Table 14.1) was less than 0.3%. The calculated corresponding cladding strains for rods G-4 and G-13 after the burnups shown in Table 14.1 were 0.36% and 0.42% greater than those calculated for rod G-1. By adding these extrapolated strains to the measured values of rod G-1, an estimate of the total end-of-life permanent cladding strain of less than 0.66% and 0.72% was obtained for rods G-4 and G-13, respectively, at the extended burnups. It was then concluded that there is sufficient margin of safety to proceed with the extended irradiation.

14.1.2.2. Analysis of "Round Robin" GE F-20 Experiment. A request was received to participate in the evaluation and round-robin analysis of the rods irradiated by General Electric in the EBR-II reactor (GE F-20 experiment). This experiment includes a total of 29 rods irradiated in three phases. Phase I consisted of a 10-day irradiation of 19 rods at power levels varying from 14.5 to 17.2 kW/ft; Phase II consisted of a

10-min irradiation at overpower (18.3 to 20.8 kW/ft power levels) to produce fuel melting; and Phase III was a 17-day irradiation at the lower power levels (15 to 17 kW/ft) after the overpower operation with fuel melting. Eight of the rods in these tests had been previously irradiated to burnups of 5 to 7 at-% at power levels from 11 to 15 kW/ft.

General Atomic will participate in the analytical effort by analyzing nine of the test rods utilizing the LIFE-III code. The evaluation is limited to those fuel rods that appear to provide the most effective support to GCFR fuel design. These are the rods listed in Table 14.2. The analysis of the rods has been initiated by the use of the present version of the LIFE-III code (July 16 version distributed by ANL). Calculations of the Phase II irradiation (10 min at overpower) of rods E-1 and S-4 were made. A comparison of the major parameters for these rods is given in Table 14.3 and the reactor power history is shown in Fig. 14.1. The capsule environment for this test was simulated in the LIFE code by manipulating the coolant inlet and outlet temperatures and flow so as to result in the proper known cladding temperature distribution for the test rods (470° to 580°C). Six axial sections were specified for each rod in order to obtain an axial temperature distribution. The radial temperature distribution predicted for the peak power axial section location in each of the rods is plotted in Fig. 14.2. This indicates that no fuel melting occurred for rod E-1 (cored fuel pellet) and that fuel melting occurred to about 8% of the fuel radius in axial section number 3 only (central section) for rod S-4 (solid fuel pellet). The formation of a central void 0.0375 in. in diameter is predicted for the initially solid fuel pellet and a central void enlargement to 0.0544 in. for the initially cored pellet. These results indicate that higher power to melt would be expected for cored pellet fuel.

14.2. DESIGN CRITERIA

The structural design criteria for the fuel, blanket, and control-rod cladding will be established under this subtask. These criteria will consist of sets of limits on stresses, strains, and displacement for all anticipated loading conditions. In the course of this effort, failure modes and related mechanisms will be identified. Work on this subtask

Table 14.2

FUEL RODS SELECTED FOR ANALYSIS IN ROUND-ROBIN EXPERIMENT

Rod No.	Fuel Pellet Form	Fuel-cladding Diametral Gap (in.)	Fuel-pellet Density (% TD)	Pre-F-20[a] Irradiation Burnup (at-%)	Irradiated In Phase
S-3	Solid	0.0056	90.4		I, II
S-4[b]	Solid	0.0057	90.6		II
F5P[a]	Solid	0.0051	94.0	5.56	II
F5G[a]	Solid	0.0043	93.8	5.58	I, II
C12	Solid	0.0032	90.0		I, II
31	Solid dished	0.0071	92.3		II
18R	Solid dished	0.0061	92.7		I, II
E-1	Annular	0.0059	90.1		II
E-2	Annular	0.0059	91.0		I, II

[a]Rods previously irradiated in EBR-II, F5P and F5G, to ∿60,000 MWd/Te.

[b]Contained melt wires.

Table 14.3

MAJOR PARAMETERS FOR RODS E-1 AND S-4 IN ROUND-ROBIN EXPERIMENT

	Rod E-1	Rod S-4
Rod OD, in.	0.2501	0.2499
Central void diameter, in.	0.0431	None
Fuel-cladding diametral gap, in.	0.0059	0.0057
Peak linear power, kW/ft	19.5	20.0
Fuel density, % TD	90.1	90.6
Cladding material	SA 316 SS	SA 316 SS
Cladding thickness, in.	0.01515	0.01505
Fuel column length, in.	13.5	13.5
Total internal fill gas, moles	0.005 He	0.00045 He
Peak fast flux, n/cm^2-sec	2.5×10^{15}	2.5×10^{15}

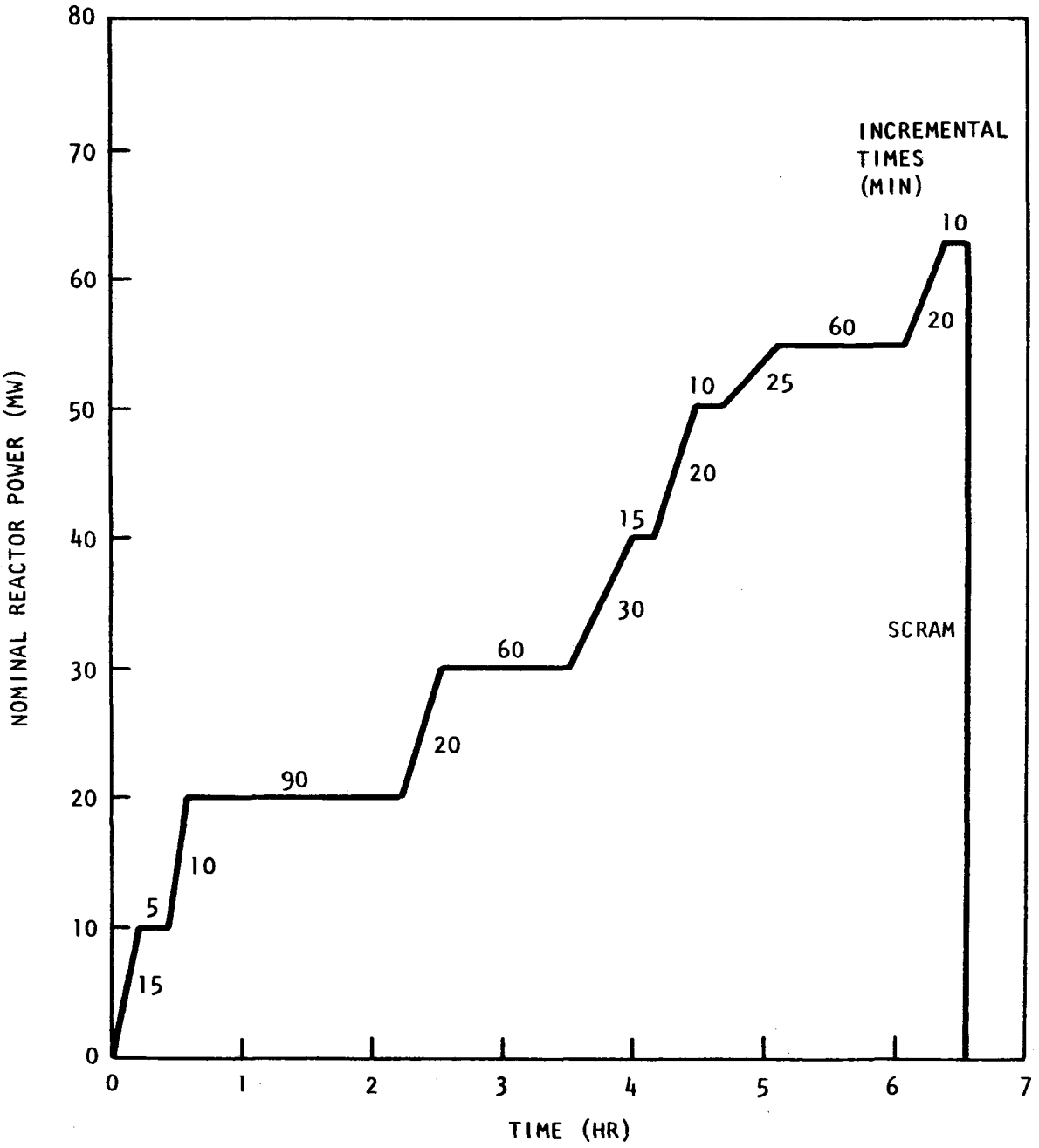

Fig. 14.1 GE F20 Phase II reactor power history

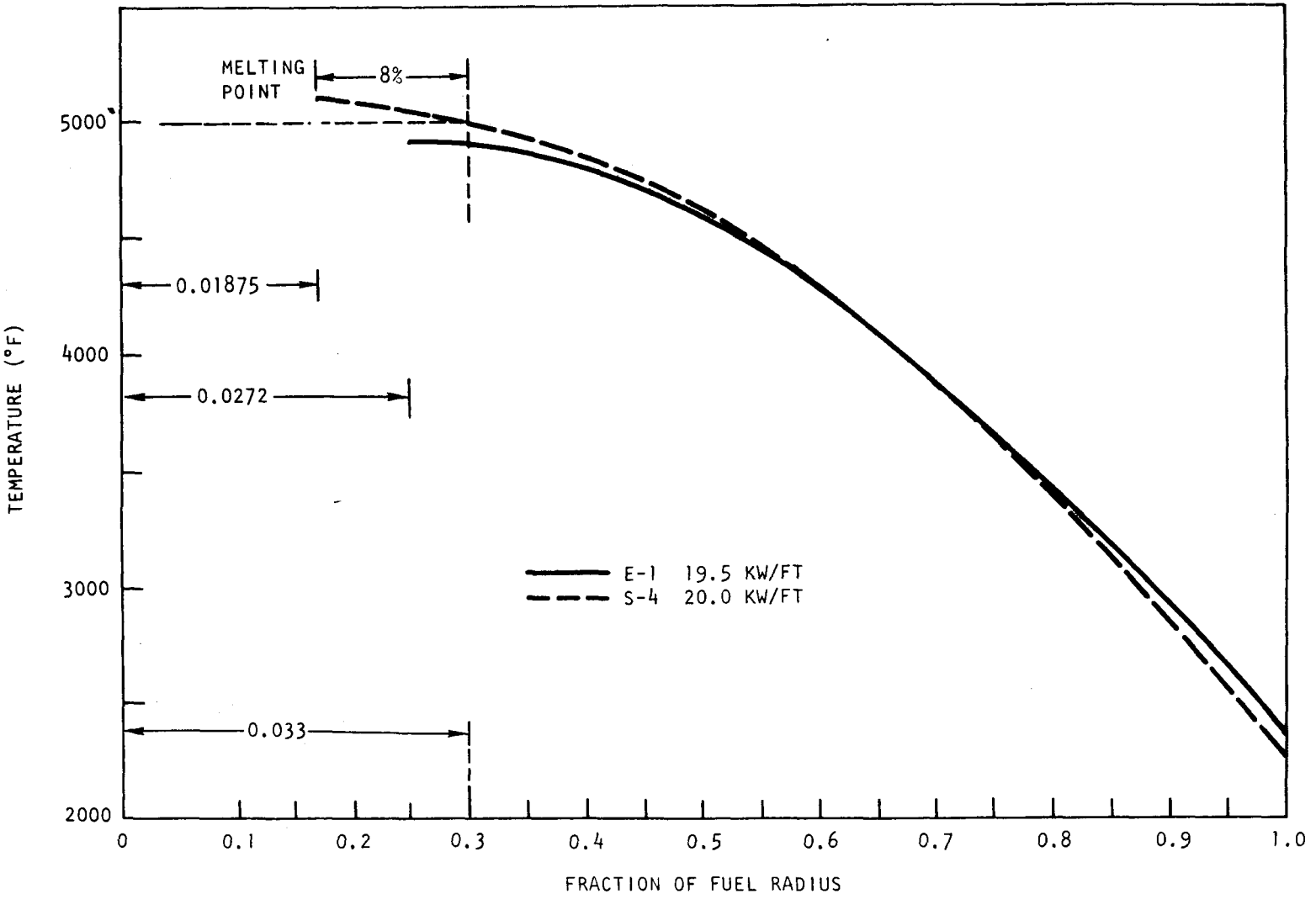

Fig. 14.2 Radial temperature distribution

commenced during the present quarter. The initial efforts have been on reviewing General Electric's report "Preliminary Draft of RDT Standard Structural Design Criteria for Core Components," and an evaluation is in progress. Based on those portions reviewed thus far, it seems likely that only minor modifications will be required to assemble GCFR criteria from the LMFBR program. The requirements of pertinent creep rupture data for the roughened and unroughened areas of the fuel rod were identified as items to be provided by ANL burst tests.

Three preliminary analyses were made to assess possible failure modes in the roughened area of the fuel rod. The effects of hertzian contact stresses were demonstrated to be negligible. At a depth of two-thirds of the rib height, the contact stresses are about 6% of those on the surface. The effect of the ribs on the hoop and meridional stresses due to fuel-cladding interaction was also determined. In the vicinity of the rib, the hoop stress was lowered 40% from that in an unribbed section. Although the meridional stress was increased over three times the value observed in the smooth section, the magnitude of these stresses is very low. Also, this is the worst combination of bending and membrane stresses in the cross section. Other sections are stressed appreciably less.

14.3. FUEL-ROD OPERATING LIMITS

Steady-state and transient operating limits on the plant system parameters will be established in this subtask. Postulated accidents and continued operation transients will be identified as well as the possible types and mechanisms of failure. The design criteria, which represent the structural upper bounds of fuel-rod operation, will be transformed into limits on power level by iteration of available analysis methods. Results of LMFBR and GCFR in-pile and out-of-pile tests will also be integrated.

Work on this subtask commenced during this quarter. Since the failure modes and design criteria must be identified and established first, the efforts have been to review LMFBR documents on criteria and rod-performance prediction to determine limits that are also applicable to GCFR. This review is in progress.

14.4. SURVEILLANCE OF OTHER PROGRAMS FOR FUEL-, BLANKET-, AND CONTROL-ROD TECHNOLOGY

The purpose of this subtask is to support the rod analysis, development, and design tasks by providing through surveillance the information and data that are available from the LMFBR program that can be used in the GCFR design and then determining what the additional requirements for information are to provide guidance for planning of supplemental tests where the GCFR fuel, blanket, and control materials differ from those of the LMFBR or where the environment is different.

GCFR personnel participated in the AEC-sponsored Fuel Pin Performance Meeting held at HEDL in September 1974. The recent results from GCFR irradiation tests and PIE data from older tests were presented. In addition, the results of recent calculations of pin performance using the LIFE-III code were presented.

Surveillance of the area of fuel-cladding interaction was continued. An information and discussion meeting was held with representatives of the Core Materials and Core Engineering Branches of General Electric Co., Sunnyvale, and plans for possible cooperative experiments are being considered.

14.5. GCFR FUEL-ROD TEST PROGRAM REQUIREMENTS

The purpose of this subtask is to maintain a continual surveillance of GCFR irradiation requirements and available data from all irradiations programs and to ensure that the GCFR irradiation schedule will provide the supplementary irradiation test data required. Also, justifications for tests, test schedules, and requests for Approvals-in-principle will be prepared.

The work planning schedule for this subtask is being revised to reflect the shortened time scale for a decision on priorities for an irradiation experiment so that detailed design and long-lead procurement can be initiated during the current fiscal year.

Five candidate experiments are being considered for initiation during the current fiscal year. Four of these were also included in a priorities list submitted by ANL.

A study of the applicable statistical techniques for the prediction of the reliabilities of fuel rods is being carried out, and preparations are being made for a review of the irradiation experiment requirements with ANL and RDD in mid-November.